UNIVERSITÀ DEGLI STUDI DELLA TUSCIA DI VITERBO

Department for Innovation in Biological, Agro-Food and Forest Systems
DIBAF

PhD in Forest Ecology, cycle XXXI

Ozone impact on ecophysiological processes of forests

BIO/07

Candidate
Adriano Conte

Supervisor
Dr. Silvano Fares
Prof. Piermaria Corona

PhD Coordinator
Prof. Mauro Moresi

Short Abstract

Tropospheric ozone is a dangerous atmospheric pollutant for forest ecosystems since it generates oxidative damage to leaves with consequent losses in carbon assimilation. Thresholds for ozone-risk assessment are commonly developed based on manipulative experiments under controlled environmental conditions. However, it is not well understood if and to which extent ozone may have an impact of the ecophysiology of trees in natural environment and common consensus that new thresholds for ozone-risk assessment should be based on accumulated ozone fluxes rather than accumulated atmospheric concentrations. In order to identify the effect of ozone on gross primary productivity (GPP) and water fluxes, this study focused on the impact of ozone exposure in a Holm Oak forest (Castelporziano, It) and a Ponderosa pine plantation (Blodgett, US) where the dominant tree species are well known to have different levels of sensitivity towards ozone. Three of most widely used formulations to simulate leaf level stomatal conductance (the Jarvis multiplicative model, the Ball-Woodrow-Berry model, and the Medlyn optimal stomatal behavior theory parameterization) were implemented with ozone impact corrections into the multi-layer canopy model FORCAsT. To evaluate if a clear phytotoxic threshold exists (expressed as cumulative ozone fluxes through stomata), and if these thresholds are variable across the study sites and during the year, I implemented the Ball Woodrow Berry ozone correction factor into AIRTREE, a multi-layer canopy model specifically calibrated for both sites. To investigate the response to ozone exposure of the studied forests, simulated GPP and Latent Heat (λE) by both models were evaluated against observations by eddy covariance flux towers. Results showed that ozone might reduce the annual GPP up to 13 % in both the study sites, and that ozone tolerance of forests changes during the year depending on exposure to tropospheric ozone concentrations and phenology. By extracting the best daily threshold values from a range of different simulations, a Jarvis-like multiplicative function was proposed as a mean to predict a more realistic forest response as a function of environmental variables during the course of the year.

Keywords:

ozone, photosynthesis, stomatal conductance, eddy covariance, multi-layer models, Gross Primary Productivity

Extended abstract

Tropospheric ozone is a powerful oxidant of particular concern for plants. It enters the stomata and induces an oxidative stress that may damage cell membranes, proteins and DNA, leading to plant growth reduction. Metrics for ozone-risk assessment are commonly developed based on manipulative experiments under controlled environmental conditions. However, it is not well understood if and to which extent ozone may have an impact of the ecophysiology of trees in natural environment and common consensus that new thresholds for ozone-risk assessment should be based on accumulated ozone fluxes rather than accumulated atmospheric concentrations. Tolerance to ozone is a typical feature of Mediterranean evergreen broadleaves, thanks to their sclerophyllous leaves, their water saving strategy and their ability to tolerate oxidative stress. At the same time, the Mediterranean climate favors massive photochemical production of ozone thanks to the characteristic strong photochemical activity and its dry-hot Summer conditions. Furthermore, rural areas downwind big cities receive plumes of ozone precursor favoring ozone formation. Therefore, the Mediterranean climate is a perfect candidate to test the effect of ozone on forests characterized by different levels of ozone tolerance. In order to identify the effect of ozone on gross primary productivity (GPP) and water fluxes, this study focused on the impact of ozone exposure in two forest sites with Mediterranean climate and history of eddy covariance measurements: a an ozone tolerant evergreen Mediterranean forest (dominated by *Quercus ilex*) in the Castelporziano (CPZ) natural state reserve (Rome, Italy), and a *Pinus ponderosa* plantation in *Blodgett* (BLD) forest research station (Georgetown, USA) where the dominant tree species are well known to have different levels of sensitivity towards ozone. Various indexes to evaluate the risks for plants exposed to ozone have been developed. These include metrics based on mean ozone concentration and stomatal ozone flux threshold. Recent studies suggest that accounting for fluxes of ozone entering stomata is a better way of assessing ozone risk for plants and crops, especially for Mediterranean ecosystems where the dynamics of tropospheric ozone concentration is often mismatched with the dynamics of stomatal concentration. To test this hypothesis, three of the most used algorithms, the empirical multiplicative model proposed by Jarvis in 1976 (JV) , the semi-empirical model proposed by Ball, Woodrow *and* Berry in 1987 (BWB) and the optimal stomatal behavior theory parametrized by Medlyn et al. in 2011 (MD) were used in this study. For each of these three stomatal conductance (g_s) models (JV, BWB and MD), correction factors describing plant

response to ozone were derived from manipulative experiments on the studied species and by retrieving data from literature studies. A g_{smax} limiting factor f_{O3} representing the linear response of g_s to ozone concentrations (Hoshika et al. 2012, 2018) based on results from Free-Air Concentration Enrichment facilities (FACE) experiments was applied to the Jarvis multiplicative algorithm (JV_{fO3}). Two correction factors F_{pO3} and F_{cO3} representing the responses of A_n and g_s to the cumulative uptake of ozone (Lombardozzi et al., 2012, 2013, 2015) were applied to the BWB model (BWB_{FO3}). Finally, a modified functional form of the Medlyn optimal behavior photosynthesis-stomatal model, modified by Hoshika et al. (2013) was used (MD_K). In addition to ozone correction factors, six different critical stomatal flux thresholds (hereafter named thr0, thr1, thr2, thr3, thr4, thr5) were tested to estimate the phytotoxic dose of ozone (PODY) entering into the stomata. These thresholds represent the maximum stomatal ozone flux the plant is able to tolerate before a toxic dose would start to accumulate. A point of weakness of current metrics for ozone-risk assessment is that they are based on sunlit leaves, and upscaling to the whole canopy is somehow critical. To apply these leaf-level relationships at the ecosystem scale a bottom-up approach is needed. This approach is intrinsic to multi-layer canopy modeling, in which the canopy gas exchange is calculated by integrating the fluxes resulting from various components (e.g. soil, understory, and crown) interacting with their specific microclimate. Through cooperation with the Lancaster University, the FORCAsT model (Ashworth et al., 2015, 2016), originally developed to study fluxes of greenhouse gases and energy together with the chemistry and transport of volatile organic compounds (VOCs) and their oxidation products in the atmosphere within and above the forest canopy, and the AIRTREE model (Fares et al., 2019), developed to study forest ecosystem services such as carbon ozone and PM deposition were implemented with ozone corrections factors. The FORCAsT model was first parametrized for the two study sites in absence of any ozone effect. The first simulations without ozone correction were performed for BWB, MD and JV and used as references for ozone correction runs. Linear regressions between observations and simulations were performed for Gross Primary Productivity (GPP) and latent heat (λE) for the whole year. The "best" model run was identified by regression that gave the best coefficient of determination (R^2) and maximum accuracy (i.e. the lowest root-mean-square error, RMSE). Two general thresholds corresponding to a stomatal ozone flux of 4 nmol m^{-2} s^{-1} for CPZ and 1 nmol m^{-2} s^{-1} for BLD were identified, leading to a reduction in annual GPP up to 13%. To evaluate if the application of the ozone thresholds would have a seasonal positive or negative effect linear regressions were performed for both the whole year and for each season. Both the MD and the

BWB models provided good results in absence of ozone effects. However, when ozone corrections were applied, the best fit with observed GPP was obtained by applying the Lombardozzi correction factor to BWB (BWB_{FO3}) in both the study sites. In both sites, regressions showed that the threshold with the highest accuracy changed on a seasonal scale. The same approach was applied to the Aggregated Interpretation of the Energy balance and water dynamics for Ecosystem services assessment (AIRTREE) model for the BWB model parameterization, after two site-specific calibration procedures were performed. Linear regressions between observations and simulations provided results similar to the FORest Canopy Atmosphere Transfer (FORCAsT) model, confirming high thresholds for CPZ and low thresholds for BLD. Interestingly, results confirmed also that the thresholds with the highest R^2 changed seasonally, thus indicating that ozone tolerance of forests changes during the year depending on exposure to tropospheric ozone concentrations and phenology. The possibility to derive a function to describe such changes without the necessity to repeat the iterative approach used in this study was hypothesized. Such a function would provide a more realistic forest response to ozone as a function of environmental variables during the course of the year. To support this hypothesis, the best critical ozone thresholds were identified from simulations at each model time step (i.e. the lowest discard from observations) and collected into a new threshold variable (THR). The Spearman's rank-order correlation index (r_s) was used to identify the environmental variables that could potentially affect THR (e.g. PAR, VPD, SWC, Tair and ozone concentration). A boundary line analysis between THR and the selected environmental variables was performed and a Jarvis-like multiplicative algorithm to predict THR was finally developed. Relatively low but statistically significant linear correlation (R^2 = 0.51 and 0.3, for CPZ and BLD, respectively) between the observed and simulated THR were obtained. This can be explained by the lack of intermediate thresholds that could best represent ozone tolerance shifts during the day and that one or more additional environmental parameter may have not been included in the analysis. However, the observed correlations support the thesis that a dynamic threshold for ozone impact on vegetation studies should be adopted in order to produce realistic estimates of ozone damage to vegetation.

Summary

1. Introduction

1.1 Tropospheric Ozone

1.1.1 Overview

There is no compound in the troposphere where the difference between actual atmospheric levels and toxic levels is so marginal as is the case for ozone (Stanners et al., 1995). Ozone (the triatomic oxygen molecule, O_3) is a greenhouse gas (GHG) naturally occurring in the atmosphere, with a lifetime of a few days to a few weeks and a radiative forcing of climate change of +0.35 W m^{-2} (Forster et al., 2007). Ozone is present in both the stratosphere and troposphere. It absorbs and emits radiation in the thermal infrared, trapping heat to warm the Earth's surface (Figure 1).
In the stratosphere (at altitude of 15 to 35 km) the ozone layer acts as a natural filter absorbing the UV radiation, protecting much of Earth's biota from this potentially damaging short wavelength radiation. This is called the stratospheric ozone, the upper layer of ozone. In the lower troposphere (up to 10-15 km above the ground), ozone is a strong oxidant that at elevated concentrations is harmful to human health, materials and plants (Sitch et al., 2007). Indeed, tropospheric ozone is considered the secondary pollutant (produced through photolytic reactions in which are involved NO_2, VOCs and OH radicals) of major concern for plants (Fares et al., 2010). Dry deposition is the main sink for ozone, controlled mainly by stomatal activity (Cieslik, 2004). Once penetrated stomata, this oxidizing agent expresses its phytotoxic action by damaging plant tissues, cell membranes, proteins and DNA (Contran and Paoletti, 2007; Fares et al., 2018), it decrease stomatal conductance, reduce primary productivity (reduced rubisco activity) and increase the secondary metabolism, leading to a reduction in carbon assimilation (Fiscus et al. 2005, Paoletti 2007b, Wittig et al., 2007). Therefore, ozone affects the ecosystem health and the productivity thus threatening food security (e.g. crops) by reducing plant growth and variety (CCAC Scientific Advisory Panel, 2014). This affects forest carbon sink, causing a reduction in net primary productivity, NPP (Ainsworth et al., 2012). Tropospheric ozone is dangerous for human health too (Anenberg et al, 2010) since it is a major component of urban photochemical smog. If inhaled, this oxidant may worsen bronchitis and emphysema, trigger asthma, and permanently damage lung tissue (Desario and Gray, 2012). Indeed, the exposure to this pollutant is responsible for an estimated 150,000 premature deaths every year (Lim et al., 2012). Ground-level ozone concentrations

limits have been set with the aim to protect human health and vegetation (Fares et al., 2014). World Health Organization (WHO) indicates the one-hour short-term limit value of 75-100 ppb for health protection and the long-term value of 30 ppb over the growing season for protection of vegetation.

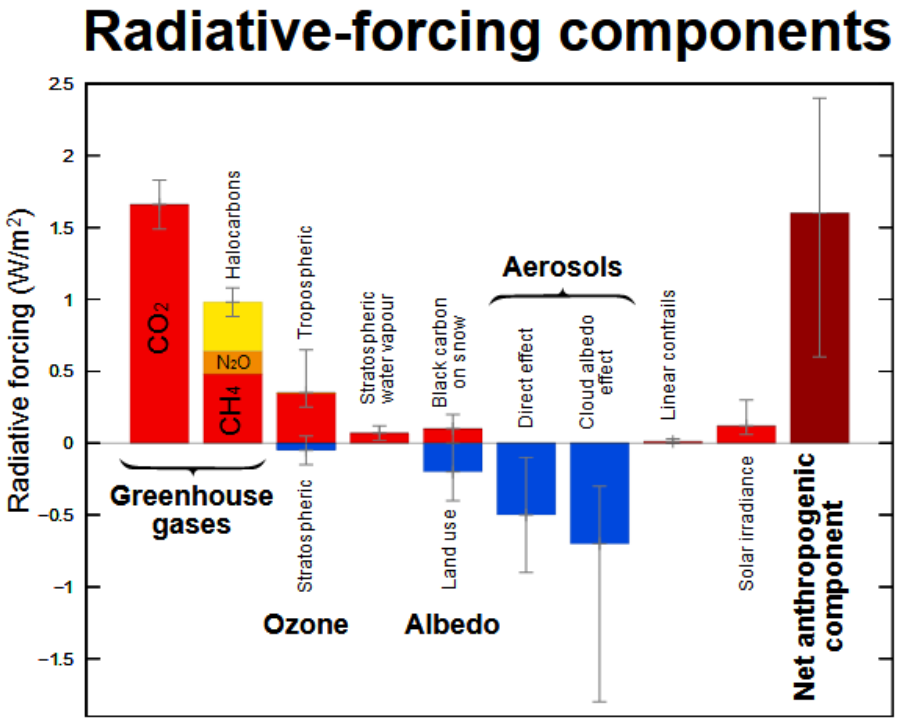

Figure 1 - GHGs Radiative Forcing - IPCC 2007 (Bernstein et al., 2008). Leland Mcinnes©

1.1.2 Ozone Formation

Ozone is a secondary pollutant. Therefore, this gas is not directly emitted but formed by sunlight-driven oxidation of other agents, called ozone precursors, in particular methane (CH_4) but also carbon monoxide (CO), non-methane volatile organic compounds (NMVOCs) and nitrogen oxides (NO_X). Chemistry that controls ozone production and destruction in the troposphere is summarized by the following reactions (Monks et al., 2015).

NO_2 is one of the main ozone precursors, primarily produced by the burning of fuel. The photolysis of NO_2 produces atomic oxygen and a molecule of ozone:

$$NO_2 + h\nu \rightarrow NO + O\cdot \qquad \text{eq.1}$$

Photodissociation of NO_2 by sunlight is the only significant anthropogenic source of ozone in photochemical smog:

$$O_2 + O\cdot + M \rightarrow O_3 + M \qquad \text{eq.2}$$

The M in eq.2 is any third molecule which is needed to stabilize the excited intermediated formed on the addition of $O\cdot$ to O_2.

$$HO_2 + NO \rightarrow OH + NO_2 \qquad \text{eq.3}$$

$$NO + O_3 \rightarrow NO_2 + O_2 \qquad \text{eq.4}$$

This series of reactions creates a null cycle, since the rapid interconversion between NO and NO_2 leads to both ozone production and destruction.
This equilibrium is altered in presence of volatile organic compounds (VOCs).

These chemical compounds are both anthropogenic and naturally occurring (i.e. most plant scents or odors are VOCs):

$$VOC + OH + O_2 \rightarrow CO_2 + HO_2 \qquad \text{eq.5}$$

VOCs oxidation produces of hydroperoxyl (HO_2), which reacts with NO (eq.3), changing the [NO]/[NO_2] ratio, leading to O_3 formation.

The major source of OH radicals is the ozone photolysis. This process is one of the main sinks for ozone, the chemical destruction:

$$O_3 + hv \rightarrow O + O_2 \qquad \text{eq.6}$$

and the subsequent reaction of the excited oxygen atom with water vapor:

$$O + H_2O \rightarrow OH + OH \qquad \text{eq.7}$$

Another ozone sink is the dry deposition that occurs in forest ecosystems through in-canopy chemistry stomatal uptake and non-stomatal uptake. Non-stomatal uptake includes all the reactions of ozone with the external surface of vegetation and soil.

1.2 Ozone impact on vegetation

1.2.1 Forests ecosystems and atmospheric pollutants

Forest ecosystems represent important resources to control atmospheric concentrations of globally relevant greenhouse gases, which emissions are the dominant drivers of climate change (Rosa and Dietz, 2012). They control the exchange of energy, carbon, water and momentum between the atmosphere and the land surface. They also represent pools that can remove (sink) or emit (source) these gases, including biogenic aerosols and their precursors in the atmosphere (Karsenty et al., 2003). These dynamics can be altered by Global climate change, reversing sinks to sources (Scholes, 1999). As a consequence, carbon stored in vegetation and soil could be released into the atmosphere with a strong impact on global climate (Heimann and Reichstein, 2008). This feedback could be one of the reasons why many of the earth's ecosystems are 'unhealthy' and their functions, also known as ecosystem services, have become impaired (Rapport, 1998).

Forest ecosystems act directly on the amount and distribution of contaminants in the atmosphere through biological, chemical and physical processes. This action has positive effects on climate and human health but can influence the physiological state of the vegetation by slowing the growth and productivity of the forest (Fares et al., 2013; Herman, et al., 2001; Rai et al., 2009). Tropospheric ozone has the most widespread negative impact on vegetation than any other air pollutant (Ashmore 2005). The effects of ambient ozone on crops and forest trees have been widely studied (Carriero et al., 2015; Kolb and Matyssek, 2003; Mills et al., 2011) but knowledge is still incomplete. At cellular level, ozone induces reductions in leaf chlorophyll content (Heagle et al., 2010; Sharma et al., 2003), reductions in the quantity and activity of the primary carboxylation enzyme Rubisco (Fiscus et al.,

2005) and/or direct damage to stomatal cells (Hassan et al. 1994; Manes et al. 2014; Torsethaugen *et al.* 2002). At leaf level it induces morphological and chemical changes which adversely affect plant growth (Karnosky et al., 2007; Matyssek et al., 2007). At plant level ozone may cause growth reduction, shift in biomass allocation (Hoshika et al., 2013b), impairment of physiological traits such as leaf gas exchange (Fares et al., 2013) and visible foliar injury (Paoletti, 2007a). At ecosystem level it affects forest carbon sink (Leisner and Ainsworth, 2012), causing a reduction in NPP (Figure 2). Tolerance to ozone is typical of the Mediterranean evergreen broadleaves, considered tolerant to ozone because of their sclerophyll leaves, their water-saving strategy and their ability to tolerate oxidative stress (Nali et al., 2004; Paoletti, 2006). These leaves presents some typical xeromorphic traits such as the compact mesophyll and strongly lignificated walls that limit the amount of pollutant that can circulate in the intercellular spaces and enter into the cells (Guerrero et al., 2013; Manes et al., 1998). Furthermore, these plants present an efficient stomatal control to ensure tolerance to yearly summer droughts (Bombelli & Gratani 2003 ; Romane & Terradas 2013), a typical water-saving strategy in which the plant closes stomata at relatively high water potentials to avoid water loss (Castell et al. 1994; de Lillis and Mirgone 1994; Savé et al. 1999) during the hottest and driest periods, thus reducing the fluxes of ozone inside the leaves (Vitale et al., 2003; Manes et al.,2007; Fares et al., 2013). In addition, evergreen broad-leaved species as Quercus ilex (De Lillis et al., 2009) are able to cope with the oxidative pressure of the Mediterranean climate (high temperatures, drought, strong sunlight, ozone pollution) by emitting monoterpenes, which have an antioxidant function (Peñuelas & Llusià, 2002; Peñuelas et al., 2005; Velikova et al., 2005).

Ozone pollution is pronounced in regions with strong photochemical activity, such as the Mediterranean area (Paoletti, 2006), which climate is characterized by seasonal changes between hot Summers with high pressure, low winds and strong solar radiation. These conditions favor massive photochemical production of ozone with

development of mesoscale processes and recirculation within air masses (Millán et al., 2000). Indeed, this region is characterized by a general spring-summer peak (Di Carlo et al., 2007; Ribas and Peñuelas, 2004) or as a double peak in mountain sites (Chevalier et al., 2007; Schuepbach et al., 2001), caused by the exchanges between stratosphere and troposphere (STE) and the transport of ozone precursors from the northern troposphere during spring and the high summer photochemical production of ozone (Lelieveld et al., 2002; Pochanart et al., 2001) In mountain sites, the first peakof ozone can be observed in spring, followed by a second peak in summer while minimum values are reached during "cold" seasons (autumn and winter), during which the ozone concentrations are about the half of the summer-spring peaks (Kouvarakis et al., 2002; Ribas and Peñuelas 2004). Furthermore, rural and forested areas downwind big cities receives plumes of ozone anthropogenic precursor favoring ozone formation (Zong et al., 2018), especially during warmer months, in presence of emitted precursos. The Mediterranean area seems to be a perfect candidate to evaluate the effect of ozone on forests characterized by different ozone tolerance. For this reason, two forest sites with Mediterranean climate with a history of eddy covariance measurements characterized by different ozone tolerance were selected: an ozone tolerant evergreen Mediterranean forest (dominated by *Quercus ilex*) in Rome (Italy), and a *Pinus ponderosa* plantation in Georgetown (California, USA). A recent study by Feng et al. (2018) suggests that the difference in tolerance between these two species (a broadleaf angiosperm and a needleleaf gymnosperm) can be related to the different leaf mass area index (LMA), the ratio of leaf dry mass to leaf area. The author found that species with high LMA are less sensitive to ozone. He proposed several explanations for this observation: a) the lower ozone load per unit leaf mass and per unit mesophyll cell mass, due to their thick mesophyll layer (Li et al., 2016). b) the cross-protection, the evolutionary adaptations to stressful environments (i.e. sclerophylly, efficient stomatal conductance and antioxidant defense) (Bussotti 2008).

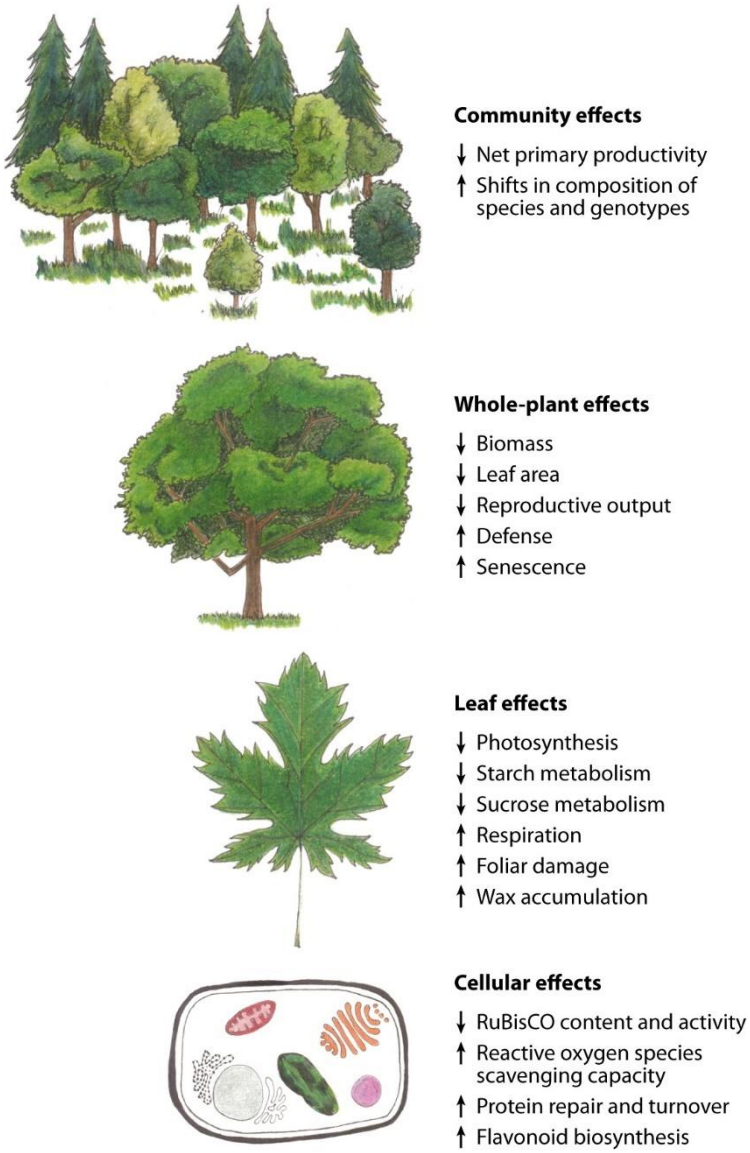

Figure 2 - Effects of O_3 on plant processes at the cellular, leaf, whole-plant, and community scales. arrows indicate directional changes of processes affected by elevated [O_3] (from Ainsworth et al., 2012).

1.2.2 Defense Mechanism

Plants evolved several defensive strategies to face the toxic effects of air pollutants. They can “avoid”, “tolerate”, or “compensate” damages caused by ozone.

1) Stomatal closure, dormancy and early senescence represents the main mechanisms of the strategy known as ozone stress “avoidance”. Avoidance consists in a physical reduction of stomatal aperture to limit the stomatal influx and thus the plant’s tissues exposure to ozone.

2) Ozone stress avoidance limits also the carbon uptake. Therefore, the synthesis of antioxidants, that represent the defensive mechanism known as ozone “tolerance”, is limited. This strategy consists in enzymatic processes and chemical reactions to detoxify photooxidants. Indeed, glutathione, vitamin C and E concentrations were found to increase rapidly in trees (*Albies alba* and *Picea abies*) exposed to low ozone concentration (Mehlhorn et al., 1986). The amount and or the synthesis rate of antioxidants as tocopherol can be interpreted as an indicator of plants tolerance to ozone (Szarka et al., 2012). Indeed, tolerant trees (*Pinus strobus*) resulted to be characterized by higher glutathione reductase and ascorbate peroxidase than sensitive species exposed to ozone (Chevone, 1991), whereas sensitive species showed increased activity in superoxide dismutase (Mehlhorn et al., 1987). The production of stress ethylene can be interpreted as another indicator of plants ozone tolerance response. In a short-term fumigation experiment its production was found to be higher in seedlings grown in free air compared to seedlings grown at high ozone concentration (preconditioned), that produced lower quantities of ethylene (Mehlhorn and Wellburn 1987). Tolerance is also dependent on leaf age, younger leaves are generally more resistant to ozone than older leaves that resulted to have lower concentrations of superoxide dismutase (SOD) (Tanaka and Sugahara, 1980).

3) A third mechanism of defense is the ozone “compensation”. This mechanism consists in the reallocation of resources form one tissue to another in response to ozone damage. This kind of response can be recognized as a change in the root to shoot ratio. Indeed, the decreased root biomass is an indirect response to ozone stress caused by a reallocation of carbon from roots to foliage (Reich,

1987; Teskey et al., 1986). The reallocation of nitrogen from a leaf to another is another typical example of compensatory response. Nitrogen is translocated from damaged older leaves to younger leaves, leading to an apparent enhanced photosynthetic activity a (Hom and Riechers 1991). Even the enhanced detoxifying compounds production in response to ozone exposure can be considered a compensatory response. However, this kind of response might not occur in nutrient-stressed plants.

In this work, I focused on the first two mechanism: ozone avoidance and ozone tolerance.

1.2.2.1 Stress Avoidance

The stomatal uptake is an important sink for tropospheric ozone (Fowler et al., 2001). Indeed, stomata represent the principal interface for ozone to penetrate into the leaves (Mills et al., 2010; Omasa & Takayama, 2002). Once enters the plant through stomata, O_3 reacts with the aqueous matrix of the cell wall (i.e. apoplast) and is immediately degraded into secondary ROS (as hydrogen peroxide, superoxide and hydroxyl radical causing oxidative stress (Bortier et al., 1999). The accumulation of reactive oxygen species (ROS) in the extracellular space activates several signaling defense cascades (Vainonen & Kangasjärvi, 2015). Ozone damages first the plasma membrane affecting its permeability (Heath & Taylor, 1997), destroys the thylakoid membranes in the chloroplast (Hippeli & Elstner, 1996), where the light-dependent reactions of photosynthesis occur, reduce the synthesis of Rubisco (Glick et al. 1995; Pell et al. 1994; Pelloux et al 2001), the enzyme responsible for the fixation of carbon from atmospheric CO_2. These damages of photosynthetic apparatus lead to the reduction of carbon assimilation by which in turn decreases photosynthesis, plant growth, and biomass accumulation (Fiscus *et al.* 2005; Wittig *et al.* 2007, 2009).
The amount of ozone entering the stomata (i.e. the stomatal flux, F_{st}) is considered the main responsible for ozone injuries to plants (UNECE, 2010). It is regulated by plants stomatal aperture that is function of environmental and physiological factors such as light, temperature, carbon dioxide (CO_2) concentration, vapor pressure deficit (VPD), phenology and water availability in the soil-plant-atmosphere system (Grünhage et al., 2012). It has been observed that high CO_2 concentrations, temperatures and hydric stress can reduce stomatal conductance (Ainsworth and Rogers 2007) and consequently the ozone flux inside the leaf. Plants' stomatal

control capacity may also be related to leaf anatomical traits such as stomatal density and size (Drake et al., 2013). Indeed, leaves characterized by high density of small stomata show a faster regulation of stomatal aperture in response to environmental stimuli (Aasamaa et al., 2002; Drake et al., 2013; Hetherington and Woodward, 2003) and therefore a faster reduction of ozone stomatal fluxes, decreasing the risk of ozone damage on leaves (Pääkkönen et al., 1996). Nevertheless, ozone damages to stomatal cells could alter these reponsest (Uddling et al., 2010). Although a rapid reduction of stomatal aperture in response to short-term exposure to ozone was reported (Wittig et al., 2007), chronic exposure reduces the ability of plants to regulate stomata, referred to as "ozone-induced stomatal sluggishness" (Carriero et al., 2015; Emberson et al., 2009; Hoshika et al., 2015, 2016, 2018b). A reduced ability in stomatal control is a serious problem for plants, since it can lead to plants inhability to regulate the loss of water (Paoletti, 2005; Sun et al., 2012).

The mechanisms behind stomatal sluggishness are still under investigation but possible explanation can be found in the up-regulation of ethylene emission (Mills *et al.* 2009), suggested to be responsible for a reduction in sensitivity to Abscisic acid (ABA) and thus to stomatal closure (Wilkinson and Davies 2010). Although the same mechanism was observed in response to water deficit (Morgan and Drew, 1997) an ozone-induced aberration lasts longer than the effect of water stress leading to an imperfect stomatal closure at night (Hoshika et al., 2013a).

In the study of gene expression Dumont *et al.* (2014) demonstrated that the CO_2 signaling pathway involved in stomatal closure was inhibited under ozone exposure.

Paoletti *et al.* (2009) related stomatal sluggishness as an indicator of early-senescence in leaf metabolism.

When the carboxylation sites are damaged by ozone, g_s and photosynthesis (A_n) may result decoupled (Figure 3). This decoupling between A_n and g_s corresponds to a change of the ratio between photosynthesis and transpiration after chronic ozone exposure. In general, the stomatal closure can be considered as an indirect response to grown internal CO_2 concentration (C_i), resulting from decreases in carbon fixation (Paoletti, 2005). Nevertheless, the rate of stomatal reduction is often different to the rate of photosynthetic decrease under chronic ozone exposure. In this situation ozone affects both carboxylation and stomatal conductance, but with different strength (Calatayud et al., 2007; Francini et al., 2007; Gregg et al., 2006; Maier-Maercker and Kock 1991; Matyssek et al., 1991; Mikkelsen 1995; Novak et al., 2005; Paoletti 2005; Paoletti and Grulke 2005; Pearson and Mansfield 1993; Tjoelker et al., 1995). Therefore, other additional ozone induced limitations (e.g. carboxylation and mesophyll limitations) may cause decoupling and may have even a more important

role than the stomatal limitation (Francini *et al.* 2007; Matyssek *et al.* 1991; Noormets *et al.* 2001; Reichenauer *et al.* 1997). An example of g_s-A_n decoupling can be found into above mentioned night stomatal aperture. During night if stomata do not close completely there would be a loss of water in absence of photosynthesis and therefore the decoupling between A_n and transpiration (Caird et al., 2007). Another example of decoupling between g_s and A_n was observed in plants exposed to high levels of both light and ozone. In that situation membranes and photosystems become oxidized, reducing carbon sequestration and stomatal conductance at different rates or magnitude (Calatayud et al., 2007; Demmig-Adams and Adams 2006; Francini et al., 2007; Maier-Maercker and Kock 1991; Matyssek et al., 1991; Paoletti and Grulke 2005; Pearson and Mansfield 1993; Tjoelker et al., 1995). Chronic exposure to ozone can lead also to the damage of plant's cuticle, increasing cuticular water loss, and increasing leaf permeability (Zhang et al., 2011). The oxidative stress exerted by reactive species (ROS) in the apoplast rapidly leads to photo inhibition (Guidi et al., 2002) and activates signal pathways that can lead to programmed cell death (Kangasjarvi *et al.* 2005). This effect is recognizable as ozone visible injuries (Paoletti et al., 2009), a symptom of ozone reduced photosynthetic capacity and stomatal conductance in leaves (Paoletti et al., 2004). These visible symptoms are visible alterations of leaf surface, generally they appear as yellow spots over the leaf (mottling) in needleleaf trees, and as small punctuate spots (stippling) in broadleaf trees (UNECE, 2004).

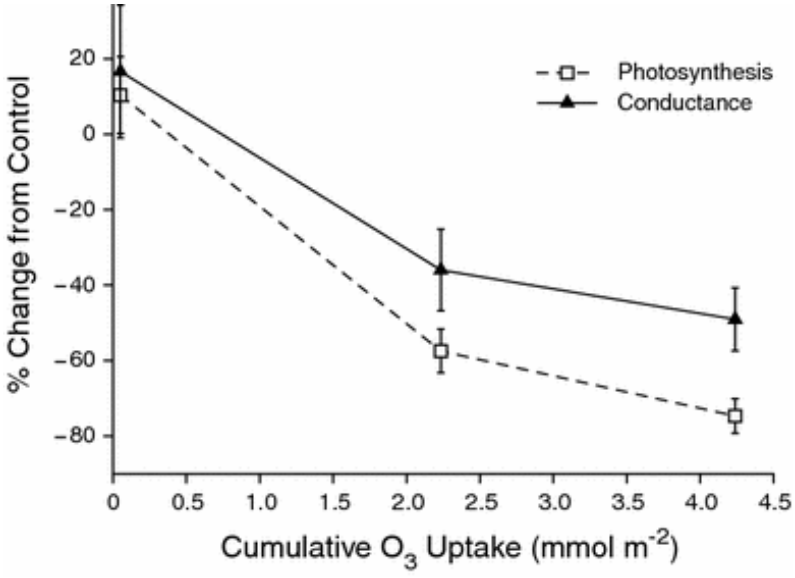

Figure 3 - Percent changes in photosynthesis (open squares) and stomatal conductance (black triangles) over a range of cumulative ozone uptakes (CUOs). Differences in the rate of change for the same CUO demonstrate that photosynthesis and stomatal conductance do not change at the same rate. Error bars represent ± bootstrap standard error (from Lombardozzi et al 2012)

1.2.2.2 Stress Tolerance

Inter and intra-species variations in ozone response to ozone have been observed (Furukawa et al., 1990; Pääkkönen et al., 1996). It can depend on leaf morphological adaptations their water saving strategy (Nali et al., 2004; Paoletti, 2006) and different characteristics of stress resistance such as avoidance by stomatal narrowing and tolerance in terms of repair and detoxification capacities (Matyssek et al., 2008; Oksanen et al., 2007). This tolerance depends on leaves available resources for repair damages or biochemical ozone detoxification (Paoletti et al., 2008; Tausz et al., 2007). Such capacity seems to increase with leaf mass per area (LMA) and photosynthetic capacity, since repair and detoxification require energy (Bussotti, 2008; Musselman and Minnick, 2000; Noctor and Foyer, 2002; Wieser et al., 2002; Zhang et al., 2012). Therefore, sensitivity to ozone may be explained by the ratio between stomatal flux and net photosynthesis (Fredericksen et al., 1996; Kolb and Matyssek, 2001), as the balance between ozone exposure and photosynthates for repair or detoxify. Indeed, in addition to regeneration of antioxidants, their synthesis rate and the repair processes of oxidized proteins can reduce ozone effects (Møller et

al., 2007; Wieser and Matyssek, 2007). Once penetrated into the leaf, ozone needs be detoxified outside of the cells, in the apoplastic space, to avoid oxidative reactions with plasma membrane and cytoplasmic compartments. The interception of ozone and reactive oxygen species (ROS) by constituents of the apoplast play a crucial role in averting cellular damage, since the plasmalemma is the site where oxidative reactions take place (Heath, 1988). Plants have a detoxification system constituted by a pool of reduced ascorbate (vitamin C, AA) in the apoplast that represents the first defense to oxidative stress (Castagna and Ranieri, 2009). The ascorbate is an antioxidant accumulated in plant tissues as chloroplasts (Foyer and Halliwell, 1976), apoplast of leaf stems (Takahama, 1993) and leaves (Castillo and Greppin, 1988; Takahama and Oniki, 1992) and its concentrations are inversely proportional to plant sensitivity to ozone (Conklin et al., 2002; Mächler et al., 1995).
This suggests that environmental factors which alter apoplast pH such as water deficit (Hartung et al., 2008), light (Mühling et al., 1995), nitrogen supply (Hoffmann et al., 1992) and gaseous pollutants (Moldau et al., 1998) may affect plant's ozone tolerance.

1.3 Assessing ozone impact on vegetation

1.3.1 Ozone risk assessment metrics

Various indexes to evaluate the risks for plants exposed to ozone have been developed (Fuhrer et al., 1997; Musselman et al., 2006). These include metrics based on mean ozone concentration and stomatal ozone flux threshold. An example concentration-based metric is the AOT40. This index is one of the most widely used in Europe and is expressed as the accumulated ozone over a threshold of 40 ppb, during daylight hours (global radiation > 50 Wm^{-2}).

$$AOT40 = \Sigma\,[[O_3] - 40]\,\Delta t \qquad \text{eq.8}$$

This index postulates that ozone is harmful for vegetation only at concentrations exceeding a threshold of 40 ppb when it is adsorbed through stomata during daylight hours (Kerstiens *et al.* 1992; Kärenlampi and Skarby 1996). However, Lombardozzi *et al.* (2013) found no correlation between ozone concentration and ozone damage across many plant species. Recent studies suggest that accounting for fluxes of ozone entering stomata would be a better approach to assess ozone risk for plants and crops, since AOT40 does not necessarily take into account the amount of ozone directly absorbed by plant stomata (Emberson et al., 2000). Therefore, the scientific community has suggested a critical level of accumulated stomatal ozone flux (Karlsson et al., 2007; Wieser and Tausz, 2006). This accumulated stomatal ozone flux index (*POD*Y), where *POD* represents the phytotoxic stomatal ozone dose above a flux threshold (Y), derived as the sum over time of the differences between hourly mean values of *F*st and Y for the period when stomatal ozone flux (*F*st) exceeds Y (Mills et al., 2011b; UNECE, 2004).

$$PODY = \int_{i=1}^{n} \max((F_{st} - Y),0)\, dt \qquad \text{eq.9}$$

Where PODY (nmol m^{-2}) is the accumulated stomatal ozone flux above a threshold Y, calculated from hourly values of F_{st}, n is the number of hours and dt = 1h.

The application of a threshold (Y) is a way to account for the ability of plants to detoxify ozone. Several studies on this topic found that ozone uptake and reductions in GPP are correlated with low threshold values (De Marco et al., 2016; Karlsson et al., 2004; Lombardozzi et al., 2015; Uddling et al., 2004). However, since plants have different detoxifying capacities even within the same species, the identification of a correct threshold is problematic (Lombardozzi et al., 2015). Indeed, in a recent study Lombardozzi *et al.* (2015) found large *CLM4*.5SP model sensitivity to ozone threshold values. Therefore, large improvements to simulated ozone responses can be expected by identifying species-specific or plant functional types threshold values.
Climatic conditions strongly affect stomatal conductance and consequently the ozone uptake and the biological response of vegetation to the pollutant (Paoletti, 2006). The ability of stomata to act as a sink for atmospheric gases (quantified by stomatal conductance) is in turn mainly controlled by water availability and other environmental factors like air water vapor pressure deficit, solar radiation, wind speed, intensity of turbulence (Emberson et al., 2000). Furthermore, an index based

on the stomatal ozone uptake requires an accurate estimate of stomatal conductance to account the actual dose of ozone received.

1.3.2 Stomatal conductance models

Plant transpiration is the process of vaporization of water from leaf tissues (i.e. the Mesophyll). This process is driven by the available energy, the drying potential of air (e.g. vapor pressure deficit, VPD), and the plant's capacity to refill the leaf tissues with water coming from the roots. This is strongly dependent on soil water availability, thus defining the water potential gradient within the soil-plant-atmosphere continuum (Pallardy and Kozlowski, 2008). Since an impermeable waxy cuticle covers the leaf surface, leaf transpiration is almost totally determined by the stomatal diffusion of water. Stomata are little pores in the leaf lamina, which regulate the diffusion of gases (CO_2, H_2O, air pollutants) from outside to inside the leaf and back, by following complex environmental, osmotic, and hormonal signal pathways. In general, stomatal aperture decreases when the evaporative demand is higher than plant's water replenishing, preventing plants from water stress (Gimenez et al., 2005). Such changes in stomatal aperture occur in the order of seconds (Fanjul and Jones, 1982; Lawson and Blatt, 2014) to optimize CO_2 uptake and water losses in rapidly changing environmental conditions (e.g. radiation, temperature, drought, VPD, wind speed, and sub-stomatal CO_2 concentrations).
Stomatal conductance is one of the most extensively modeled processes of the last decades. Empirical and semi-empirical approaches are widely used to simulate g_s.

1.3.2.1 Jarvis multiplicative algorithm

One of the most used algorithms is the empirical multiplicative model proposed by Jarvis in 1976, based on the observed responses of g_s to environmental factors. This model applies a set of covariates to reduce a maximal g_s:

$$gs = f(Q) \cdot f(T_l) \cdot f(VPD_l) \cdot f(C_a) \cdot f(SWC) \quad \text{eq.10}$$

Each covariate is a function (*f*) describing the observed response to each environmental factor independently from the others (Damour et al., 2010) and can be

derived by boundary line analysis (Webb, 1972). The hypothesis behind this approach is that g_s is sensitive to multiple environmental influences (e.g. light intensity Q, leaf temperature T_l, VPD_l, CO_2 concentration C_a, and SWC). The weak point of this approach is that it does not take in account any physiological feedback loops among stomatal conductance and internal CO_2 concentration, transpiration, humidity deficits and leaf water potential (Quiang et al., 2004).

1.3.2.2 The Ball, Woodrow & Berry model

These interactions have been implemented into semi-empirical models, such as the Ball, Woodrow & Berry model (BWB) that linearly relates photosynthesis (A_n) and g_s (Ball et al., 1987; Farquhar et al., 1978). Indeed, the BWB formulation, photosynthesis is influenced by changes in g_s that regulates internal carbon dioxide concentration (C_i), which drives the biochemical components of photosynthesis. The A_n-g_s empirical relationship corresponds roughly to the value of maximum g_s that maximizes productivity (Patwardhan et al., 2006). This model has been developed after Wong et al. (1979) demonstrated that stomata regulate to plant water status but also on leaf A_n, maintaining a near constant ratio between intercellular (C_i) and ambient (C_a) CO_2 concentrations. Ball modeled leaf conductance as a function of leaf photosynthesis, leaf surface relative humidity, and surface CO_2 concentration.

$$g_s = g_0 + g_1 (A_n RH / C_a) \qquad \text{eq.11}$$

where g_0 and g_1 are fitted parameters, A_n is net assimilation rate ($\mu mol\ m^{-2}\ s^{-1}$), RH is relative humidity at the leaf surface (dimensionless), and C_a is atmospheric CO_2 concentration at the leaf surface ($\mu mol\ mol^{-1}$).

This formulation implies the necessity to couple g_s with a photosynthesis model (e.g. the Farquhar biochemical model 1982) and to solve for them both simultaneously. An example of this approach can be found into the analytical solution proposed by Baldocchi (1994).
A weak point of this model is that stomata appear to respond to transpiration (Monteith 1995; Mott and Parkhurst 1991; Oren et al. 1999) rather than directly to relative humidity (Ball et al. 1987; Grantz 1990; Katul et al. 2009; Monteith 1995).

1.3.2.3 The optimal stomatal behavior model

A different approach can be found in the Medlyn formulation, focused on the 'regulatory' role of stomata (Medlyn et al., 2011). This formulation was developed with the aim to reconcile the empirical approaches previously described (based on experimental observations) with the optimization theory approach into a model whose parameters have theoretical meaning. The theory of the optimal stomatal behavior (Cowan and Farquhar, 1977) postulates that stomata act to maximize photosynthesis while minimizing transpiration (E). The ratio between these two optimizations is defined as the "marginal water cost of carbon gain", λ (mol H_2O mol^{-1} C).
The use of this approach was limited, probably because λ was difficult to estimate. However, the possibility to directly estimate the empirical model parameters from data made it easier to use (Duursma, 2015; Medlyn et al., 2011).
Medlyn et al. (2011) derived a unified model in a BWB-like form based on the optimal stomatal conductance theory, providing to model parameters a biological meaning.
This approach was developed following Cowan and Farquhar (1977).

Stomata act to minimize the marginal water cost of plant carbon gain.

$$\frac{\delta E}{\delta A} = \lambda \qquad \text{eq.12}$$

Where E is the transpiration rate, A is the CO_2 assimilation rate, λ is a Lagrange multiplier that represents the marginal water cost of plant carbon gain. This stomatal behavior would be optimal if stomatal apertures varied to maintain the δA/δE ratio constant.

Eq. 12 can also be written as:

$$\frac{\delta E/\delta gs}{\delta A/\delta gs} = \lambda \qquad \text{eq.13}$$

In this form eq. 13 describes the sensitivity of photosynthesis (*A)* and transpiration *(E)* to changes in stomatal conductance (g_s).

The full equations are (Cowan and Farquhar, 1977):

$$\frac{\partial E}{\partial g} = \frac{r_s^2 E}{r_s + r_b + r_b^* \left(\frac{L}{C_p}\right)\left(\frac{\partial w'}{\partial T_l}\right)} \qquad \text{eq.14}$$

Where r_s is the stomatal resistance (equal to $1/g_s$), r_b is the boundary layer resistance, T_l is the leaf temperature (K), L is the latent heat of vaporization of water (J mol^{-1}), , C_p is the heat capacity of air (J mol^{-1} K^{-1}),, $\delta w' / \delta T_l$ is the slope of the curve relating the saturation vapor pressure of water to temperature , r_b is the effective boundary layer resistance to transfer of sensible heat and thermal radiation.*

$$\frac{\partial A}{\partial g_s} = \frac{1.6 r_s^2 A - 1.6 r_b^* \left(\frac{L}{C_p}\right)\left(\frac{\frac{\delta A}{\delta T_l}}{\frac{\delta A}{\delta C_i}}\right)\left(\frac{\delta E}{\delta g_s}\right)}{1.35 r_b + 1.6 r_s \sigma \left(\frac{1}{\delta A / \delta C_i}\right)} \qquad \text{eq.15}$$

Where, σ is the Stefan-Boltzmann constant (5.67 x 10^{-8} W m^{-2} deg^{-4}), C_i is the intercellular partial pressure of CO_2 within the leaf.

Making the assumption that r_b and r^*_b are expected to be relatively low, they can be ignored and equation (14) and (15) becomes:

$$\frac{\partial E}{\partial g_s} = r_s E = D \qquad \text{eq.16}$$

$$\frac{\partial A}{\partial g_s} = \frac{1.6 r_s^2 A}{1.6 r_s + \frac{1}{\partial A / \partial C_i}}$$

Where D is the leaf-to-air vapor pressure deficit,

Combining with eq. 13:

$$\lambda = \frac{D\left(1.6r_s + \frac{1}{\partial A/\partial C_i}\right)}{1.6r_s^2 A} \qquad \text{eq.17}$$

According to Farquhar and Sharkey (1982), A can be also written as:

$$A = \frac{C_a - C_i}{1.6r_s} \qquad \text{eq.18}$$

So:

$$\lambda = \frac{D\left(1.6 + \frac{g_s}{\partial A/\partial C_i}\right)}{C_a - C_i} \qquad \text{eq.19}$$

Rearranging and substituting:

$$A = \frac{\delta A}{\delta C_i}\frac{[\lambda(C_a - C_i)^2 - 1.6D(C_a - C_i)]}{1.6D} \qquad \text{eq.20}$$

Eq. 20 can also be expressed as a quadratic equation with respect to Ci, e.g. $aC_i^2 + bC_i + c$, which can be solved in a normal way, but expressions for A and $\delta A/\delta C_i$ are needed.

According to Farquhar *et al.* (1980) the photosynthesis can be written as

$$A = min\{A_c, A_J\} \qquad \text{eq.21}$$

where A_c is the rate of CO_2 assimilation limited by the potential rate of Rubisco carboxylation, and A_J is the rate of CO_2 assimilation limited by the potential rate of ribulose-1,5 bisphosphate regeneration, usually considered to be limited by the rate of electron transport J.

According to previous study (e.g. Shimazaki 1989), stomatal behavior could be regulated by electron transport (Aj) rather than rubisco carbon fixation (Ac). Therefore, by taking in consideration A_j only:

$$A_J = \frac{J}{4}\frac{C_c - \Gamma^*}{2\Gamma^* + C_c} \qquad \text{eq.22}$$

Where A_J is the rate of CO_2 assimilation limited by the potential rate of ribulose-1,5 bisphosphate regeneration, usually considered to be limited by the rate of electron transport J, Cc is the partial pressure of CO_2 at the sites of carboxlation in the chloroplast, Γ^* is the CO_2 compensation point in the light.

The derivate with respect to C_c is:

$$\frac{\delta A_J}{\delta C_c} = \frac{J}{4}\frac{3\Gamma^*}{[2\Gamma^* + C_c]^2} \qquad \text{eq.23}$$

Under the assumption that $C_i = C_c$ (Arneth et al. 2002) it is possible to substitute eq. 23 in eq. 20 can be expressed as a quadratic equation respect of C_i :

$$\left(\lambda - \frac{1.6D}{3\Gamma^*}\right)C_i^2 + \left(1.6D - 2C_a\lambda + \frac{1.6D\Gamma^*}{3\Gamma^*}\right)C_i + (\lambda C_a - 1.6D)C_a + \frac{1.6D\Gamma^{*2}}{3\Gamma^*} = 0 \qquad \text{eq.24}$$

The optimal C_i is given by a root of the quadratic $aC_i^2 + bC_i + c$.
where $a = 3\Gamma^* - L$, $b = 2\Gamma^*(L - 3C_a)$ and $c = L(2\Gamma^{*2} - 3C_a\Gamma^*) + 3C_a^2\Gamma^*$ and L represents the combination of terms (= 1.6 D / λ).

The discriminant $\Delta = b^2 - 4ac$, can be calculated to be:

$$\Delta = 12\Gamma^* L(C_a^2 + C_a\Gamma^* - C_a L + \Gamma^* L - 2\Gamma^2) \qquad \text{eq.25}$$

Under the assumption that $C_a >> \Gamma^*$, this expression simplifies to:

$$\Delta \approx 12\,\Gamma^{*} L\, C_a^{2}$$

eq.26

The solution to the quadratic equation leads to:

$$\frac{C_i}{C_a} \approx \frac{3\Gamma^{*} - \sqrt{3\Gamma^{*} L}}{3\Gamma^{*} - L}$$

eq.27

This expression can be simplified by completing the square in the denominator, giving:

$$\frac{C_i}{C_a} \approx \frac{\sqrt{3\Gamma^{*}}}{\sqrt{3\Gamma^{*}} + \sqrt{L}}$$

eq.28

Substituting in optimal C_i/C_a from equation to (Farquhar and Sharkey, 1982) and rearranging:

$$g_s \approx 1.6 \left(1 + \sqrt{\frac{3\Gamma^{*}\lambda}{1.6D}}\right)\frac{A}{C_a}$$

eq.29

This equation can then be re-written in a form that is analogous to the empirical models:

$$g_s \approx 1.6\left(1 + \frac{g_1}{\sqrt{D}}\right)\frac{A}{C_a} \quad g_s{}^{*} \approx 1.6\left(1 + \frac{g_1}{\sqrt{D}}\right)\frac{A}{C_a}$$

eq.30

Where the model parameter g_1 is given by the parameter combination $\sqrt{3\ \Gamma^{*}\lambda/1.6}$ and has units of $kPa^{0.5}$ The parameter g_1 is a species-specific parameter representing the sensitivity of the conductance to the assimilation rat*e that can readily be estimated by fitting the equation to data, yielding in turn an estimate of λ.*

The optimal stomatal conductance theory predicts that stomatal conductance should be zero when net photosynthesis is zero. However, there is accumulating evidence that stomatal conductance can be non-zero when photosynthesis is zero, including during the night. Therefore, an intercept term g0 can be added:

$$g_s \approx g_0 + 1.6\left(1 + \frac{g_1}{\sqrt{D}}\right)\frac{A}{C_a}$$

eq.31

The main assumption of this theory is that stomata are controlled mainly by RUBP regeneration than by carbon fixation rate. Medlyn et al., (2011) gave two main justifications for this procedure. The first one is that the guard cells have a significant capacity for electron transport and a low capacity for rubisco C fixation (Outlaw et al., 1979; Outlaw and De Vlieghere-He, 2001; Shimazaki, 1989). The second is that RuBP regeneration is the major limiting factor in leaves below light saturation and a co-limiting factor in light-saturated leaves (Farquhar et al., 1980; Woodrow, 1994).
Although such analytical approximations may be interpreted as a model limitation if compared to the numerical solution solving for both Ac and Aj (e.g. Baldocchi, 1994), it has been demonstrated (Bonan et al 2014, De kawe et al 2015) that model performance using the optimisation scheme is comparable to the original empirical stomatal conductance scheme (Ball et al., 1987) and less computationally intensive.

1.4 Ozone correction factors derivation

Since tropospheric ozone is considered a threat for forest ecosystems (Paoletti, 2007a), the lack of a specific parameterization of its impact on g_s may lead to estimation errors in simulating canopy gas exchanges (e.g. carbon sequestration, transpiration). Direct measurement of forests gas exchanges at ecosystem level can be performed by the eddy covariance (Aubinet et al., 2012). This technique has the advantage that fluxes of a target gas (i.e., CO_2, H_2O, or O_3) are recorded at ecosystem level and are therefore representative of an entire plant community in the footprint of an experimental tower (Fares et al., 2018). The disadvantages are the lack of a direct control on the environmental covariates influencing the ecosystem ecophysiological processes and that the measured overall ozone flux cannot be directly partitioned in its stomatal and non-stomatal sinks. Therefore, isolating the effect of ozone directly by ecosystem level measurements is not possible. However, correction factors accounting for plant response to ozone can be derived by manipulative experiments. To isolate the effect of ozone exposure by the natural occurring environmental changes structures such as Open Top Chambers (OTCs) or Free Air Concentration Enrichment (FACE) facilities are needed (Figure 4). Through these experimental structures it is possible grow plants in under close to natural conditions (Leadley et al., 1997), under different ozone fumigation treatments (e.g. ambient air ozone concentration, AA; charcoal filtered air CF, doubled ambient air ozone concentration AA*2), at different moisture availability by excluding drought stress (i.e. well-

watered treatment, WW) or by inducing it (e.g. WW*0.5) to evaluate if a cumulative response to both ozone and drought stress exists.
Leaf gas exchanges measurements, plant, stem, root growth, defoliation, ozone visible injuries are then evaluated during the experimental period for each treatment to evaluate the effect of ozone treatments on plant's ecophysiology compared to a control that was exposed to ambient or filtered air for the whole study (Macháčová, 2010; Paoletti et al., 2017).
As for ecosystem level measurements with eddy covariance, these methods have some limitations as the "chamber effect" that alters the chamber microclimate (Macháčová, 2010), the space limitations in OTCs that can affect plant growth (Uprety et al. 2006,Vanaja et al. 2006) and the age of the plants (often seedlings) that can affect a mature tree response. These limitation can be solved by FACE facilities, but the high cost limits their use.

Figure 4 - *Two examples of structure for manipulative experiments. On the left: Open Top Chambers (OTCs), Newcastle University (UK) Close House field station (Simon Fraser©). On the right: Free Air Concentration Enrichment facility (FACE), National Research Center (CNR), Sesto Fiorentino (Italy).*

1.4.1 Jarvis fO_3 multiplicative factor

Several studies were successfully achieved in deriving a g_{max} limiting factor *fO_3* for the Jarvis multiplicative algorithm for crops (Pleijel et al., 2002, Oue et al., 2008, Grüters et al., 1995; Danielsson et al., 2003). Hoshika *et al.* in 2012 and 2018 developed a *fO_3* for forests (i.e. *F. crenata, B. platyphylla* and *Q. mongolica)* representing the linear response of g_s to ozone concentrations observed under free-air conditions experiments (FACE). By identifying non-limiting g_s data (PPFD >500 µmol m^{-2} s^{-1}, VPD < 1.2 kPa) they estimated a potential g_{smax} value without ozone (0 nmol mol^{-1}) by extrapolating it from g_s data collected on plants exposed to ambient (ambient air ozone concentration) and at enhanced ambient ozone concentrations (ozone fumigated). This value was assumed to be the g_{smax} without any ozone effect. Finally, the extrapolation line between the g_s data and average hourly ozone concentrations of each ozone treatment over the experimental period was used to derive the ozone-induced stomatal closure response (*fO3*) (Figure 5). This approach has the advantage to be easy to apply, being related to a multiplicative model based on direct observation on dose-response relationships. A possible problem could be found in data availability, since these observations can be collected most easily with manipulative experiments on a limited number of species. A second point of weakness is the fact that this approach is based on ozone concentration rather than on ozone fluxes, and as previously discussed concentrations do not necessarily take into account the amount of ozone directly entering through stomata (Emberson et al., 2000).

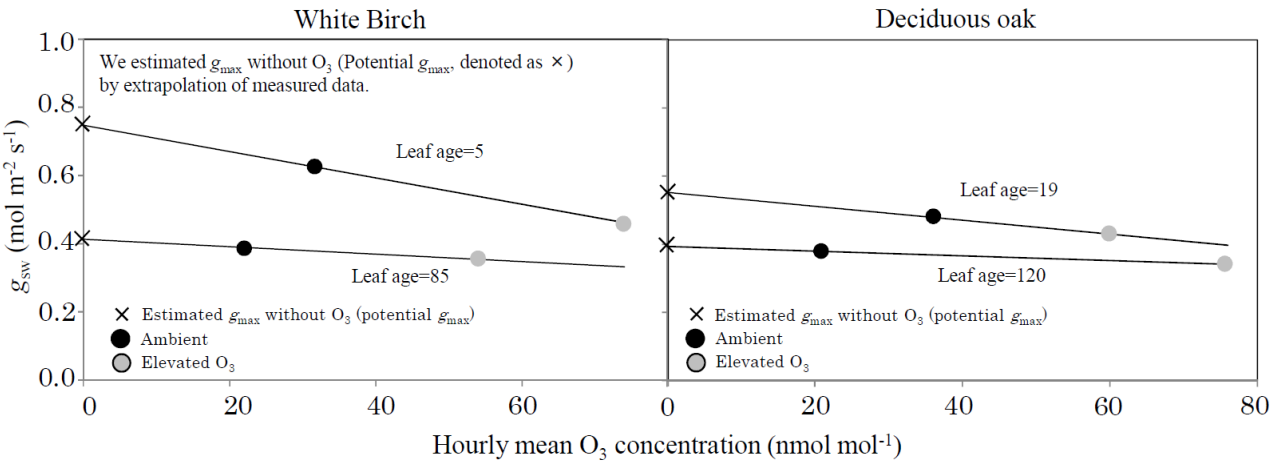

Figure 5 - Relationships between stomatal conductance (g_s) and hourly mean ozone concentration in white birch and deciduous oak. From Hoshika et al (2018)

1.4.2 BWB F_{pO3} and F_{cO3} correction factors

A flux-based approach was proposed by Lombardozzi *et al.* (2012, 2013 and 2015). This approach was developed to account for the decoupling effect between A_n and g_s observed under growing ozone exposure (Fares et al., 2018; Lombardozzi et al., 2012). This approach was developed to account for conditions that increase or decrease photosynthesis without changing g_s. Conditions that cannot be predicted by a direct dependence of stomatal conductance calculations on the photosynthetic rate. An example can be found in models using the Farquhar/Ball-Berry equations to predict ozone damage to photosynthesis with proportional responses in conductance (Felzer et al., 2007; Ollinger et al., 1997; Sitch et al., 2007). Indeed, the BWB model equation (eq. 11) clearly shows a direct linear dependence between g_s and A. Therefore, a reduction of A would proportionally affect g_s since the two parameters results to be inter-dependent (or coupled). If the response of g_s to ozone is independent of the response of A to ozone, this A-g_s dependence might lead to overestimate the ozone impact on g_s (or A) and may worsen when up-scaling from leaf to ecosystem/regional level (Lombardozzi et al., 2012). Since damages to carboxylation and stomata would change the ratio between water loss per carbon gain, Lombardozzi (2013, 2015) developed two independent multiplicative correction factors (F_{pO3} and F_{cO3}) for the BWB model representing the responses of A_n and g_s to the cumulative uptake of ozone (CUO) by retrieving data covering different plant functional types (PFTs) from literature studies. Since the impact of ozone on gs is

independent of the impact of ozone on A these corrections must be applied only after potential (uncorrected) A and g_s are simulated. The CUO is a metric used to standardize plant responses to chronic ozone exposure by integrating ozone flux into the leaf through time. Its calculation has two main limits: 1) it does not directly account for plant detoxification capacity, and 2) that plants exposed to high concentrations for short periods can have the same CUO to plants exposed to lower concentrations for longer periods (Lombardozzi et al., 2012). Regardless these limitations, stronger correlations between the CUO and photosynthesis (Reich, 1987; Wittig et al., 2007), biomass (Karlsson et al., 2004; Uddling et al., 2004) or relative crop yield (Pleijel et al., 2004, 2002), than metric based ozone concentration (Matyssek et al., 2007; Musselman and Massman, 1998; Reich, 1987; Wieser, 1997) were found. Cumulative uptake of ozone can be calculated multiplying the cumulative exposure to ozone (CEO_3), that is the cumulative ozone concentrations above 0 ppb over total exposure time, equivalent to AOT00 and SUM00 (Lombardozzi et al., 2012; Nunn et al., 2006; Reich, 1987; Wittig et al., 2007), to the mean leaf-level stomatal conductance to ozone, therefore obtaining a flux-based metric. The correction factors are then derived by the extrapolation line between the treatment to control ratio of both A_n (F_{pO3}) and g_s (F_{cO3}) and the calculated CUO (fig 6). This method modifies the optimal rates of A_n and g_s directly after they were calculated in the model, thus allowing to separate the response of g_s to ozone from the response of A_n to ozone and without altering photosynthesis calculations in the model (Lombardozzi et al., 2015).

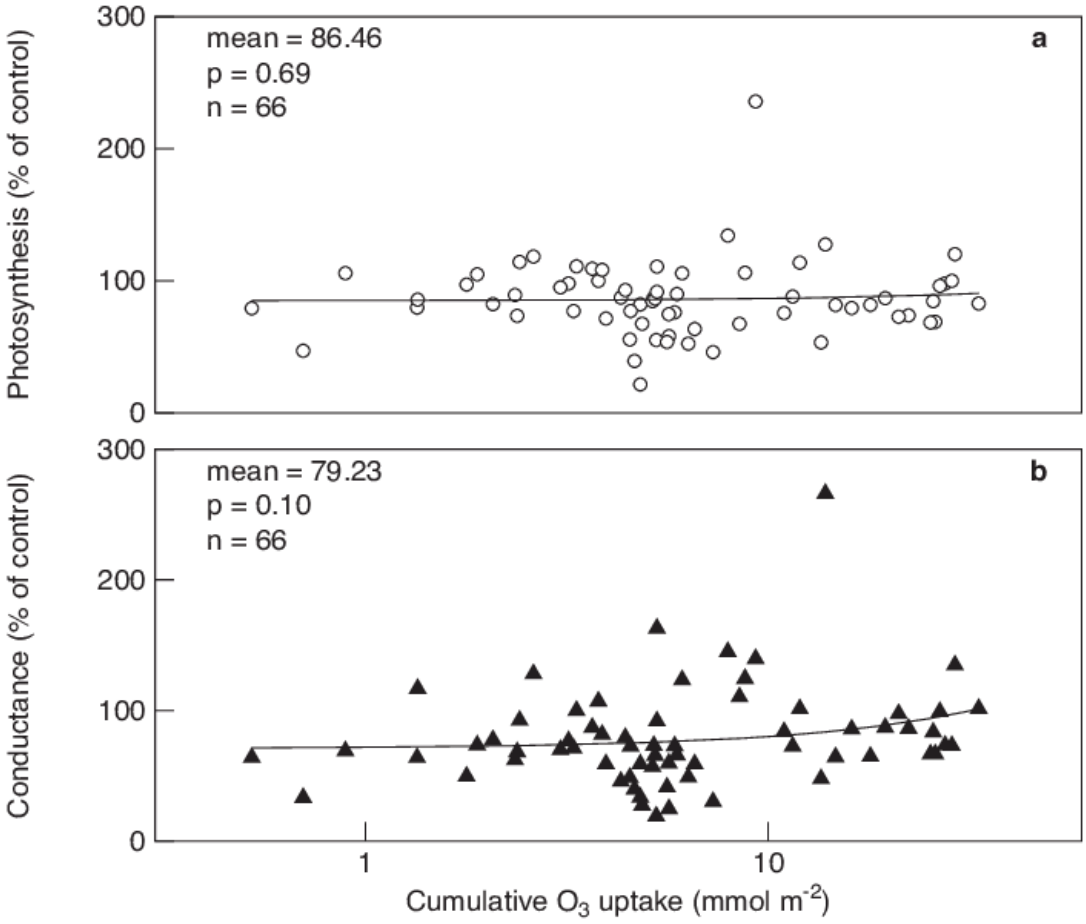

Fig. 6. *The correlation of photosynthesis (open symbols;* ***a****) and conductance (closed symbols;* ***b****) to CUO. Response values are reported as % of control (treatment/control). In this example on "high-confidence" data (CUO was presented in the publication) extracted from 11 studies, no correlations between CUO and photosynthesis or stomatal conductance were found. Figure from Lombardozzi et al., (2013).*

1.4.3 Ozone avoidance implementation for the optimization model

A modified functional form of the Medlyn optimal stomatal behaviour model was proposed by Hoshika et al. (2013c) to account for ozone stress avoidance by stomatal closure observed in a free air exposure experiment on *F. crenata*, and in a recent study (Hoshika et al., 2019) on *P. angustifolia, Q. ilex, Q. pubescens* and *Q. robur.* According to the optimal stomatal theory by Cowan (1978), Hoshika postulated that in addition to minimize water loss stomata act to minimize ozone flux.

The optimization can be expressed as:

$$\frac{\partial A}{\partial g_s} - \frac{1}{\lambda} \cdot \frac{\partial E}{\partial g_s} - \frac{1}{\lambda^{\circ}} \cdot \frac{\partial F_{\mathrm{st}}}{\partial g_s} = 0 \qquad \text{eq.32}$$

where λ^{o} is the marginal ozone damage of plant carbon gain (mol O_3 mol^{-1} CO_2) and F_{st} is stomatal ozone flux.

F_{st} is given by:

$$F_{\mathrm{st}} = \frac{g_s}{1.6}\left([O_3]_{\mathrm{air}} - [O_3]_{\mathrm{leaf}}\right) \qquad \text{eq.33}$$

where $[O_3]_{air}$ is the ambient ozone concentration, and $[O_3]_{leaf}$ is the ozone concentration inside the leaf, assumed to be approximately zero (e.g., Laisk et al. 1989; Omasa et al. 2011). The coefficient of 1.6 is the ratio of the diffusion coefficients for water vapor to ozone (Hicks et al., 1987).

Eq. 32 can be rewritten as:

$$\frac{\delta A}{\delta g_s} - \frac{1}{\lambda}\left(\frac{\delta E}{\delta g_s} + k\frac{\delta F_{st}}{\delta g_s}\right) = 0 \qquad \text{eq.34}$$

where k is the ratio of λ/λ^{o} (mol H_2O mol^{-1} O_3).
Therefore, λ can be given as:

$$\lambda = \frac{\frac{\delta E}{\delta g_s} + k\frac{\delta F_{st}}{\delta g_s}}{\frac{\delta A}{\delta g_s}} \qquad \text{eq.35}$$

Similarly, to $\delta E/\delta g_s$ and $\delta A/\delta g_s$ in Medlyn et al., (2011), according to the assumption of $[O_3]_{leaf} = 0$ (Laisk et al. 1989; Omasa et al. 2011), $\delta F_{st}/\delta g_s$ can be given as:

$$\frac{\delta F_{st}}{\delta g_s} = \frac{\delta\left(\frac{g_s}{1.6}\cdot\left([O_3]_{air} - [O_3]_{leaf}\right)\right)}{\delta g_s} = \frac{[O_3]_{air}}{1.6} \qquad \text{eq.36}$$

Therefore, λ in eq.19 can be rewritten as:

$$\lambda = \frac{\left(D+k\frac{[O_3]_{air}}{1.6}\right)\times\left(1.6+\frac{g_s}{\delta A/\delta C_i}\right)}{(C_a-C_i)} \qquad \text{eq.37}$$

Then, rearranging and substituting again with "A= (C_a-C_i)/1.6·r_s",

$$A = \frac{\delta A}{\delta C_i}\left[\frac{\lambda\cdot(C_a-C_i)^2-(C_a-C_i)(1.6D+k\cdot[O_3]_{air})}{1.6D+k\cdot[O_3]_{air}}\right] \qquad \text{eq.38}$$

Following Medlyn et al., (2011), an expression for A and "$\delta A/\delta C_i$" is given by the limitation of A by electron transport. Therefore, by merging eq. 22 and eq.23 into the eq. 38 :

$$\frac{J}{4}\cdot\frac{C_i-\Gamma^*}{2\Gamma^*-C_i} = \frac{J}{4}\cdot\frac{3\Gamma^*}{[2\Gamma^*+C_i]^2}\left[\frac{\lambda\cdot(C_a-C_i)^2-(C_a-C_i)(1.6D+k\cdot[O_3]_{air})}{1.6D+k\cdot[O_3]_{air}}\right] \qquad \text{eq.39}$$

If L=(1.6D+k[O_3] $_{air}$)/λ the quadratic functional form "$\alpha C_i^2+\beta C_i+\gamma=0$" is obtained. Solving the quadratic equation accordingly to Medlyn et al., (2011) leads to the final form:

$$g_s = g_0 + 1.6\left[1+\frac{g_1}{\sqrt{(D+(k/1.6)[O_3]_{air})}}\right]\frac{A}{C_a} \qquad \text{eq.40}$$

Where $g_1 = \sqrt{3\Gamma^*\lambda/1.6}$.

A point of weakness of the three above mentioned methods is that leaf gas-exchange measurements are taken on a limited number of individuals (often seedlings) and the resulting observations could be not representative of a whole mature ecosystem (Hendrey et al., 1999; Saxe et al., 1998).

1.5 The eddy covariance technique

The study of GHGs and air pollutants fluxes (O_3, CO_2, H_2O, and PM) at the ecosystem level requires high-resolution data. Fluxes, emissions and exchange rates can be accurately characterized starting from punctual measures, using fixed or movable flux towers, helicopters, planes etc. Eddy covariance (EC) is a micro-meteorological technique that have long been applied to measure mass and energy fluxes between forest ecosystems and the atmosphere (Figure 7). The advantage is

that fluxes of targeted gases (i.e., water vapor or ozone) are recorded at ecosystem level and are therefore representative of an entire plant community in the footprint of an experimental tower. EC produces advantageously continuous and long-term measurements, provided the terrain is rather homogeneous. Measurements took place in the surface layer, 10 m (up to 50 m in case of unstable stratification) above the earth's surface. Inside this layer, the atmospheric turbulence is the dominant transport mechanism. The EC technique implies that a field site should be equipped with a three-dimensional sonic anemometer to measure wind velocity and sonic virtual temperature fluctuations at high frequency (conventionally 10 Hz, sample interval of 0.1 s). The anemometer should be mounted next to the inlet of sampling line or right next to an open path sensor (i.e. infrared gas analyser, IRGA). In a typical configuration, air is sampled continuously at one inlet through Teflon tubes located near the sonic anemometer. In the last decades, several models of fast ozone sensors have been developed, mostly through chemiluminescence and using coumarin dyes. The chemiluminescence detectors are calibrated against average ozone concentrations from a UV ozone monitor and correlated with vertical wind velocity, according to EC methodologies extensively described in Aubinet et al. (2012). In this technique a variable, a scalar (x) (usually gas concentration, temperature or momentum) or wind component (u, v, or w), is decomposed into its mean ($\bar{x}$) and its fluctuating component (x'). The vertical flux is calculated as the covariance of x' and vertical wind velocity. Positive fluxes indicate gas release to the atmosphere while negative fluxes indicate uptake from the atmosphere:

$$F_x = \overline{x' w'} \qquad \text{eq.41}$$

where F is any flux measured with EC, w is the vertical wind velocity, and c the concentration of the gas at the measurement height. The prime indicates deviations from the 30-min means threshold, and the overbar indicates a time average.

Measurements of quality assurances are needed to obtain reliable data. A number of processing routines are ultimately needed to compute fluxes, that is, identifying the time lag for sampling and instrument response by maximizing the covariance between vertical wind velocity (w') and scalar (x') fluctuations. Several methods are applied to correct for errors due to sensor separation and damping of high-frequency eddies, rotation of wind-related data, and selection of quality data after filtering for turbulence levels below thresholds considered valid for EC application (Aubinet et al., 2012). The eddy covariance technique directly measures the net ecosystem

exchange (NEE) of CO_2 and λE. In this study, Gross Primary Production (GPP) rather than NEE (Net Ecosystem Exchange - NEE) was assumed to be representative of the forest photosynthesis, since GPP is in theory the closest metric to express photosynthesis at the canopy level with Eddy Covariance data not accounted for ecosystem respiratory processes (Fares et al. 2013a). Although GPP is not directly measured, it can be derived by applying different post-processing methods. Further details can be found in Lasslop et al. (2010). Since GPP is derived from a model, its estimation carries some uncertainties, which however do not exceed 10% (as highlighted in a comparison of different methods of estimation) (Desai et al. 2008).

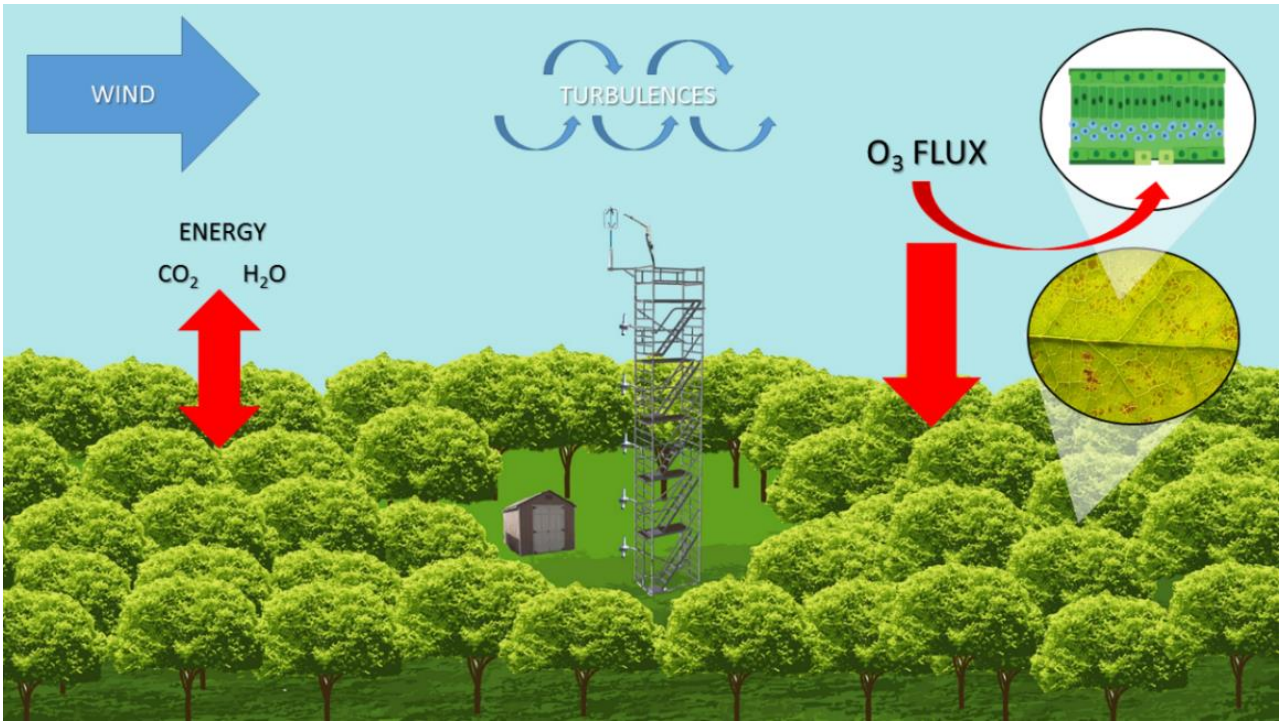

Figure 7 - View of a typical eddy covariance tower. equipped with fast sensors (i.e. a 3D sonic anemometer coupled to a gas analyzer) for ozone flux measurement. The air flow (on the top) is represented as an horizontal flow (wind) of numerous rotating eddies (turbulences). Exchanges of energy and gases is us represented by red arrows. The snapshot of single leaves shows ozone penetrating stomata (ozone dry deposition) and causing oxidative damage in the form of visual necrotic spots.

1.6 Multi-layer canopy models

To test these leaf-level relationships to the ecosystem scale, corresponding ecosystem level estimates of An and transpiration in a bottom-up approach are needed. This approach is intrinsic to multi-layer canopy models. These models combine models of penetration of light with models to resolve energy balance in the canopy based on leaf-level photosynthesis, and models of gas/energy transport within the canopy (Lowman and Rinker, 2004). Canopy photosynthesis (gross primary productivity GPP), and transpiration (latent heat, λE) and other gas exchanges are calculated by integrating fluxes resulting from various components (e.g. soil, understory, crown) that interact with their specific microclimate (e.g. profiles of light, humidity and temperature) (Journet and Etherington, 2006). A variety of multilayer models differing in spatial (i.e. local, regional and global model) and temporal resolution are

actually available. In function of their final scope and data availability, different approaches to simulate g_s and A_n are used. In this work the FORCAsT model (Ashworth et al., 2016, 2015), developed to study the chemistry and transport of volatile organic compounds (VOCs) and their oxidation products in the atmosphere within and above the forest canopy, and the recently published AIRTREE model (Fares et al., 2019), developed to study forest ecosystem services such as ozone and PM deposition, were used. In both these models, the incoming solar radiation is reflected, transmitted and absorbed depending on the canopy structure. The canopy architecture is constructed during the initialization routines within both FORCAsT and AIRTREE models. The canopy can be divided into a variable number of layers (up to 10) between the trunk level and the top of the canopy, and characterised by different leaf angle classes and by both sunlit and shaded leaves. The light extinction within the canopy is the results of an exponential attenuation (e.g. Beer's law) by foliage at each layer (i.e. Leaf Area Index, LAI) calculated at each model time step. As radiation and temperature decay through the canopy layers, leaf level ecophysiological processes variate between layers and angle classes within a single layer. Dry deposition of particles and gases on leaves is calculated at all models' levels by following resistance schemes and is dependent on the individual resistances of in-canopy aerodynamic resistance (R_a), soil resistance (R_g), quasi-laminar boundary layer resistance (R_b), mesophyll (R_m), cuticular (R_{cut}) and stomatal resistance (R_{st}). Stomatal resistance is therefore calculated according to the canopy environment at each time step, for each leaf angle class in each canopy layer it. In FORCAsT stomatal resistance (R_{st}) is needed also to simulate BVOCs emission and ozone deposition and is calculated accordingly to the Jarvis multiplicative algorithm. Conversely, the AIRTREE model needs g_s ($g_s=1/R_{st}$) to simulate both gross primary productivity (GPP) and ozone deposition, thus using a photosynthesis sub-model based on the analytical solution of the coupled BWB A-g_s model proposed by Baldocchi (1994).

The simulation of stomatal conductance provides the potential to estimate the flux of any gaseous species into the vegetation and therefore the damage to plant cells due to the uptake of ozone. Stomatal ozone fluxes were calculated by multiplying ozone concentration at the leaf level (see methods shown in Gerosa et al. 2005 and Fares et al. 2018) by stomatal conductance to ozone. By considering their scopes, the implementation of ozone corrections could represent a significant improvement for both these models, leading to a more accurate simulation of the stomatal ozone dose

entering into the stomata, emission of BVOCs, sequestration of carbon and loss of water.

1.7 Thesis objectives and structure

In the previous paragraphs the role of ozone for the health of Mediterranean forest ecosystems was defined. It is important to identify and/or improve proper metrics (e.g. PODY) for ozone risk assessment.
In this work meteorological variables, biometric data and leaf level gas exchange measurements have been used to parametrize two multi-layer canopy models. These models were implemented with specific formulations for the quantification of ozone impact on plant's ecophysiological processes. Fluxes of carbon and water measured through the eddy covariance technique have been used to calibrate and validate the models' output and finally quantify the impact of ozone on forests' ecophysiological processes (Figure 8).

In this study, formulations to quantify ozone damage in plants' ecophysiological processes were derived by manipulative experiments under controlled conditions. However, in natural condition ozone stress occurs simultaneously with other stressors (e.g. drought stress). Since plants can use the same response mechanism to different stressors (i.e. avoidance of ozone and drought stress by stomatal control) the impact of ozone alone would result to be difficult to quantify. Therefore, a first question can be formulated:

A) Can a multi-layer canopy model parameterized with a relatively small set of environmental input variables (e.g. RH, Tair, PAR, Precipitation, SWC, air pressure) estimate reductions in carbon assimilation due to ozone dose/exposure?

If so, the impact of this gas on carbon sequestration should be different depending on the species-specific strategies to face ozone stress (i.e. avoidance) and their level of sensitivity to ozone (i.e. tolerance). Therefore, while in an ozone sensitive species the impact of ozone is expected to have an impact up to 30% (Sitch et al., 2007), low or no reduction might be observed in ozone tolerant species. For the latter case, a model implementation would be useless. Consequently, a second scientific question is:

B) Is it possible to define a threshold of phytotoxic ozone dose for trees with known differences in ozone sensitivity?

In order to find the answer to these scientific questions this PhD work will pursue two main objectives: (1) to evaluate which model parameterization best fits the observations in simulating the ecophysiology of the studied ecosystems and (2) to propose possible improvements to metrics for ozone risk assessment based on phytotoxic ozone dose (amount of ozone entering stomata).

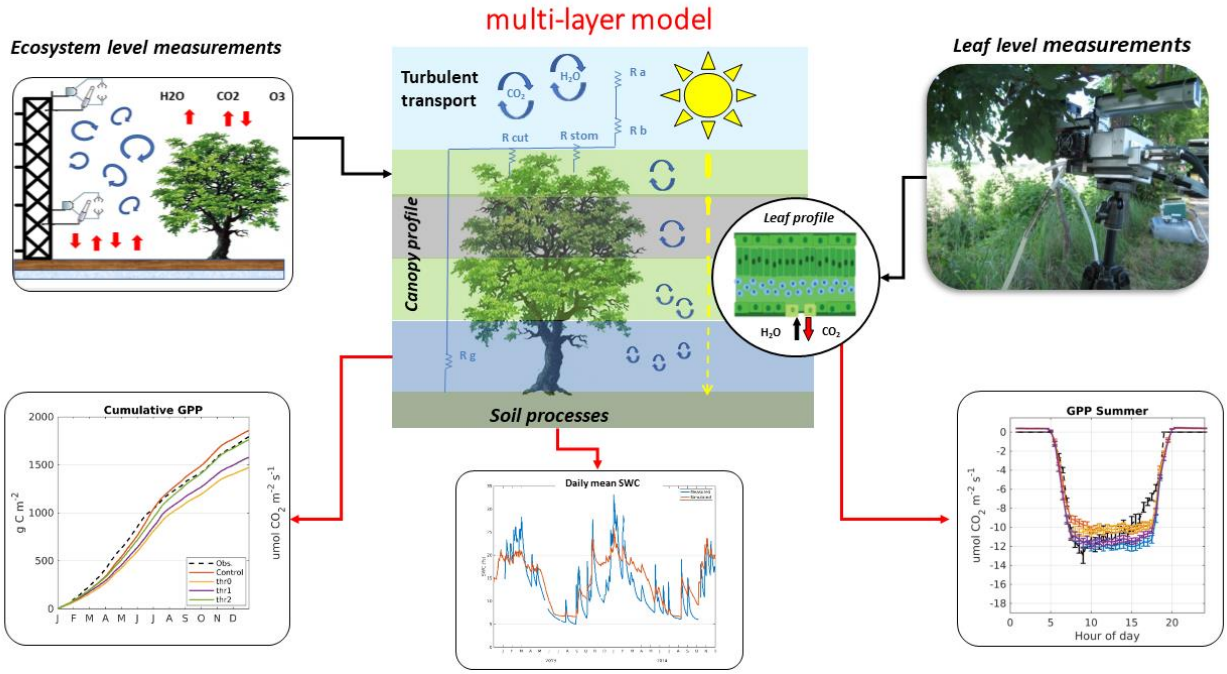

Figure 8 – Description of a multi-layer model. Ecosystem level measurements of fluxes and meteorological data and leaf level gas exchange measurements (black lines) are used as model input, the model then computes output fluxes at each layer, that can be integrated to the canopy level (red arrows) l.

2. Materials and Method

2.1 Sites Description

2.1.1 Castelporziano (IT-Cp2)

The presidential Estate of Castelporziano represents a hotspot for biodiversity in the Mediterranean area, which hosted more than 1000 plants species (Davison et al., 2009). It is a protected area of about 4800 ha, of which 85% are forests. It is located on the coast of the Tyrrhenian sea, 25 km from Rome downtown (Figure 9). The study site (hereafter named CPZ), named Grotta di Piastra (Fluxnet code IT-Cp2), is located in a wild coastal rear dune ecosystem within the estate, 1.5 km from the seashore (41°70'42''N, 12°35'72''E).
The vegetation is covered almost prevalently by a 64 years old even-aged (Romane & Terrada 2013) evergreen holm oak forest (*Quercus ilex* L). The forest main height was 14 m and the Leaf Area Index (LAI) was 3.69 m^2 leaf m^{-2} ground, measured using a LAI 2000 instrument (Li-Cor, USA). The understory vegetation is poorly developed and formed prevalently by small shrubs of mock privet (*Phillyrea latifolia* L.). Soil has a flat topography, with a sandy texture (84% sand, 14 % silt, 3% clay), and low water-holding capacity.

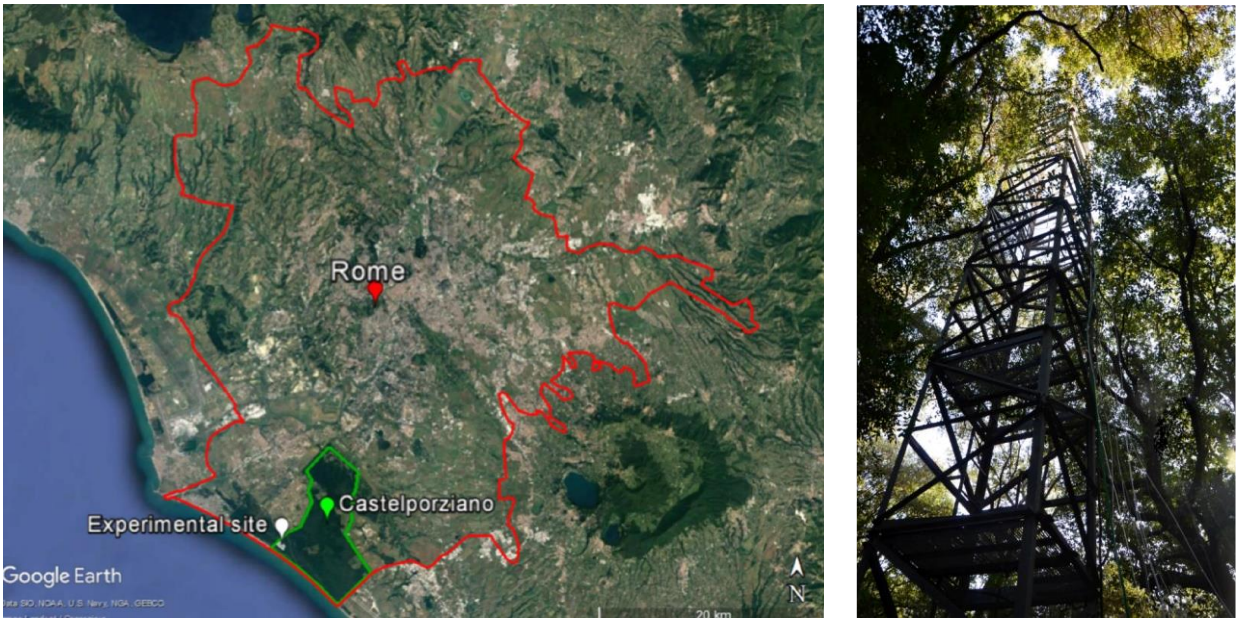

Figure 9 - The figure shows (on the left) the location of the IT-Cp2 experimental site (white sign) in the Castelporziano natural reserve (in green), within the area of Rome (in red) and (on the right) the IT-Cp2 EC flux tower into the Grotta di Piastra holm oak forest.

Wind circulation followed a sea-land breeze regime, the dominant wind direction is S-SW during the morning and N-NE during the afternoon (Figure 12). The site is characterized by the typical Mediterranean climate, with pronounced seasonality. Summer is hot and dry and Winters are moderately cold. Precipitation occurs prevalently during Spring and Autumn. Mean annual precipitation are around 700-800 mm y^{-1} and mean monthly temperatures, averaged over the same period, range between 7 °C and 24 °C (Figure 11). The site can experience high Summer levels of tropospheric ozone up to 90 ppb (Fares et al., 2014). Air temperature, precipitation, relative humidity, net solar radiation, wind direction, soil humidity and soil temperature were recorded every minute and averaged for 30 min intervals with a Davis vantage pro meteorological station (Davis Instruments Corp. CA, USA). For more details on the site and meteorology see Fares et al. (2014). The fluxes continuous measurements started in 2012 and measurements are still ongoing. Flux measurement equipment was installed on 20 m scaffold tower. Tridimensional sonic anemometer (GILL HS-50) was used to measure instantaneous wind speed and temperature fluctuations. H_2O and CO_2 concentrations were measured with an infrared gas analyzer (Licor LI-7200). Data were recorded at 10 Hz for all trace gases. Castelporziano is included in the Long-Term Ecosystem Research network (LTER – Italy), furthermore, as an EC site is part of the Fluxnet and ICOS international networks.

2.1.2 Blodgett Forest (US-Blo)

The Blodgett Ameriflux site (Fluxnet code US-Blo) is located at 1315 m above sea level in the Sierra Nevada Mountains of California, USA, near Georgetown (38°53’42.9’’ N 120°37’57.9’’ W). Trees were planted in 1990 at a density of 1300 trees/ha, and underwent a precommercial thinning in 2000, removing 60% of the trees and cutting back all the shrubs. The dominant tree species is ponderosa pine (*P. ponderosa L.*), an ozone sensitive species (Anderson et al., 2001; Coyne and Bingham, 1982). The major understory shrubs are *Arctostaphylos manzanita* (Mazanita) and *Ceonothus cordulatus* (Ceanothus). The total LAI increased from 1.2 in 2001 to 2.9 in 2006, with a mean height increasing from 4 m to 7.6 m during the same period. The soil has 60% sand, 11% clay and 29% loam. The site is characterized by a Mediterranean climate, with warm dry Summers and cold wet Winters, and with a typical mountain wind regime bringing daytime air up the mountain slopes from the nearby Sacramento valley urban area, while at night a

gentle downslope wind reverses the direction (Figure 12). Air temperature and vapour pressure deficit (VPD) followed similar annual patterns across the years, with the higher values during Spring and Summer, and large sub-weekly variation due to the passage of weather fronts. Annual precipitations are around 800-900 mm, and are concentrated almost exclusively in Spring and Winter with low precipitations in Fall, and total absence of precipitation in Summer except for 2003 and 2004 (38 mm and 22 mm, respectively) which were the years used in this study (Figure 11). Also this site experiences Summer levels of tropospheric ozone above 100 ppb, as described in detail by Fares et al. (2010b).

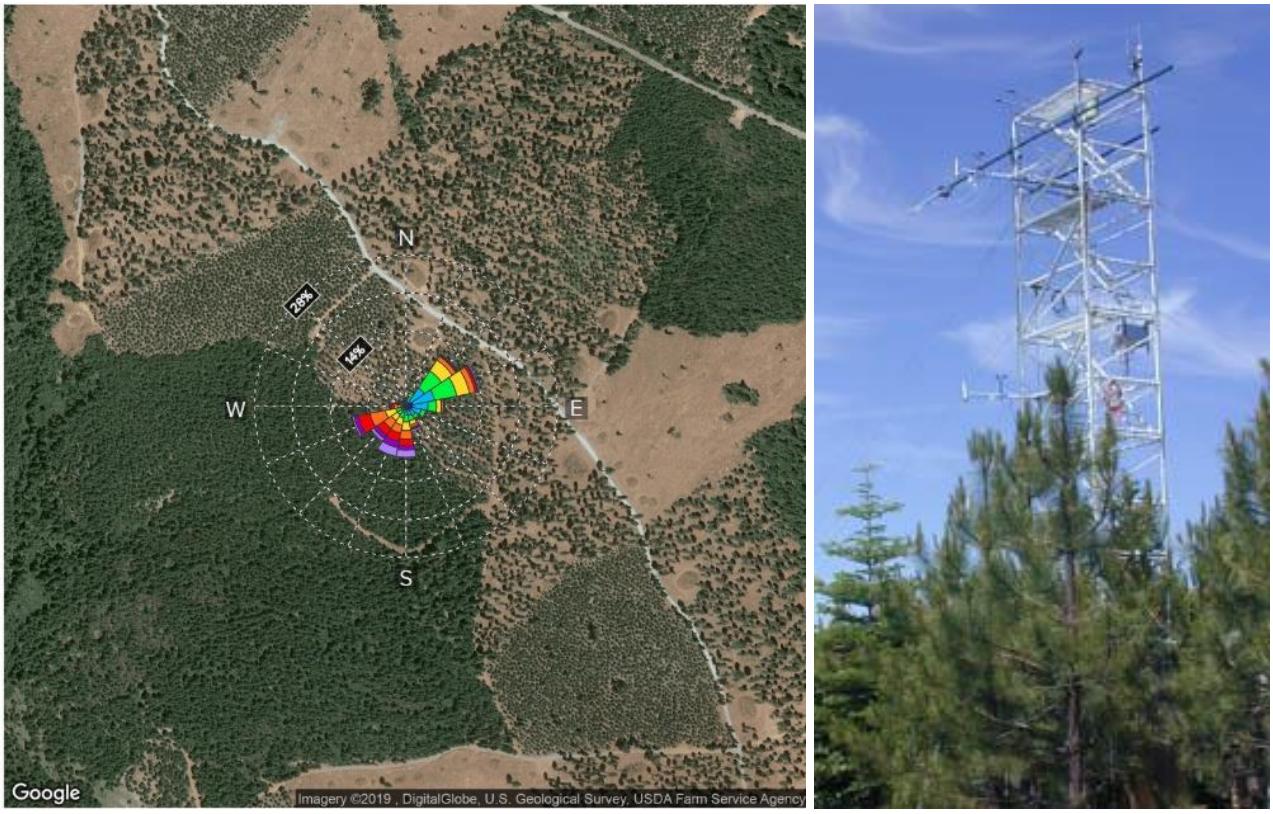

Figure 10 - The figure shows (on the left) the annual wind rose of the US-Blo experimental site in the Sierra Nevada Mountains, and (on the right) the US-Blo EC flux tower above the Ponderosa pine forest.

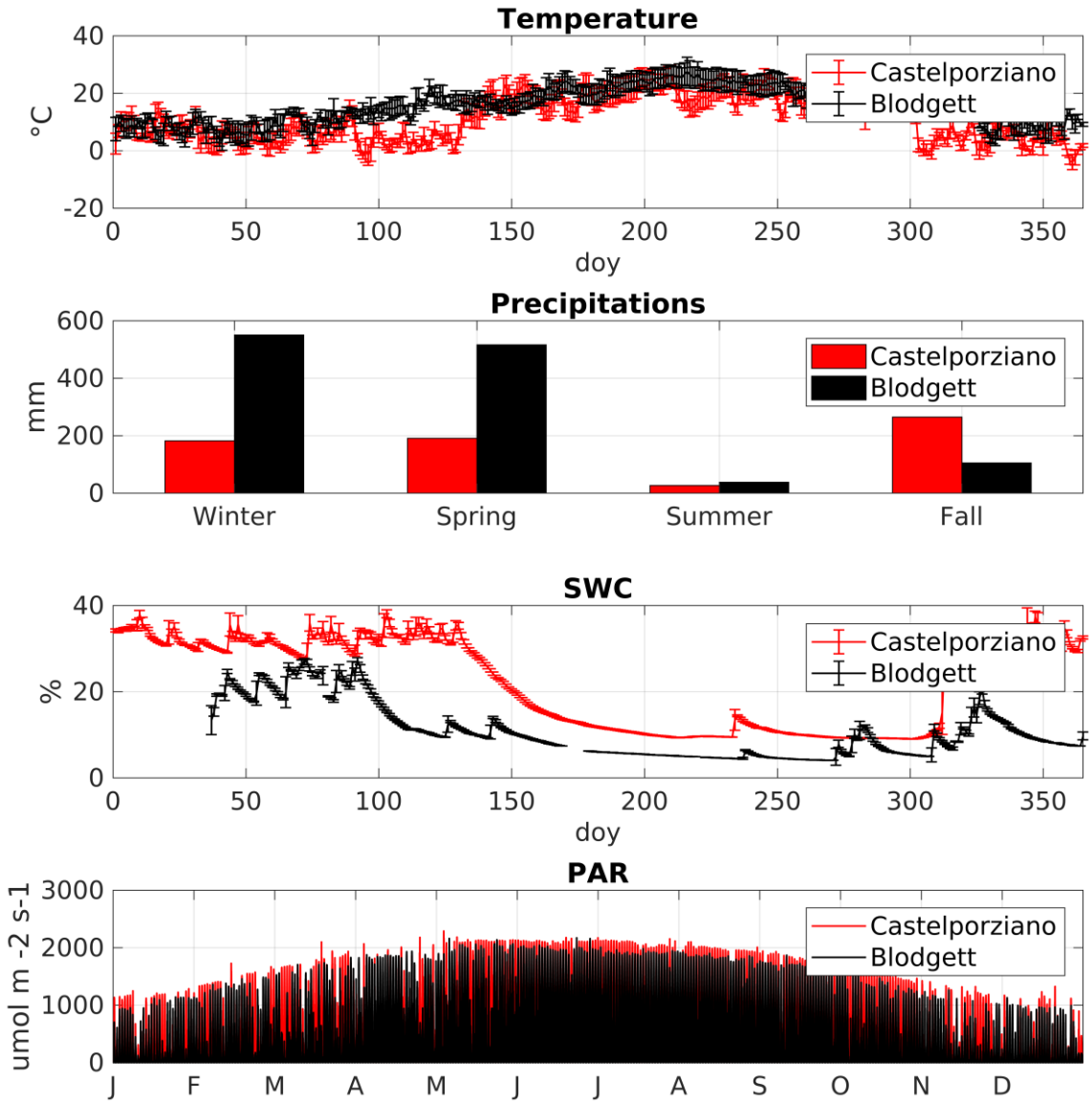

Figure 11 - The figure shows the sites' climatic characteristics. Average temperatures (in the top), cumulative seasonal precipitations (in the middle), daily mean soil water content (SWC) measured at 10 cm of depth (in the bottom) and photosynthetic active radiation (PAR) for the year 2013 and 2003 collected in Castelporziano (in black) and Blodgett (in red) sites, respectively.

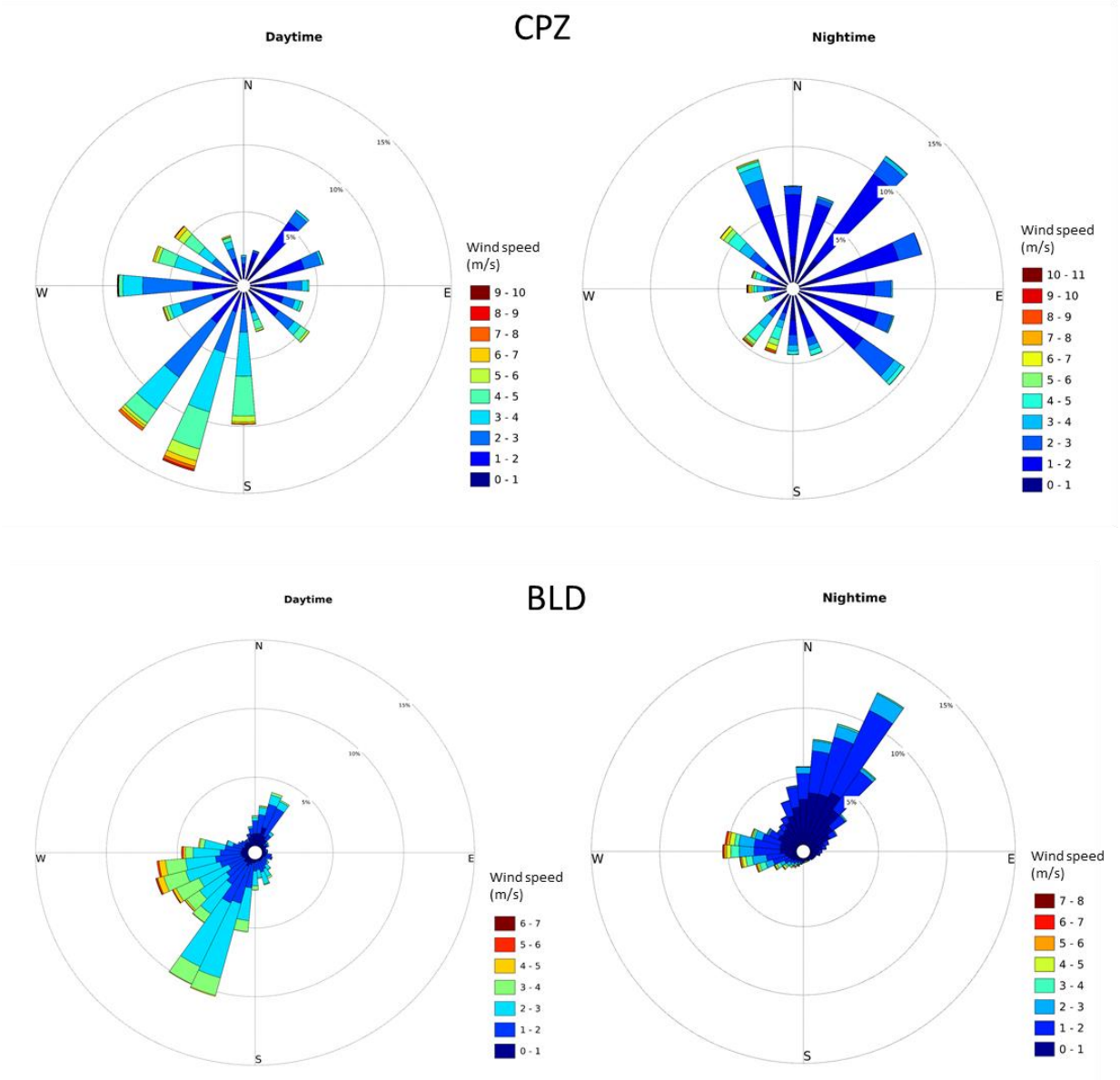

Figure 12 – Wind rose plots of two study sites. On the top: Castelporziano wind regime, during the day (left) wind blows from SW (from the sea) while during the night (right) wind blows from N-NE (the city of Rome). On the bottom: Blodgett wind regime, during the day (left) wind blows upslope from SW (from the city of Sacramento) while during the night (right) wind blows downslope in the opposite direction (N-NE).

2.2 The FORCAsT Model

The FORest Canopy Atmosphere Transfer (FORCAsT) model is a single column (1-D) model that incorporates atmospheric chemistry and dynamics and land surface modelling to study the emission, deposition, chemistry and transport of volatile organic compounds (VOCs) and their oxidation products in the atmosphere within and above the forest canopy (Figure 13). FORCAsT is based on the Canopy Atmospheric CHemistry Emission (CACHE) model (Bryan et al., 2012; Forkel et al., 2006), updated with the gas phase chemistry scheme CACM (Caltech Atmospheric Chemistry Mechanism, Chen and Griffin 2005; Griffin et al. 2002, 2005), and the aerosol module MPMPO (Model to Predict the Multiphase Partitioning of Organics, Chen and Griffin 2005; Griffin et al. 2003, 2005). Energy balances and radiative transfer within the canopy are calculated accordingly to the CUPID soil–plant-atmosphere model (Norman, 1979; Norman and Campbell, 1983). The default model vertical resolution is of 40 vertical layers the (half of them are in the vegetation canopy space) from the land surface to a maximum height set by the user. The lower level of the column represents the soil, where soil heat and moisture storage and transfer to the atmosphere are computed (Forkel et al., 2006). The canopy levels are further sub-divided into a trunk space and crown space which height, canopy shape, leaf angle distribution, leaf area index (LAI), and the fraction of the total LAI in each canopy layer are user defined. The transfer of radiation is simulated through the canopy, thus providing leaf temperatures, latent and sensible heat fluxes for both sunlit and shaded foliage at each canopy level. The incoming solar radiation (provided by user as a model input variable) is divided between visible (0.4– 0.7 μm), near-infrared (0.7–4 μm) and the thermal radiation (4–100 μm). The reflection, transmission and absorption of all incoming radiation and the total back-scattered or up-welling radiation are dependent on the canopy structure and the angle of the leaves relative to the incident radiation. The incoming solar radiation is further divided into direct and diffuse radiation based on the proportion of back-scattered radiation. The model considers nine angle classes for sunlit leaves that receive components of both direct and diffuse radiation, and designates an additional class to the shaded leaves within each layer receive only diffuse radiation. The light attenuation within the canopy is based on Beer's law and of the absorption of thermal radiation at each model time step. The radiation that penetrates to lower canopy layer decays due to shading from leaves in the layers above. Therefore, the biogenic emissions, driven by radiation and leaf temperature change among layers and angle classes even within a single layer. This full multi-level representation of vegetation

structure affects also the processes governing deposition rates. The model simulates gases and particles dry deposition on vegetation following the resistance scheme (Gao et al. 1993; Meyers and Baldocchi 1988; Wesely 1989).

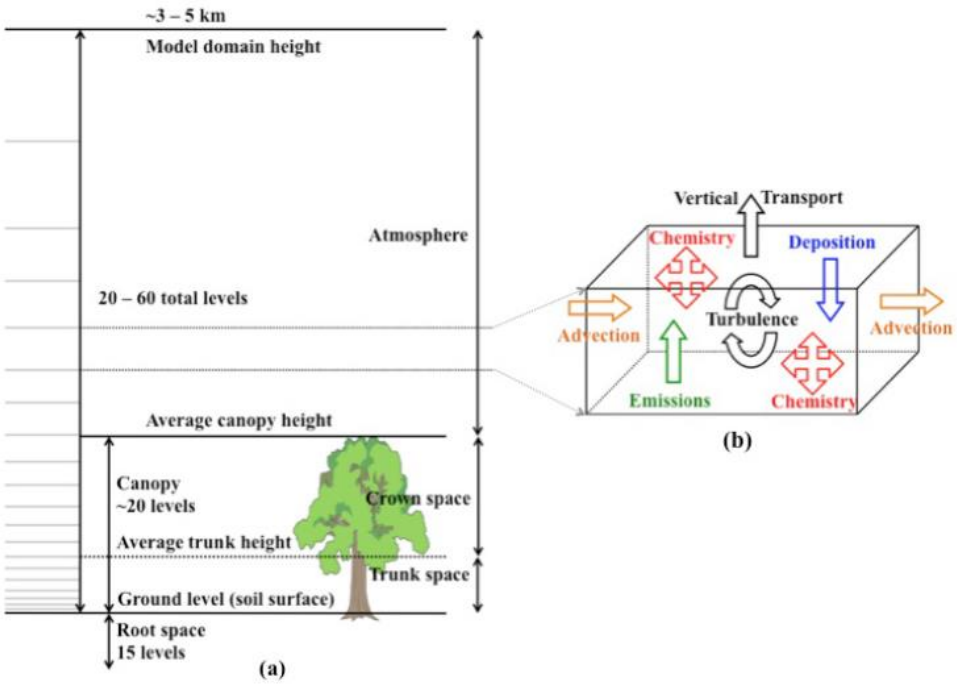

Figure 13 – (a) schematic of the FORCAsT column model. Each level within the column is a box model (b) incorporating the processes involved in canopy–atmosphere exchange of energy and mass appropriate for that level (form Ashworth et al. 2015)

Leaf resistance is dependent on the individual resistances of the quasi-laminar boundary layer at the leaf surface, the mesophyll and cuticular resistances, and stomatal resistance. The soil resistance is modelled after Gao et al. (1993). And calculated at each time step based on the temperature and soil moisture profile at that time. Stomatal conductance is calculated at each time step for each leaf angle class, in each canopy layer according to the canopy environment, accounting for changes in temperature, light levels above and within the canopy, and vapor pressure deficit by the Jarvis (1976) multiplicative algorithm. Deposition velocities of gases and particles are calculated by FORCAsT before being passed to the chemistry scheme, where they are included as a loss term in the computation of reaction rates. As the simulation of stomatal conductance within FORCAsT occurs on-line, this provides the potential to estimate the flux of any species into the vegetation, allowing simulation of damage to plant cells due to the uptake of powerful oxidizing agents such as ozone.

Since the aim of this study was to evaluate ozone impact on simulated stomatal conductance and consequently on GPP and λE the chemistry and the advection modules were deactivated and measured ozone concentrations were directly used as input for the model Table 1.

Table 1 - *list of the continuous environmental variable needed by the FORCAsT model in this study.*

Variable	***Description***	***Unit measure***
PPFD	Photon flux density	μmol m^{-2} s^{-1}
Press	Atmospheric pressure	Pa
RH	Relative humidity	%
SWC	Soil water content	%
Tsoil	Soil temperature	C°
Tair	Air temperature	C°
O_3	Ozone concentration	ppb
CO_2	CO_2 concentration	ppm
u*	Friction velocity	m s^{-1}
ubar	Surface wind speed	m s^{-1}
sigmaw	Std. dev. of wind vertical component	m s-1

Heat and water vapor balance of the air in the canopy space is expressed by the transient heat conduction equations, accordingly to Norman (1982):

$$\frac{\varepsilon\rho}{p}\cdot\frac{\delta e}{\delta t}=\frac{d}{\delta z}\left(\frac{\varepsilon k(z)\delta e}{c_p\, p\, \delta z}\right)+Q_E \qquad \text{eq.42}$$

$$\rho c_p\cdot\frac{\delta T}{\delta t}=\frac{d}{\delta z}\left(K(z)\frac{\delta T}{\delta z}\right)+Q_H \qquad \text{eq.43}$$

Where T and e are temperature and water vapor pressure of air respectively, K(z) is the eddy thermal conductivity (J m^{-1} s^{-1} $°C^{-1}$) and $\varepsilon K(z)/(c_p p)$ is the eddy conductivity for water vapor (Kg m^{-1} s^{-1} Pa^{-1})), Q_H (W m^{-3}) and Q_E is the source or sink of heat

respectively water vapor. Q_H and Q_E are derived from the leaf energy balance equation.

Leaf energy and water balance equations for each leaf angle class in each layer are solved simultaneously. Canopy photosynthesis (GPP), and latent heat (λE) results from the integration of fluxes resulting from each layer. Since this work is not focused on the model capability to simulate atmospheric chemistry and the advection of pollutants and ozone precursor, the description of these modules is not here reported, further details can be found in Ashworth et al. (2015).

2.3 The AIRTREE model

The Aggregated Interpretation of the Energy balance and water dynamics for Ecosystem services assessment (AIRTREE) model, is a one-dimensional multi-layer model that couples soil, plant and atmospheric processes to predict exchanges of CO_2, water, ozone, and particulate matter (PM) between leaves and the atmosphere.

The AIRTREE model is constituted by four different modules (see figure 8):

1) The radiative transfer model, which calculates leaf temperature and the radiation through canopy.

2) The photosynthesis module, that calculates A_n and g_s.

3) The deposition module, which calculates resistances to gas diffusion and deposition of gases and pollutants.

4) The hydrological model, which predicts the ecosystem hydrological status.

The model requires a limited number of input variables (Table 2) to estimate individual leaf gas exchanges and integrate fluxes through five layers to obtain fluxes (e.g. GPP, λE, PM, O_3) at the canopy level. The model incorporates a canopy environmental module to determine the leaf temperature (T_l), stomatal conductance, and radiative transfers at different levels from the top to the bottom of the canopy. Since T_l and g_s influence the photosynthesis and the gas exchanges with the atmosphere, they are calculated iteratively by coupling an energy conservation equation (Goudriaan and Van Laar, 1994) with photosynthesis (Müller et al., 2008), under the assumption that the energy balance affects A_n and the T_l and that A_n and gs affect the latent heat in the energy balance. The leaf photosynthetic rate (A_n) is calculated from the minimum value between the carboxylation rate when ribulose

bisphosphate (RuBP) carboxylase/oxygenase is saturated (W_c) and carboxylation rate when RuBP regeneration is limited by electron transport (Wj). AIRTREE uses the analytical solution proposed by Baldocchi (1994) to calculate *A and* g_s, by coupling the FVcB-BWB model (eq. 11). Drought limitation to photosynthesis and g_s was modelled as piece-wise linear function of soil water content (W_{fac}) multiplied by *A*, as reported by Keenan et al. (2010).

$$W_{fac} = \begin{cases} 1, & if\ \Theta \geq \Theta max \\ \left[\frac{\Theta - \Theta min}{\Theta max - \Theta min}\right]^q, & if \Theta < \Theta max \end{cases} \qquad \text{eq. 44}$$

where Θ is volumetric soil water content, Θmax is the relative soil water content for the 4.5 m soil column at which reductions are first evident, Θmin is the wilting point, and q is a measure of the non-linearity of the effects of soil water stress on physiological processes.

Finally, *A* and g_s for the whole canopy were obtained by integrating values calculated for each layer according to the fraction of sunlight and shaded leaf area. Deposition on vegetation surfaces is calculated through a resistance scheme. The canopy resistance was calculated as proposed by Zhang et al. (2002).

$$\frac{1}{Rc} = \frac{1 - W_{st}}{R_{st} + R_m} + \frac{1}{R_{ac} + R_g} + \frac{1}{R_{cut}}; \qquad \text{eq. 45}$$

where W_{st} is the fraction of stomatal blocking under wet conditions (equal to 0 for dry conditions); R_{st} is the stomatal resistance (inverse of stomatal conductance to O_3), R_m is the mesophyll resistance (10 s m^{-1}), R_a and R_g are in-canopy aerodynamic resistance and soil resistances, respectively, and R_{cut} is the cuticular resistance estimated according to Erisman et al. (1994), Zhang et al. (2002) and Mészáros et al. (2009).

Ozone fluxes resulted from the integration of each layer contribution. The total fluxes were calculated as the product between the measured concentration and the velocity of deposition (V_d) for each canopy level (see methods in Gerosa et al., 2005).

$$V_d = \frac{1}{R_a + R_b + R_c}; \qquad \text{eq. 46}$$

Where R_a is aereodynamic resistance, calculated at each layer elevation accordingly to Killus et al., (1984), and R_b is quasi-laminar boundary layer resistance (R_b) was calculated as suggested by Hicks et al. (1987). The formalism to explain resistances is detailed in Fares et al. (2019).

The sensible (H) and latent (λE) heat fluxes inside each canopy layer from the leaves to the atmosphere are computed as (Lhomme, 1988):

$$H = \rho c_p g e_c (T_l - T_a) \quad \text{eq.47}$$

$$\lambda E = \left(\frac{\rho c_p}{\gamma}\right) g e_v (e_s - e_a) \quad \text{eq.48}$$

Where ρ is the air density, c_p is the specific heat of air at constant pressure, ge_c is the equivalent conductance for horizontal heat transfer, Tl is the leaf temperature, Ta is the air temperature, γ is the psychrometric constant, ge_v is the equivalent conductance for horizontal vapour transfer, e_s is the saturated vapour pressure at leaf temperature, e_a is the air water vapour pressure.

These variables are calculated iteratively by coupling the energy conservation equation (Goudriaan and Van Laar, 1994) with the photosynthesis process (Müller et al., 2008) under the assumption that the energy balance affects photosynthesis and the leaf temperature, while the photosynthesis and stomatal conductance affect the latent heat in the energy balance.
The hydrological sub-model implemented in AIRTREE is derived from the BRTSim general-purpose hydrological and biogeochemical solver (Maggi, 2018, Maggi, 2019). The soil moisture dynamics are described by means of the Richards equation (Richards, 1931; Richardson, 2007) which couples the continuity equation to the Darcy's law (Darcy, 1856) and solves for the unsaturated-saturated flow regimes. In this application, the soil column is described by a sequence of twenty finite volumes; the solver discretizes the Richards Equation over the finite volumes and tests the convergence of solution against a tolerance. Full details of the convergence criteria are provided in the User Manual and Technical Guide of the BRTSim v3.1a package (Maggi, 2018) and are not replicated here.
The AIRTREE model was developed to be a site-specific model calibrated on site observations, to provide the most accurate simulations of ecosystem gas exchanges. The first step of the model calibration required to set a range for each initializing parameter, during the calibration other sets of parameter vectors were generated and evaluated with respect to the first set of parameters. The calibration was performed on a random sample (splitted in two parts: the 80% was used for calibration, and the

remaining part for validation) of the input dataset (17520 half hourly data for one year of study) and include the sensible heat, latent heat, GPP, and soil humidity. To evaluate the impact of ozone corrections on the model performances, input data collected at ambient ozone concentrations above 40 ppb were excluded from this procedure. The calibration iterated until a satisfactory user-defined efficiency threshold (Kling-Gupta efficiency, Gupta et al., 2009) was met. The sensitivity analyses of the AIRTREE model identified the canopy depth, LAI, and leaf length, Vc_{max} and m (the BWB slope parameter) as the most important parameters for the model (Fares et al., 2019). Concerning PM deposition, the model incorporates traditional atmospheric models to predict particle deposition. Since this work is not focused on the model capability to simulate particulate matter deposition, the description of these models is not here reported, a detailed description of the AIRTREE model can be found in Fares et al. (2019).

Table 2 - list of the continuous environmental variable needed by the AIRTREE model in this study.

Variable	***Description***	***Unit measure***
RAD	PPFD + Near Infrared Radiation, NIR	W m^{-2}
T_{air}	Air temperature	C°
RH	Relative humidity	%
ubar	Wind speed	m s^{-1}
CO_2	CO_2 concentration	ppm
O_3	Ozone concentration	ppb
Press	Air pressure	Pa
PM	PM concentration	ppm
rain	Precipitations	mm
ustar	Friction velocity	m s^{-1}

2.4 Meteorological and flux data

Two-year datasets for both Castelporziano (2013 and 2014) and Blodgett (2003 and 2004) sites were used to parameterize and evaluate the model. The datasets with the lowest number of missing data were selected to avoid unrealistic predictions and artifacts in the simulations.

The main characteristic of the two sites are resumed in Table 3. In both sites, fluxes measurement with Eddy Covariance were performed from the top of a tower. H_2O and CO_2 concentrations were measured with closed-path infrared gas analyser (see details in references provided for each site). Ozone fast measurements were performed by a chemiluminescence methods which uses coumarin dye reaction with ozone, thanks to a customized instrument developed by the National Oceanic and Atmospheric Administration (NOAA, Silver Spring, MD).

Table 3 - Overview of the main climatic characteristic and species included in this study.

Site Name	**Castelporziano**	**Blodgett Ameriflux site**
Coordinates	41°70′42″N 12°35′72″E	38°53’42” N 120°37’57” W
Altitude	13 m	1315 m
Vegetation	Holm oak forest (*Quercus ilex*)	Ponderosa pine plantation (*Pinus ponderosa*)
Tree mean height	14 m	7 m
LAI	3,69 m^2 m^{-2}	2,9 m^2 m^{-2}
Soil texture	Sandy	Sandy loam
Climate	Mediterranean	Mediterranean
Mean Temperature	15° C	12° C
Annual Precipitation	790 mm	870 mm
Summer mean ozone concentration	40 ppb	57 ppb
Ozone sensitivity	Tolerant	Sensitive

The chemiluminescence detector was calibrated against 30 min average ozone concentrations from a UV ozone monitor. Data were recorded at 10 Hz for all gases using data loggers (CR-3000, Campbell Scientific, Shepshed, UK).
In this study GPP was calculated from ecosystem scale fluxes of CO_2 (NEE) by adding the ecosystem respiration term (R_{eco}) to NEE, since NEE represents the balance between CO_2 sequestrated and emitted by the photosynthetic (GPP) and respiratory (R_{eco}) processes of the ecosystem.

$$NEE=GPP-R_{eco} \qquad \text{eq. 49}$$

The separation of NEE into its component is necessary to derive GPP and R_{eco}. In absence of light GPP is assumed to be zero and therefore NEE measured at night is representative of R_{eco}. Conversely, during light hours Reco cannot be directly derived by NEE and an estimation of daytime R_{eco} is needed. Therefore, an Arrhenius-type model (Lloyd and Taylor, 1994) describing R_{eco} dependence to temperature, is fitted to nighttime NEE.

$$R_{eco} = rb\ exp\left(E_0\left(\frac{1}{T_{ref-T_0}} - \frac{1}{T_{air} - T_0}\right)\right) \qquad \text{eq. 50}$$

where rb ($\mu mol\ \ C\ \ m^{-2}\ \ s^{-1}$) is the base respiration at the reference temperature [T_{ref} (°C), set to 15 °C], E_0 (°C) is the temperature sensitivity, T_{air} is the air temperature, and parameter T_0 (°C) is kept constant at −46.02 °C as in Lloyd & Taylor (1994). For E_0 a constant value is used for the whole year while rb was estimated every 5 days using a 15 days window (as in Reichstein et al., 2005).

Finally, by using daytime temperature in place of nighttime temperature, daytime respiration is derived, and the difference between modeled R_{eco} and measured NEE yields estimated GPP (Lasslop et al. 2010).
Methods that rely on night-time data for partitioning may be biased due to the frequent night-time suppression of turbulence and dominance of advective fluxes not measured by conventional EC systems (Goulden *et al.*, 1996; Feigenwinter *et al.*, 2004; Aubinet, 2008). Compared to GPP values derived from biometric measurements Campoli et al. (2016) observed an uncertainty of night-time based NEE partitioning of GPP of 5±5% and the 2 to 15% if compared to automated ecosystem-chambers dark Reco measurements (Galvagno & Worfart 2015).

Daily gross primary productivity (GPP), water fluxes (ET) and ozone concentrations of the first year of study (2013 and 2003 for Castelporziano and Blodgett, respectively) for both the study sites are shown in Figure 14.

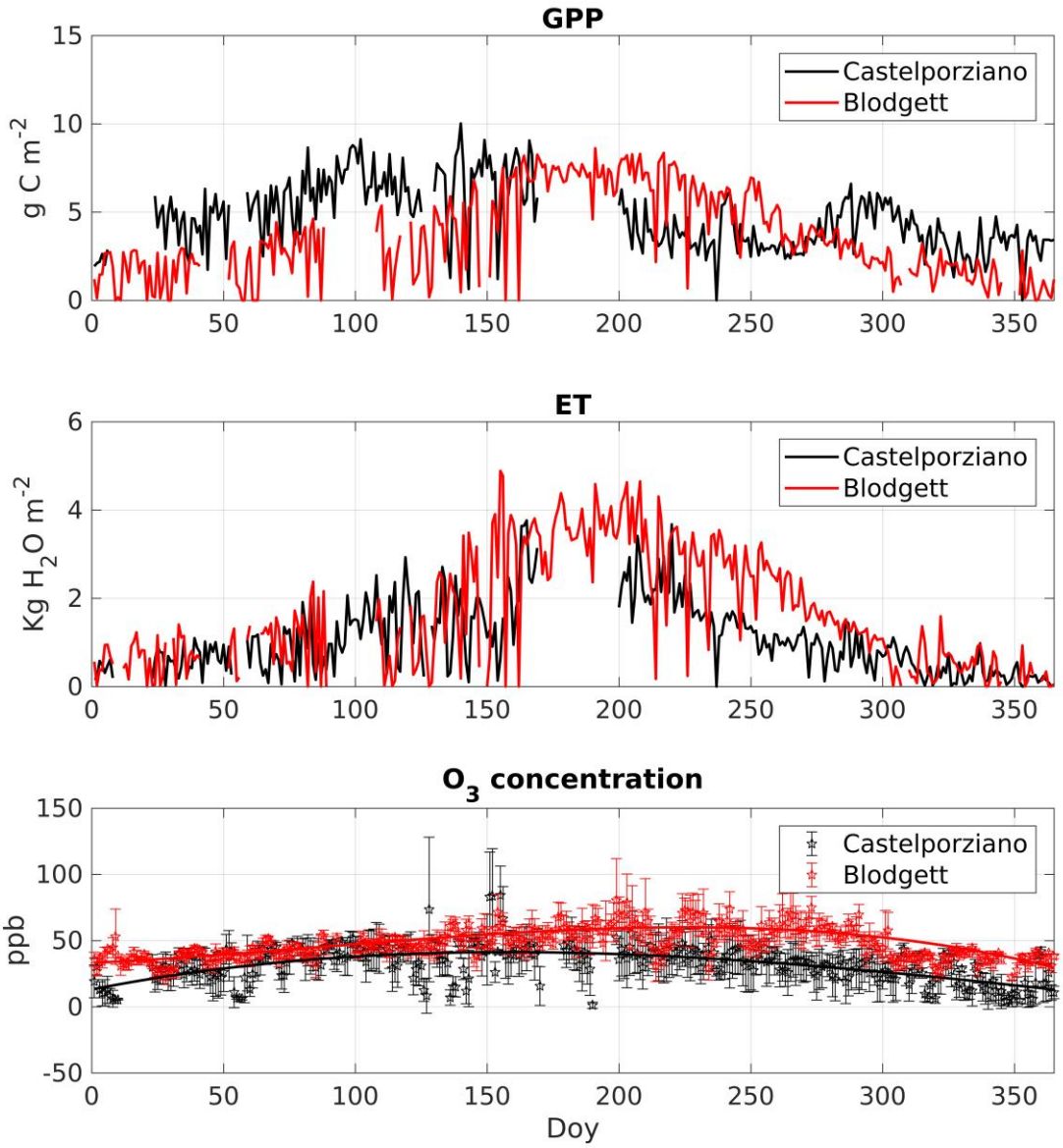

Figure 14 - the figure shows both sites GPP (top), ET (middle) and ozone concentrations (bottom) for the year 2013 and 2003 for Castelporziano (in black) and Blodgett (in red) sites, respectively.

2.5 Leaf-level gas exchange measurements

Gas exchange measurements were performed in Castelporziano holm oak forest with a portable gas analyzer (mod. Li-cor 6400). Full developed sunlit leaves were acclimated to the chamber at 25°C, a chamber-air CO_2 concentration of 400 ppm, and a saturated photosynthetic photon flux density (PPFD) of 1800 μmol m^{-2} s^{-1} until the photosynthetic rate (A) stabilized. In order to estimate the velocity of carboxylation (Vc_{max}), the electron transport rate (J_{max}), dark respiration (R_d) of the plant, A-Ci curves consisting of 10 different intercellular CO_2 concentrations (C_i) increasing from 70, 90, 120, 160, 220, 260, 400, 800, 1100, 1300 ppm were built. The Farquhar, von Caemmerer and Berry model of photosynthesis (FvCB) was fitted to measurements of photosynthesis and C_i by using the 'fitaci' function in 'plantecophys' package in R (Duursma, 2015). This method fits the hyperbolic minimum of A_c and A_j instead of the minimum function of two non-linear equations (eq.21) that is sometimes difficult to fit, avoiding discontinuity:

$$A_m = \frac{A_c + A_j - \sqrt{(A_c + A_j)^2 - 4\theta A_c A_j}}{2\theta} - R_d \qquad \text{eq.51}$$

where θ is a shape parameter, and A_m is the hyperbolic minimum of A_c and A_j.

The velocity of carboxylation (Vc_{max}) used in this study was measured in september 2018 below and above the canopy on fully expanded sunlight leaves (8 replicates per level). By adopting a Beer's law type function (eq. 52) different Vc_{max} from the bottom to the top of the canopy were reproduced as reported by Bonan et al. (2011, 2014) to take into account the different levels of Nitrogen (Kn) and in general different capacity of carboxylation (Vc_{max}) between shade and light adapted leaves in the canopy profile.

$$Vc_{max}^{opt}(x) = Vc_{max}^{opt}(0)e^{-K_n x} \qquad \text{eq.52}$$

Where Vc^{opt}_{max} (0) is defined at the top of the canopy. Kn scales with Vc^{opt}_{max} at the canopy top following (Bonan et al.*, 2014)*

2.6 Ozone correction factors implementation

Three stomatal conductance models, the Jarvis (hereafter referred to as JV) multiplicative algorithm proposed by Jarvis in (1976), the BWB coupled A-gs model proposed by Ball, Woodrow & Berry in 1987 and the optimal stomatal behavior model (hereafter referred to as MD) proposed by Medlyn et al. (2011) have been incorporated into the FORCAsT model for this study.

2.6.1 Jarvis parameterization and the fO_3 correction factor (JV_{fO3})

For this study, the modified formulation of the JV model developed for ozone flux estimates (Büker et al., 2007; Emberson et al., 2000, 2007, 2009) was adopted. Such formulation is indicated into the UNECE guidelines for ozone assessment and integrated into the DO3SE model (Emberson et *al.*, 2004).
Stomatal conductance is calculated as:

$$G_s = G_{max} \cdot f_{phen} \cdot f_{light} \cdot max\{f_{min} \cdot (f_{temp} \cdot f_{VPD} \cdot f_{SWC})\} \cdot fO_3 \qquad \text{eq.53}$$

Where G_{max} is the maximum g_s (mol m^{-2} s^{-1}) derived from leaf gas exchange measurements under non limiting conditions, f_{phen}, f_{light} , f_{temp} , f_{vpd} and f_{swc} are the variation in G_{max} with leaf age, photosynthetic photon flux density at the leaf surface (PPFD, µmol photons m^{2} s^{-1}), temperature (T, °C), vapor pressure deficit (VPD, kPa), and volumetric soil water content (SWC, m^3m^{-3}).

The effect of changes in leaf age (f_{phen}) on stomatal conductance was modelled as:

$$if\ doy \leq astart \qquad \text{eq.54}$$

$$f_{phen} = fphen_c$$

$$if astart < doy < astart + fphen_a$$

$$f_{phen} = (1 - fphen_c) * ((jday - astart)/fphen_a) + fphen_c$$

$$if(astart + fphen_a) < doy < (aend - fphen_b)$$

$$f_{phen} = 1$$

$$if (aend - fphen_b) < doy \leq aend$$

$$f_{phen} = (1 - fphen_d) * ((aend - jday)/fphen_b) + fphen_d$$

$$if aend < doy$$

$$f_{phen} = fphen_d$$

Where the parameters astart and aend are the start and the end of the growing season, respectively (doy), $fphen_a$ and $fphen_b$ represent the number of days of fphen to reach its maximum and the number of days during the decline of fphen to the minimum value, respectively. The parameter $fphen_c$ and $fphen_d$ represent maximum fraction of fphen at astart and aend, respectively.

The response of stomatal conductance to light (f_{light}) is given by:

$$f_{light} = 1 - exp(-a \cdot PPFD) \quad \text{eq.55}$$

Where a is a species-specific parameter defining the shape of the exponential relationship.

The response of stomatal conductance to vapor pressure deficit (VPD, kPa) is given by:

$$if\ VPD \geq VPDmin \quad \text{eq.56}$$

$$f_{VPD} = fmin$$

$$if\ VPD \leq VPDmax$$

$$f_{VPD} = 1$$

If VPD > VPDmax or VPD < VPDmin

$$f_{VPD} = \big(((1 - fmin) * (VPDmin - VPD))/(VPDmin - VPDmax)\big) + f_{min}$$

where VPDmin and VPDmax denote the threshold of VPD for attaining minimum and full stomatal opening derived from leaf gas exchange measurements, respectively. If

VPD exceeds VPDmin then fVPD is set to fmin. If VPD is lower than VPDmax then fVPD is 1.

The effect of leaf temperature variation on stomatal conductance (f_{temp}) is calculated as:

$$f_{temp} = \frac{(T - T_{min})}{(T_{opt} - T_{min})} \cdot \frac{(T_{max} - T)}{(T_{max} - T_{opt})}^{\frac{(T_{max} - T_{opt})}{(T_{opt} - T_{min})}} \quad \text{eq.57}$$

where T_{min}, T_{max} and T_{opt} are the minimum, maximum and optimum temperature for stomatal conductance in °C.

The response of stomatal conductance to soil water content (%) follows the functions of Büker et al. (2015).

$$if \theta \geq \theta_f \quad \text{eq.58}$$

$$f_{SWC} = 1$$

$$if\ \theta < \theta_f$$

$$S = (\theta - \theta_w)/(\theta_f - \theta_w)$$

$$if\ k1 \leq S \leq 1$$

$$f_{SWC} = 1$$

$$if 0 < S < k1$$

$$f_{SWC} = (1 - fmin) * S/k\,1 + f_{min}$$

Where θ, θw, θ_f are the volumetric soil water content (SWC), wilting point and field capacity respectively with units of m^3m^{-3}. k1 is a threshold of SWC above which gs is at a maximum

The fO_3 multiplicative factor was implemented as an additional multiplicative factor to the JV model (eq.53). This factor has been derived accordingly to Hoshika et al. (2018b) to the results reported in OTCs and FACE facility studies on *Q.ilex* (Fusaro et al., 2016; Vitale et al., 2008) and on *P. ponderosa* (Beyers et al. 1992; Panek 2004) where seedlings were exposed to different ozone treatments with open-top chambers.

$$fO_3 = 1 - q * [O_3] \quad \text{eq.59}$$

Where q is the parameter reflecting stomatal sensitivity to ozone *concentration given by the extrapolation line between the* g_s *data and hourly mean* ozone *concentrations, and* $[O_3]$ *is hourly mean* ozone *concentration (ppb).*

The rate of carbon assimilation (A) was calculated by using Fick's Law as:

$$A = g_s(C_s - C_i) \quad \text{eq.60}$$

Where C_s *is the* CO_2 *at the leaf surface and* C_i *is the intercellular* CO_2 *concentration calculated by assuming a constant Ci/Cs ratio* (Wong et al., 1979).

Average g_s values measured at different ozone exposures were extrapolated from tables and graphs. When not available, the mean ambient ozone (AA) and the mean concentrations of each enhanced ozone treatment (e.g. AA x 0.5, AA x 1.5, AA x 2) were derived from cumulated concentrations or from AOT40 values as the ratio between Cumulated Concentrations and hours of exposure. Since this approach was developed for ozone FACE facilities studies, where plants are fumigated with different growing ambient air (AA) ozone concentrations. In this studies, stomatal conductance in absence of ozone cannot be directly measured, so Hoshika derived it as the intercept of the extrapolation line when x (i.e. $[O_3]$) was equal to zero (0 ppb). In OTCs experiments the g_s response at 0 ppb is usually available as the Charcoal Filter (CF) treatment used as "control" for g_s, representing the plant growth without ozone limitations. The other treatments represent the non-filtered ambient air ozone treatment (i.e NF, same as AA) and enhanced ambient ozone concentrations (i.e. NF+, same as AAx_i) respectively. In this study, plants' responses to different hourly ozone concentrations were derived from the extrapolation lines between g_s measured in the CF, NF, and NF+ treatments, at ozone concentrations representing the mean hourly value of the period of exposure. In many studies, g_s response to ozone was

usually tested in parallel with g_s response to drought. Since a specific f_{SWC} was already implemented in the Jarvis multiplicative formulations, only data derived from well-watered (WW) soil moisture conditions were considered.

2.6.2 Ball Woodrow Berry correction factors (BWB_{FO3})

Two correction factors (F_{CO3} and F_{PO3}), are applied to A_n and g_s of the BWB model. These correction factors are derived accordingly to Lombardozzi et al. (2013 and 2015) on the results reported in Alonso et al. (2014) and Vitale et al. (2008) for *Q. ilex* and in Beyers et al. (1992) for *P. ponderosa*. A linear regression was used to identify the correlation between change in photosynthesis or stomatal conductance relative to plants exposed to little or no ozone (% of control) with CUO (an indicator of ozone plant physiological damage through time).

$$F_{cO_3} = a_c * CUO + b_c \qquad \text{eq.61}$$

$$F_{pO_3} = a_p * CUO + b_p$$

Where a and b are slope and intercept constants for gs and A with the Cumulative Uptake of ozone *(CUO) that represents the flux of ozone entered into the stomata for the considered time interval.*

$$CUO = CEO_3 \times g_s \times 1.67 \times 3600 \times 10^{-6} \qquad \text{eq.62}$$

Where CEO_3 is the cumulative ozone *exposure (i.e. SUM00, AOT00 etc.) that represents the environmental condition of ambient ozone the plant was exposed to.*

2.6.3 Optimal stomatal behavior model for ozone avoidance (MD_K)

Finally, for the MD model, the Hoshika formulation (Hoshika et al., 2013c) for assessing ozone impact on g_s was used.

$$g_s = g_0 + 1.6\left(1 + \frac{g_1}{\sqrt{D + (k/1.6)[O_3]_{air}}}\right)\frac{A}{C_a} \qquad \text{eq.63}$$

Where g_0 is stomatal conductance at zero A, and g_1 is a slope parameter. D and O_3 are VPD (kPa) and ozone concentration (ppb), respectively. k is the ratio of the marginal water cost of plant carbon gain (λ) to the marginal O_3 damage of plant carbon gain ($\lambda°$) (mol H_2O mol^{-1} O_3), the 1.6 outside a parenthesis is the ratio of the diffusion coefficients for water vapour to CO_2, and the 1.6 inside a parenthesis is the ratio of the diffusion coefficients for water vapour to O_3 (Hicks et al 1987).

Depending on plants responsivity to water stress k ranges between 0.1*k and k (Hoshika et al 2013c). In this study the maximum value of k was used.

2.7 Modeling and statistics

The FORCAsT model was first optimized without applying any ozone correction (i.e. no ozone damage). Therefore, since the vegetation was constantly exposed to ambient air ozone concentrations, possible underestimation of ozone impact on simulated fluxes was expected. The resulting model runs (hereafter named Control) were performed for BWB, MD and JV and then used as reference for ozone correction-implemented model simulations. With the goal to identify (if exists) the threshold that gives the best fit with the field observations from eddy covariance, different thresholds ranging from 0 to 5 nmol m $^{-2}$ s $^{-1}$ representing high to low sensitivity to ozone, respectively were applied in both sites' simulations. These six additional model simulations differed only by the critical ozone dose threshold (hereafter named thr0, thr1, thr2, thr3, thr4, thr5).
Both the AIRTREE and FORCAsT Control simulations were compared with the threshold (thr0 to thr5) simulations. Thresholds (defined as critical ozone threshold) in this study are considered critical stomatal ozone fluxes above ozone stress occurred. Consequently, correction factors have been applied only when stomatal ozone fluxes were above selected thresholds. No correction to either A_n and g_s was

applied when the stomatal ozone flux at each time step of the model was lower than the selected thresholds.
Linear regressions between observations and simulations were performed for GPP and λE. To evaluate if the application of the ozone thresholds would have a seasonal positive or negative effect linear regressions were performed for both the whole year and for each season. The "best" model run was identified by the regression that gave the best coefficient of determination (R^2) and maximum accuracy (i.e. the lowest root-mean-square error, RMSE). While the R^2 provides information about the percentage variation in the dependent variable (y) explained by the predictors (x-variables), the RMSE measures the average error performed by the model in predicting the outcome for an observation. Lower values of RMSE indicates better fit. In addition, to evaluate the ozone corrections impact on model performances data were filtered for ozone concentration above a threshold of 40 ppb, thus indicating a potential ozone exposure (as in AOT40).
The AIRTREE natively includes the BWB A_n-g_s model and only corrections for the BWB model were tested. In addition to the above described approach used to identify the best threshold at both the seasonal and annual scale, the best (i.e. the lowest discard from observations, Obs) simulation's values (thr_i) were identified also at each model time step (half-hourly time resolution). These corresponding thresholds were collected into a dynamic threshold variable (THR).

$$\mathrm{THR} = \frac{1}{n}\sum \min |\mathrm{Obs} - \mathrm{thr}_i| \qquad \text{eq.64}$$

At each model time step the THR variable indicates which threshold (thr_i) provides the simulated value closest to observation (Obs).

The Spearman's rank-order correlation index (r_s) was used in order to evaluate if the changes of the ozone threshold (THR) can be due to changes in environmental conditions (e.g. PAR, VPD, SWC, T_{air} and ozone concentration). The choice of the Spearman non-parametric correlation index instead of the most traditional Pearson's one-moment correlation coefficient was adopted with the aim to analyse together linear and non-linear correlations among variables (Conte et al., 2019, Salvati et al., 2014). Once identified which environmental variable had a statistically significant correlation with THR, a Jarvis-like approach to simulate THR was performed. A boundary line analysis (Webb 1972) between THR/THR_{max} and the selected environmental variables was performed and a Jarvis-like multiplicative algorithm to predict THR was finally developed. The functions were between THR/THR_{max} and the selected environmental variable, were derived by plotting the relative THR (THR/THR_{max}) against each environmental variable separately. The upper limit of the scatter diagram indicates the response of THR to the particular independent variable. The response functions were derived by using the MATLAB® Curve Fitting Toolbox. A series of linear and nonlinear models (e.g. Exponential, Gaussian, Power, Rational

models) were fitted to data and compared. Finally, the function with the lowest RMSE was selected and used as THR/THR_{max} reducing factor in the multiplicative model. As stated before, the main criticism of this approach is that the interactive effects between environmental factors are not considered, and the multiplicative nature of the model doesn't account any synergistic interaction.

The main input parameter for the stomatal conductance models used in this study are reported in Tables 4 to 6.

Table 4 - Parameters for the Jarvis multiplicative gs model and the Hoshika fO_3 correction factor used in FORCAsT model calculated in this study.

Input	***Description***	***Q.ilex*** [a]	***P. ponderosa*** [b]	***Units***	***Reference***
G_{max}	maximum gs	0.352	0.12	mol m^{-2} s^{-1}	[a] Hoshika et al., 2017 [b] Misson et al., 2004
f_{min}	minimum gs	0.03	0.01	mol m^{-2} s^{-1}	[a] Hoshika et al., 2018a [b] Misson et al., 2004
VPD_{min}	VPD for minimum gs	7.4	3	kPa	[a]Hoshika et al., 2018 [b]Bičárová et al. 2017
VPD_{max}	VPD for maximum gs	0.8	0.6	kPa	[a]Hoshika et al., 2018a [b]Bičárová et al. 2017
Θ_f	SWC at field capacity (FC)	0.3	0.19	m^3 m^{-3}	[a,b] this study
Θ_w	SWC at wilting point (WP)	0.07	0.05	m^3 m^{-3}	[a,b] this study
K1	SWC for max g_s	0.32	0.19	%	[a]Hoshika et al., 2018a [b] this study
Trsmin	Minimum Tair for g_s	6	1	°C	[a]Hoshika et al., 2017 [b]Bičárová et al. 2017
Trsmax	Maximum Tair for g_s	50	36	°C	[a]Hoshika et al., 2017 [b]Bičárová et al. 2017
Trsopt	Optimal Tair for g_s	20	18	°C	[a]Hoshika et al., 2017 [b]Bičárová et al. 2017
astart	Start of the growing season	91	70	doy	[a] Hoshika et al. 2018a [b] this study
fphena	number of days for max fphen	89	88	doy	[a] Hoshika et al. 2018a [b] this study
fphenb	number of days for min. fphen	80	99	doy	[a] Hoshika et al. 2018a [b] this study
fphenc	maximum fraction of fphen at Astart	0.9	0.3	-	[a] Fares et al. 2013a [b] UNECE 2004
fphend	maximum fraction of fphen at aend	0.9	0.3	-	[a] Fares et al. 2013a [b] UNECE 2004
aend	end of the growing season	304	310	doy	[a] Fares et al. 2013a [b] this study
a	shape of the hyperbolic relationship	0.022	0.008	μmol m^{-2} s^{-1}	[a] Fares et al. 2013a [b]Bičárová et al. 2017

Table 5 - Ball Berry model parameterization for the FORCAsT and for the AIRTREE models

Input	*Description*	*Q.ilex* [a]	*P. ponderosa* [b]	*Units*	*Reference*
Vc_{opt}	Vc_{max} at optimal temp. - canopy top	78	52	µmol m^{-2}	[a] this study [b] Misson et al. 2006
J_{opt}	J_{max} at optimal temp. – canopy top	100	90	µmol m^{-2}	[a] this study [b] Misson et al. 2006
k_{ball}	slope of Ball-Berry model	6	8	-	[a] this study [b] Law et al. 2000
bprime	intercept for H_2O	0.03	0.01	mol m^{-2} s^{-1}	[a] this study [b] Misson et al. 2004

Table 6 - Medlyn model parameterization for the FORCAsT model

Input	*Description*	*Q.ilex* [a]	*P. ponderosa* [b]	*Units*	*Reference*
g0	intercept for H_2O	0.03	0.01	mol m^{-2} s^{-1}	[a] this study [b] Misson et al. 2004
g1	Slope coefficient	3.6	2.35	$kPa^{0.5}$	[a] this study [b]De Kauwe et al., 2015
alpha	Quantum yield of electron transport	0.3	0.22	mol mol^{-1}	[a]Guardia, et al., 2012 [b]Panek 2004
theta	Shape of light response curve	0.75	0.81	-	[a]Gomez-Aparicio et al., 2006 [b]Varela et al., 2016
J_{opt}	Jmax at optimal temp. – canopy top	100	90	µmol m^{-2} s^{-1}	[a] this study [b] Misson et al. 2006
Vc_{opt}	Vcmax at optimal temp. -canopy top	78	52	µmol m^{-2}	[a] this study [b] Misson et al. 2006

3. Results

3.1 Ozone correction factors

Similar to Hoshika et al. (2012; 2018), the fO_3 correction factor for the Jarvis multiplicative algorithm (JV_{fO3}) was derived from literature data. The stomatal conductance response to ozone for *Q.ilex* was derived from the study of Fusaro et al., (2016), in which seedlings from the Castelporziano (CPZ) Estate nursery were studied in OTCs. Ozone AA concentrations (derived from AOT40) values were 40.9 ppb, and consequently, 52 ppb and 70 ppb for the NF+ (supplemented with + 30% ambient air ozone) and NF++ (supplemented with +74% ambient air ozone), respectively. For *Pinus ponderosa*, g_s responses to different ozone exposures were derived from the study of Beyers et al. Beyers *et al.* (1992), in which 2-years old seedling from the Whitaker Forest at 1600 m a.s.l. in California, 200 miles from Blodgett forest (BLD). Ozone concentration for each ozone treatment were directly available in the text indicating 13, 62 and 95 ppb for CF, NF, and NF150 exposure treatments, respectively. The extrapolation lines provided a slope (i.e. q in eq. 59) of $3.2x10^{-3}$ and $2x10^{-4}$ for *Q.ilex* and *P.ponderosa*, respectively (Figure 15). Thus, allowing to calculate fO_3 at each model time step for CPZ and BLD sites.

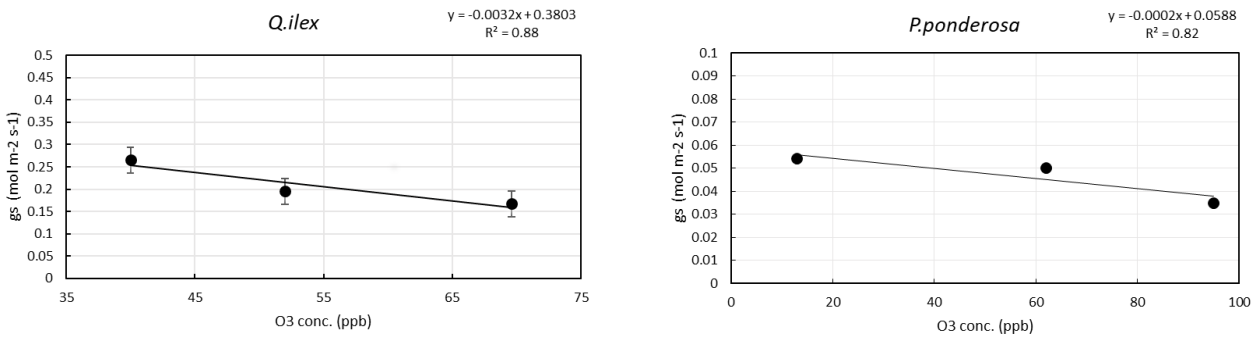

Figure 15 - The two scatterplots show the extrapolation lines between stomatal conductance to water vapour and hourly ozone concentration accordingly to Hoshika et al. (2018)

For CPZ, the correction factors F_{cO3} and F_{pO3} for the Ball-Berry model (BWB_{FcO3} and BWB_{FpO3}) were derived accordingly to Lombardozzi *et al.* (2013, 2015) on the results reported in Alonso *et al.* (2014) on *Q.ilex* responses to different cumulated ozone dose, since not enough (only two) replicates were reported in Fusaro et al. (2016). The CEO_3 was derived for each season by multiplying the average enhanced

treatment ozone concentration NFA+ (AA+40 ppb) for the daily hours of exposure (10 hours per day) and for the number of days between the start of the fumigation and each measurement. The same approach was used for BLD, by using data derived from Beyers et al. (1992). Since ozone fumigations were not continuous during the 3 years of study, CEO_3 was calculated as the sum of ambient CEO_3 (62 ppb) of the days excluded by fumigations, and the CEO_3 cumulated during the NF150 ozone fumigations (95 ppb). CUO was then calculated by multiplying each g_s measurements for the corresponding CEO_3 (eq. 61-62). Intercept and slope of the linear regression between CUO and the ratio between gs measured in NFA+ treatment and in CF treatment were used to derive F_{cO3} and F_{pO3} (Table 7).

Table 7 - Values used to parameterize plants' sensitivity to ozone (F_cO_3, F_pO_3). Slopes and intercepts (unitless) are derived from literature data accordingly to Lombardozzi et al. (2013, 2015).

Species	***Photosynthesis***		***Conductance***	
	Slope (a_p)	***Intercept (b_p)***	***Slope (a_c)***	***Intercept (b_c)***
Q.ilex	-0.0003	0.7930	-0.0009	0.8572
P.ponderosa	-0.0005	0.9152	-0.0007	1.0671

Finally, for the parameterization of the optimal stomatal behavior model for ozone avoidance (MD_K) proposed by Hoshika *et al.* (2013c) the k parameter (eq. 63) was calculated online directly from leaf level VPD and ozone concentrations. The parameter g1 in eq. 63 was derived by fitting measures of leaf level g_s (8 replicates) collected from mature trees inside the CPZ experimental site to the photosynthesis-stomatal model (figure 16), accordingly to (Hoshika et al., 2013c). The estimated value of g1 was 3.6 and it was used as input for the FORCAsT model.

Since measurement of leaf level gas exchange for *P.ponderosa* were not available, g1 could not be directly estimated. Therefore, a value of 2.35 representative of the evergreen needleleaf plant functional types (PFTs) was used (De Kauwe et al., 2015).

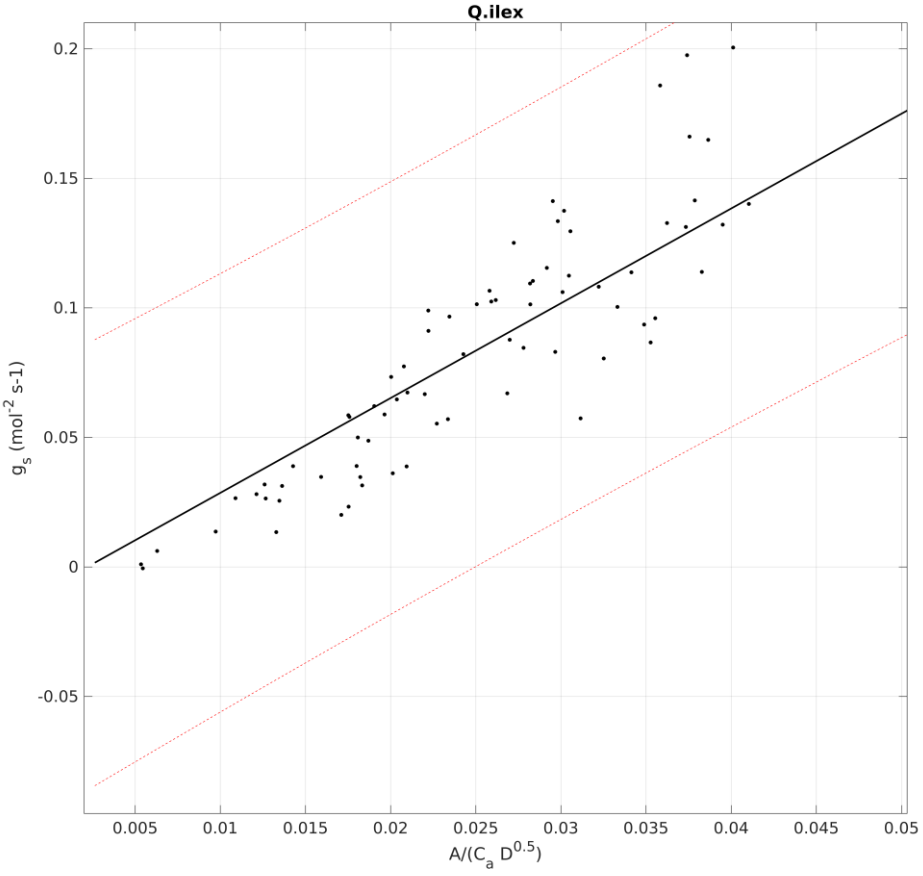

Figure 16 – Relationship between stomatal conductance and the dominant parameter of the photosynthesis stomatal model assuming that ozone stress is zero (k=0). Red lines are confidence bounds.

3.2 Leaf level gas exchange measurements

Vc_{max} and J_{max} values measured at the experimental site are reported in table 5 and 6. A-C_i curves applied to measurements at the top and at the bottom of the canopy collected in September 2018 provided values of Vc_{max} of 44 and 78, and J_{max} values of 68 and 100, for the bottom and the top of the canopy leaves (Figure 17). Vc_{max} was scaled through the canopy accordingly to eq. 52. K_n was calculated iteratively up to reach the observed values at the top and at the bottom of the canopy (Table 8).

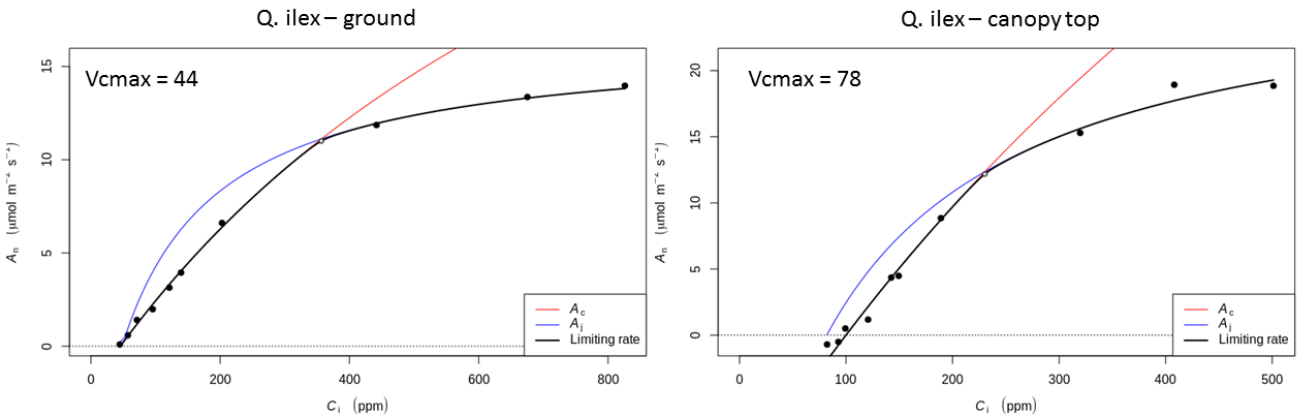

Figure 17 - A_n is the net photosynthetic rate, C_i the intercellular CO_2 concentration. Symbols are measurements, the black line the fitted FvCB model of photosynthesis. Colored lines indicate the two photosynthesis rates in the FvCB model. The fitaci function estimates V_{cmax}, J_{max} and R_d from the fitted curve.

Since these measurements were not available for BLD site, a K_n value of 0.15 for evergreen needleleaf plant functional types (PFTs) was applied (Bonan et al., 2011), accordingly to the maximum measured values available in literature studies on *Pinus ponderosa* (Table 5-6).

Table 8 - Vc_{max} values scaled at each canopy layer, according to Bonan et al (2011, 2014a). Cumulative layer of a round canopy are reported for both AIRTREE (5 canopy layers) and FORCAsT (10 canopy layers) from the top of the canopy (layer 1) to the ground (layers 5 and 10 for AIRTREE and FORCAsT, respectively). The K_n value referred to this table is K_n=0.15, for a LAI of 3.69.

Layer	AIRTREE		FORCAsT	
	LAI cumulated	Vc_{max}	LAI cumulated	Vc_{max}
1	0.43	73	0.3	74
2	1.32	64	0.65	70
3	2.37	54	1.07	66
4	3.25	48	1.52	62
5	3.69	45	2.06	57
6	-	-	2.51	53
7	-	-	2.94	50
8	-	-	3.24	48
9	-	-	3.49	46
10	-	-	3.69	45

3.3 Model simulations

3.3.1 FORCAsT

3.3.1.1 Castelporziano – *Quercus ilex*

Linear regressions between observed and simulated GPP for the years 2013 and 2014 are shown in table 9. The best "Control" runs (i.e. no ozone effect) between simulated and observed GPP were provided by the MD model (R^2 of 0.64 and 0.40, RMSE of 4.89 and 7.03 for 2013 and 2014, respectively) and by the BWB model (R^2 of 0.6 and 0.47, RMSE of 6.35 and 7.72 for 2013 and 2014, respectively), followed by the JV model (R^2 of 0.58 and 0.35, RMSE of 7.81 and 10.67 for 2013 and 2014, respectively). Regressions between observed and simulated λE identified MD as the best model (R^2 of 0.72 and 0.53, RMSE of 41.23 and 65.66 for 2013 and 2014, respectively) followed by BWB (R^2 of 0.67 and 0.52, RMSE of 61.27 and 79.00 for 2013 and 2014, respectively), and JV (R^2 of 0.65 and 0.44, RMSE of 40.98 and 73.89 for 2013 and 2014, respectively).

When compared to their relative Control runs, the application of ozone corrections led to improvements in model accuracy in simulating GPP by applying the Lombardozzi BWB_{FO3} correction (RMSE decreased up to 28 and 22% in 2013 and 2014, respectively), the Hoshika JV_{fO3} correction (RMSE decreased up to 26% and 21% in the two years of study) and the Hoshika MD_K model (RMSE decreased up to 2.5% and 0.36% in the two years of study). Similar results were found for λE (Table 9). Indeed, improvements in model accuracy were observed by applying the BWB_{FO3} correction (RMSE decreased up to up to 22 and 13% in 2013 and 2014, respectively) and the JV_{fO3} correction (RMSE decreased up to 8% and 6% in the two years of study). Nevertheless, the implementation of the MD_K model did not ameliorate the accuracy of λE simulations (Table 9). Similar results for both GPP and λE were found by linear regressions on data filtered at high ozone concentrations (above 40 ppb, not shown). In general, for the whole year, simulations including ozone corrections (thr_i) with critical ozone thresholds (Y) of 3, 4 and 5 nmol m^{-2} s^{-1} (thr3, th4, thr5) led to an overall increase (β,R^2, RMSE) in the accuracy of all three g_s models when compared to the "Control" run. In particular, the ozone correction providing the best results was the Lombardozzi et al. (2013 and 2015) correction factor for the BWB model (BWB_{FO3}).

On a seasonal scale, by focusing on data filtered at high ozone concentrations, the ozone correction that provided the best results in simulating GPP (Table 10) for 2013 in Summer (R^2 = 0.65, RMSE = 3.35) and Fall (R^2 = 0.61, RMSE = 4.35) was the MD_K , while in Winter (R^2 = 0.84, RMSE = 2.5) and Spring (R^2 = 0.68, RMSE = 4.56) the BWB_{FO3} performed better than the others. In 2014 the best results were provided by BWB_{FO3} in Winter (R^2 = 0.72, RMSE = 3.48), Summer (R^2 = 0.62, RMSE = 4.49) and Fall (R^2 = 0.54, RMSE = 5.07) while the MD_K model provided the best results (R^2 = 0.54, RMSE = 5.69) in Spring (Table 11). Considering λE, in 2013 the best results were provided by the BWB_{FO3} in Winter (R^2 = 0.78, RMSE = 21.08) and Spring (R^2 = 0.75, RMSE = 34.50) and by JV_{fO3} correction in Summer (R^2 = 0.54, RMSE = 62.62) and Fall (R^2 = 0.56, RMSE = 39.99). In 2014 the best results were provided by BWB_{FO3} in all seasons.

In synthesis, the BWB_{FO3} resulted to be the correction factor that ameliorated both GPP and λE in both two years of study (Table 9-11). Therefore, by focusing on this approach, the critical ozone threshold that increased the model accuracy in simulating GPP was thr5 in Winter (R^2 = 0.84 and 0.72 in 2013 and 2014, respectively) and Spring (R^2 = 0.69 and 0.48, respectively). In Summer, thr0-thr1 (R^2 = 0.63 and 0.61, respectively) resulted to be the most appropriate thresholds in both years. In Fall, during 2013 the best model fit was obtained by applying critical ozone thresholds between 0 and 2 nmol O_3 m^{-2} s^{-1} (R^2 =0.6), while thr4 (R^2= 0.54) resulted to be the best threshold in 2014. A similar pattern was found for λE. In 2013 indeed, thr5 (R^2= 0.77), thr3 (R^2= 0.75), thr0 (R^2= 0.58) and thr1 (R^2= 0.61) provided the best results in Winter, Spring, Summer and Fall, respectively. In 2014, the best thresholds for Winter and Spring was thr5 (R^2= 0.49 and 0.44, respectively), while thr0-thr1 provided the best results for Summer and Fall (R^2= 0.56 and 0.49, respectively).

Table 9 - Linear correlations between modelled versus measured GPP and λE for the whole years 2013 and 2014 under different ozone thresholds. Thresholds (thr) are critical ozone fluxes above 0, 1, 2, 3, 4, 5 nmol m^{-2} s^{-1}. Thr0 to thr5 = high to low sensitivity to ozone. Intercept was forced to zero. Slope, R-squared and RMSE values are marked in bold where ozone corrections ameliorates or provide the same values of the control run simulation (no ozone effect). Values marked in red indicate the best values. For all the regressions both Slope (t-test) and model (Ftest) pValues resulted to be statistically significant (pValues <0.05).

Variable	year	Run	β			R^2			RMSE		
			BWB	MD	JV	BWB	MD	JV	BWB	MD	JV
GPP	2013	control	1.13	1.00	1.27	0.60	0.64	0.58	6.35	4.89	7.81
		thr0	**0.90**	0.65	**1.13**	0.60	**0.70**	**0.61**	**5.03**	5.22	**6.17**
		thr1	**0.92**	0.87	**1.14**	**0.61**	0.62	**0.61**	**4.97**	**4.77**	**6.17**
		thr2	**0.94**	0.95	**1.15**	**0.62**	0.61	**0.62**	**4.88**	5.02	**6.19**
		thr3	**0.97**	0.96	**1.17**	**0.63**	0.62	**0.62**	**4.94**	4.95	**6.32**
		thr4	**1.01**	0.98	**1.19**	**0.62**	0.63	**0.62**	**5.23**	**4.85**	**6.51**
		thr5	**1.05**	0.97	**1.21**	**0.61**	0.63	**0.61**	**5.55**	**4.86**	**6.83**
	2014	control	1.07	0.89	1.19	0.47	0.40	0.35	7.27	7.03	10.67
		thr0	0.85	0.58	**1.05**	**0.47**	**0.51**	0.36	**6.14**	**6.98**	**8.86**
		thr1	0.87	0.76	**1.05**	**0.47**	0.39	0.36	**6.17**	**6.92**	**8.86**
		thr2	0.88	0.84	**1.06**	**0.48**	0.39	0.37	**6.07**	7.07	**8.80**
		thr3	**0.91**	0.84	**1.08**	**0.50**	0.39	0.38	**5.95**	**7.00**	**8.79**
		thr4	**0.95**	0.87	**1.10**	**0.51**	**0.40**	0.39	**6.00**	**6.93**	**8.92**
		thr5	**0.99**	0.86	**1.12**	**0.51**	**0.41**	0.39	**6.21**	**6.86**	**9.18**
λE	2013	control	1.34	1.11	0.97	0.67	0.72	0.65	61.27	41.23	40.98
		thr0	**1.19**	0.37	0.86	**0.67**	0.56	**0.65**	**50.33**	54.94	**37.91**
		thr1	**1.19**	0.77	0.86	**0.68**	0.54	**0.66**	**50.62**	46.13	**37.89**
		thr2	**1.20**	**0.98**	0.87	**0.68**	0.64	**0.66**	**50.92**	43.44	**37.87**
		thr3	**1.22**	**0.99**	0.89	**0.67**	0.63	**0.66**	**52.45**	44.32	**38.03**
		thr4	**1.25**	**1.05**	0.91	**0.67**	0.67	**0.66**	**55.30**	43.15	**38.12**
		thr5	**1.28**	**1.06**	0.93	**0.67**	0.68	**0.66**	**57.65**	42.82	**38.69**
	2014	control	1.04	0.83	0.77	0.52	0.53	0.44	79.00	65.66	73.89
		thr0	0.92	0.29	0.69	**0.52**	0.47	**0.44**	**70.14**	85.08	**70.36**
		thr1	0.93	0.57	0.69	**0.53**	0.43	**0.45**	**70.51**	72.47	**70.34**
		thr2	0.93	0.74	0.70	**0.53**	0.47	**0.45**	**70.72**	70.14	**69.75**
		thr3	0.95	0.74	0.71	**0.53**	0.47	**0.46**	**71.49**	69.52	**69.50**
		thr4	**0.97**	0.80	0.72	**0.53**	0.52	**0.46**	**73.46**	66.14	**69.61**
		thr5	**1.00**	0.80	0.73	**0.52**	0.51	**0.46**	**75.42**	66.97	**70.11**

Table 10 - Linear correlations between modelled versus measured GPP and λE for each season on the year 2013 under different ozone thresholds. Slope, R-squared and RMSE values are marked in bold where ozone corrections ameliorates or provide the same values of the control run simulation (no ozone effect). Values marked in red indicates the best values. For all the regressions both Slope (t-test) and model (Ftest) pValues resulted to be statistically significant (pValues <0.05).

Year	season	Run	GPP O_3 > 40 ppb									λE O_3 > 40 ppb								
			β			R^2			RMSE			***β***			R^2			RMSE		
			BWB	**MD**	**JV**	**BWB**	**MD**	**JV**	**BWB**	**MD**	**JV**	**BWB**	**MD**	**JV**	**BWB**	**MD**	**JV**	**BWB**	**MD**	**JV**
2013	Winter	Control	0.99	1.11	1.16	0.84	0.79	0.77	2.55	3.64	4.30	0.91	1.15	0.75	0.77	0.81	0.81	20.20	23.75	21.22
		thr0	0.78	0.75	**1.01**	**0.84**	0.78	**0.78**	3.50	4.03	**3.14**	0.80	0.28	0.65	**0.78**	0.67	0.80	21.08	45.85	24.98
		thr1	0.78	**1.03**	**1.01**	**0.84**	0.76	**0.78**	3.50	**3.38**	**3.14**	0.80	**0.95**	0.65	**0.78**	0.59	0.80	21.08	31.22	24.98
		thr2	0.78	**1.11**	**1.02**	**0.84**	**0.79**	**0.78**	3.50	**3.64**	**3.14**	0.80	**1.15**	0.65	**0.78**	**0.81**	0.80	21.08	**23.62**	24.94
		thr3	0.83	**1.05**	**1.03**	0.79	0.72	**0.79**	3.33	3.86	3.09	0.83	**1.03**	0.66	**0.77**	0.66	**0.81**	20.67	28.88	24.60
		thr4	0.95	**1.11**	**1.10**	0.83	**0.79**	**0.78**	2.57	**3.64**	3.61	0.89	**1.15**	0.70	**0.77**	**0.81**	0.80	20.62	**23.63**	22.99
		thr5	0.98	**1.06**	**1.15**	**0.84**	0.74	**0.77**	**2.50**	3.67	4.18	**0.91**	**1.05**	0.74	**0.77**	0.69	0.80	20.30	27.57	21.55
	Spring	Control	1.16	1.16	1.45	0.67	0.73	0.61	6.21	5.50	10.69	1.14	1.12	1.05	0.75	0.79	0.69	41.34	35.70	41.76
		thr0	**0.92**	0.68	**1.24**	**0.67**	**0.78**	**0.62**	**4.65**	5.67	**7.65**	**1.01**	0.27	0.91	**0.75**	0.64	**0.69**	**34.53**	70.79	**37.30**
		thr1	**0.92**	**0.91**	**1.24**	**0.67**	0.54	**0.62**	**4.65**	5.91	**7.65**	**1.01**	0.67	0.91	**0.75**	0.42	**0.69**	**34.53**	56.23	**37.30**
		thr2	**0.92**	**1.05**	**1.24**	**0.67**	0.61	**0.62**	**4.65**	5.86	**7.64**	**1.01**	**0.97**	0.91	**0.75**	0.65	**0.69**	**34.56**	42.43	**37.25**
		thr3	**0.93**	**1.07**	**1.25**	**0.67**	0.63	**0.63**	**4.61**	5.67	**7.62**	**1.01**	**0.93**	0.92	**0.75**	0.62	**0.69**	**34.50**	43.45	**37.09**
		thr4	**0.95**	**1.11**	**1.26**	**0.68**	0.69	**0.65**	**4.56**	**5.37**	**7.67**	**1.02**	**1.00**	0.92	**0.75**	0.67	**0.69**	**34.75**	41.76	**36.85**
		thr5	**1.01**	**1.09**	**1.31**	**0.69**	0.67	**0.67**	**4.70**	**5.46**	**7.98**	**1.05**	**0.97**	0.94	**0.75**	0.64	**0.70**	**36.50**	43.44	**36.35**
	Summer	Control	1.72	1.10	1.57	0.63	0.63	0.55	8.88	3.54	7.92	1.51	1.07	0.93	0.58	0.57	0.52	115.65	70.06	66.72
		thr0	**1.36**	0.74	**1.33**	**0.63**	**0.65**	**0.57**	**5.57**	**3.35**	**5.67**	**1.33**	0.45	0.81	**0.58**	0.50	**0.52**	**93.69**	79.52	**62.63**
		thr1	**1.36**	**0.91**	**1.33**	**0.63**	0.57	**0.57**	**5.57**	**3.33**	**5.67**	**1.33**	0.67	0.81	**0.58**	0.40	**0.52**	**93.70**	75.20	**62.63**
		thr2	**1.36**	**1.00**	**1.34**	**0.63**	0.55	**0.58**	**5.58**	3.66	**5.70**	**1.33**	0.88	0.82	**0.58**	0.47	**0.52**	**94.00**	71.36	**62.87**
		thr3	**1.37**	**1.02**	**1.40**	**0.63**	0.59	**0.59**	**5.69**	**3.49**	**6.15**	**1.34**	**0.92**	0.86	**0.58**	0.46	**0.53**	**95.99**	75.24	**63.01**
		thr4	**1.43**	**1.05**	**1.45**	0.60	0.60	**0.59**	**6.37**	**3.51**	**6.61**	**1.38**	**1.02**	0.90	0.57	0.51	**0.54**	**102.62**	73.78	**62.62**
		thr5	**1.51**	**1.09**	**1.50**	0.58	**0.63**	**0.59**	**7.27**	**3.53**	**7.00**	**1.43**	**1.07**	0.92	0.57	**0.57**	**0.54**	**107.58**	70.18	**62.77**
	Fall	Control	1.40	1.02	1.43	0.60	0.56	0.61	8.09	5.30	8.15	1.74	1.35	1.11	0.61	0.63	0.53	84.46	54.28	47.07
		thr0	**1.12**	0.68	**1.25**	**0.60**	**0.59**	**0.62**	**5.54**	**4.81**	**6.29**	**1.53**	0.50	**0.98**	**0.61**	0.53	**0.54**	**68.72**	**43.91**	**40.14**
		thr1	**1.12**	0.92	**1.25**	**0.60**	**0.61**	**0.62**	**5.54**	**4.35**	**6.28**	**1.53**	**0.97**	**0.98**	**0.61**	0.47	**0.54**	**68.71**	**47.41**	**40.13**
		thr2	**1.12**	**0.98**	**1.26**	**0.60**	0.53	**0.62**	**5.54**	5.39	**6.39**	**1.53**	**1.23**	**1.00**	**0.61**	0.53	**0.56**	**68.77**	55.35	**39.99**
		thr3	**1.15**	**1.01**	**1.28**	0.59	0.55	**0.63**	**5.93**	**5.30**	**6.53**	**1.57**	**1.30**	**1.02**	0.60	0.59	**0.56**	**71.91**	53.85	**40.79**
		thr4	**1.20**	**1.01**	**1.31**	0.58	**0.56**	**0.64**	**6.53**	**5.23**	**6.69**	**1.62**	**1.33**	**1.04**	0.60	0.62	**0.56**	**75.84**	53.69	**41.62**
		thr5	**1.25**	**0.99**	**1.37**	0.57	**0.56**	**0.62**	**7.03**	**5.16**	**7.32**	**1.67**	**1.32**	**1.08**	0.60	0.61	0.54	**79.47**	53.59	**44.82**

Table 11 - Linear correlations between modelled versus measured GPP and λE for each season on the year 2014 under different ozone thresholds. Slope, R-squared and RMSE values are marked in bold where ozone corrections ameliorates or provide the same values of the control run simulation (no ozone effect). Values marked in red indicates the best values. For all the regressions both Slope (t-test) and model (Ftest) pValues resulted to be statistically significant (pValues <0.05).

Year	season	Run	GPP O_3 > 40 ppb									λE O_3 > 40 ppb								
			β			R^2			RMSE			β			R^2			RMSE		
			BWB	MD	JV	BWB	MD	JV	BWB	MD	JV	BWB	MD	JV	BWB	MD	JV	BWB	MD	JV
2014	Winter	Control	1.05	1.21	1.26	0.71	0.67	0.68	3.63	5.24	5.74	0.95	1.20	0.76	0.49	0.47	0.43	41.30	53.65	37.92
		thr0	0.84	0.81	**1.09**	**0.71**	**0.68**	**0.69**	**3.56**	**3.84**	**4.03**	0.83	0.29	0.67	**0.49**	**0.49**	**0.44**	**37.09**	**39.48**	**35.69**
		thr1	0.84	**1.12**	**1.09**	**0.71**	0.62	**0.69**	**3.56**	**4.88**	**4.03**	0.83	**1.01**	0.67	**0.49**	0.40	**0.44**	**37.10**	**50.26**	**35.69**
		thr2	0.84	**1.21**	**1.10**	**0.71**	**0.67**	**0.70**	**3.56**	5.25	**4.01**	0.83	**1.20**	0.67	**0.49**	**0.47**	**0.44**	**37.09**	**53.48**	**35.68**
		thr3	0.89	**1.14**	**1.11**	0.70	0.62	**0.70**	**3.38**	**5.08**	**4.10**	0.87	**1.06**	0.68	**0.49**	0.40	**0.44**	**37.91**	**52.87**	**35.46**
		thr4	**1.00**	**1.21**	**1.19**	0.70	**0.67**	**0.69**	**3.49**	5.25	**4.87**	0.93	**1.20**	0.73	**0.49**	**0.47**	**0.44**	**40.22**	**53.49**	**36.18**
		thr5	**1.04**	**1.15**	**1.25**	**0.72**	0.64	**0.69**	**3.48**	**4.92**	**5.51**	**0.95**	**1.12**	**0.76**	**0.49**	0.44	**0.44**	**40.80**	**50.94**	**37.46**
	Spring	Control	1.22	1.21	1.51	0.44	0.46	0.39	9.09	8.65	13.63	0.93	0.91	0.83	0.44	0.45	0.37	71.54	67.78	73.45
		thr0	**0.97**	0.73	**1.29**	**0.44**	**0.54**	**0.41**	**6.81**	**5.69**	**10.49**	0.82	0.21	0.72	0.43	0.40	**0.37**	**65.29**	78.62	**67.87**
		thr1	**0.97**	**0.97**	**1.29**	**0.44**	0.40	**0.41**	**6.81**	**7.34**	**10.49**	0.82	0.57	0.72	0.43	0.31	**0.37**	**65.30**	70.20	**67.87**
		thr2	**0.97**	**1.11**	**1.30**	**0.44**	0.41	**0.41**	**6.80**	**8.25**	**10.48**	0.82	0.78	0.72	0.43	0.37	**0.37**	**65.32**	71.07	**67.84**
		thr3	**0.98**	**1.12**	**1.31**	**0.45**	0.42	**0.42**	**6.72**	**8.24**	**10.47**	0.82	0.75	0.73	0.43	0.38	**0.37**	**65.41**	69.78	**67.70**
		thr4	**1.01**	**1.16**	**1.33**	**0.47**	0.45	**0.43**	**6.64**	**8.26**	**10.54**	0.83	0.82	0.73	**0.44**	0.42	**0.37**	**65.87**	67.89	**67.54**
		thr5	**1.07**	**1.14**	**1.37**	**0.48**	0.44	**0.44**	**6.92**	**8.14**	**10.92**	0.86	0.79	0.74	**0.44**	0.40	**0.38**	**66.77**	69.00	**67.45**
	Summer	Control	1.23	0.79	1.29	0.61	0.50	0.31	6.54	5.48	11.66	1.25	0.92	0.92	0.56	0.56	0.44	106.12	72.37	90.60
		thr0	**0.97**	0.53	**1.08**	**0.61**	**0.59**	**0.32**	**4.51**	7.32	**9.06**	**1.11**	0.37	0.80	**0.56**	0.49	**0.45**	**88.09**	103.89	**82.84**
		thr1	**0.97**	0.62	**1.08**	**0.61**	0.43	**0.32**	**4.51**	6.85	**9.06**	**1.11**	0.55	0.80	**0.56**	0.39	**0.45**	**88.09**	92.75	**82.84**
		thr2	**0.97**	0.73	**1.09**	**0.61**	0.45	**0.32**	**4.51**	6.06	**8.99**	**1.11**	0.78	0.80	**0.56**	0.45	**0.46**	**88.25**	82.80	**82.01**
		thr3	**0.98**	0.72	**1.13**	**0.61**	0.45	**0.36**	**4.49**	6.07	**8.80**	**1.12**	0.79	0.83	**0.56**	0.45	**0.47**	**89.38**	83.08	**81.05**
		thr4	**1.03**	0.76	**1.15**	**0.62**	0.48	**0.37**	**4.64**	5.68	**8.81**	**1.15**	0.88	0.85	0.55	0.53	**0.47**	**94.30**	74.83	**80.92**
		thr5	**1.09**	0.77	**1.18**	**0.62**	**0.50**	**0.38**	**5.02**	5.55	**9.00**	**1.19**	0.90	0.87	0.55	0.53	**0.47**	**98.97**	76.10	**81.62**
	Fall	Control	1.02	0.67	0.86	0.46	0.40	0.31	6.46	6.70	7.77	1.07	0.82	0.63	0.49	0.51	0.38	92.00	70.69	83.10
		thr0	0.81	0.49	0.75	**0.46**	**0.51**	**0.34**	**5.78**	7.83	**7.18**	**0.94**	0.32	0.55	**0.49**	0.47	**0.39**	**80.97**	93.42	**82.14**
		thr1	0.81	0.59	0.75	**0.46**	**0.49**	**0.34**	**5.78**	6.83	**7.17**	**0.94**	0.60	0.55	**0.49**	0.46	**0.39**	**80.97**	74.62	**82.12**
		thr2	0.81	0.65	0.79	**0.46**	0.38	**0.37**	**5.77**	6.91	**6.76**	**0.94**	0.73	0.58	**0.49**	0.44	**0.41**	**81.05**	78.52	**79.78**
		thr3	0.86	0.66	0.80	**0.51**	0.39	**0.37**	**5.30**	6.83	**6.78**	**0.97**	0.77	0.59	**0.49**	0.46	**0.41**	**82.66**	75.68	**79.40**
		thr4	0.93	**0.67**	0.81	**0.54**	**0.40**	**0.36**	**5.07**	**6.70**	**6.88**	**1.02**	**0.82**	0.60	**0.50**	**0.51**	**0.40**	**84.00**	**70.59**	**80.29**
		thr5	0.97	**0.67**	0.83	**0.52**	**0.41**	**0.34**	**5.48**	**6.63**	**7.27**	**1.05**	0.81	0.61	**0.50**	**0.51**	**0.38**	**87.57**	**70.36**	**82.55**

3.3.1.2 Blodgett – *Pinus ponderosa*

Linear regressions between observed and simulated GPP for the years 2013 and 2014 are shown in Table 12. The best "Control" runs (i.e. no ozone effect) between simulated and observed GPP were provided by MD (R^2 of 0.82 and 0.76, RMSE of 3.69 and 4.78 for 2003 and 2004, respectively) and by BWB (R^2 of 0.78 and 0.76, RMSE of 3.92 and 4.70 for 2003 and 2004, respectively), followed by JV (R^2 of 0.67 and 0.53, RMSE of 6.88 and 7.36 for 2003 and 2004, respectively) g_s models. Regressions between observed and simulated λE identified MD (R^2 of 0.78 and 0.72, RMSE of 48.96 and 47.48 for 2003 and 2004, respectively) and BWB (R^2 of 0.78 and 0.76, RMSE of 50.62 and 55.09 for 2003 and 2004, respectively) as the best models, followed by JV (R^2 of 0.72 and 0.68, RMSE of 69.06 and 68.07 for 2003 and 2004, respectively).

Focusing on GPP, when compared to their relative control runs, improvements in model accuracy were observed only by applying the BWB_{FO3} correction in both years (RMSE reduced up to 3 and 18% in 2003 and 2004, respectively). However, none of the correction factors implemented in this study were found to ameliorate the model accuracy in simulating λE (Table 12). Linear regressions on data filtered at high ozone concentrations (above 40 ppb) provided similar results (not shown). In general, for the whole year, simulations including ozone corrections with critical ozone thresholds (Y) of 0 and 1 nmol m^{-2} s^{-1} (thr0 and thr1) led to an overall increase (RMSE reduced by 14 and 18% in 2003 and 2004, respectively) in the accuracy of the BWB g_s model in simulating GPP, when compared to the "Control" run.

On a seasonal scale, focusing on data filtered at high ozone concentrations (Table 13-14), the ozone correction that provided the best results in simulating GPP and λE for 2003 and 2004 was the application of the BWB_{FO3} model. Focusing on the BWB_{FpO3} model, in both 2003 and 2004, the critical ozone threshold that increased the model accuracy in simulating GPP was thr1 in Winter (R^2 = 0.88 and 0.85, RMSE = 1.43 and 1.34) and Spring (R^2 = 0.71 and 0.80, RMSE = 3.10 and 2.76). In Summer, thr4 (R^2 = 0.46, RMSE = 5.04) and thr5 (R^2 = 0.75, RMSE = 5.36) resulted to be the most appropriate thresholds for the years 2003 and 2004, respectively. In Fall 2003, the best model run was observed in thr4 (R^2 = 0.77, RMSE = 3.75), while thr3 (R^2 = 0.56, RMSE = 5.76) resulted to be most appropriate in 2004. Focusing on λE in 2003, the critical ozone threshold that increased the model accuracy was thr5 in Spring (R^2 = 0.76, RMSE = 42.05) and thr2 in Fall (R^2 = 0.73, RMSE = 43.94). In 2004, thr5 (R^2 = 0.6, RMSE = 23.33) and thr3 (R2=0.66, RMSE= 40.68) resulted to be the most

appropriate simulations for Winter and Fall, respectively. No relevant ameliorations from control run were observed For MD_K and JV_{fO3} models.

Table 12 - Linear correlations between modelled versus measured GPP and λE for the whole years 2003 and 2004 under different ozone thresholds. Thresholds (thr) are critical ozone fluxes above 0, 1, 2, 3, 4, 5 nmol m^{-2} s^{-1}. Thr0 to thr5 = high to low sensitivity to ozone. Intercept was forced to zero. Slope, R-squared and RMSE values are marked in bold where ozone corrections ameliorates or provide the same values of the control run simulation (no ozone effect). Values marked in red indicates the best values. For all the regressions both Slope (t-test) and model (Ftest) pValues resulted to be statistically significant (pValues <0.05).

Variable	year	Run	β			R^2			RMSE		
			BWB	MD	JV	BWB	MD	JV	BWB	MD	JV
GPP	2003	control	1.14	1.16	1.35	0.78	0.82	0.67	3.92	3.69	6.88
		thr0	**1.01**	0.34	0.13	0.71	0.61	0.58	**3.82**	7.70	9.96
		thr1	**1.01**	0.74	**0.75**	0.71	0.41	0.24	**3.80**	6.05	8.35
		thr2	**1.02**	**0.84**	**0.98**	0.71	0.48	0.37	**3.90**	5.52	7.51
		thr3	**1.04**	**1.06**	**1.18**	0.72	0.68	0.50	3.93	4.38	7.24
		thr4	**1.09**	**1.13**	**1.24**	0.75	0.77	0.56	**3.81**	3.95	7.04
		thr5	**1.10**	**1.15**	**1.15**	0.75	0.81	0.49	**3.91**	3.76	7.12
	2004	control	1.30	1.31	1.36	0.76	0.76	0.53	4.70	4.78	7.36
		thr0	**1.16**	0.40	0.15	0.72	0.63	**0.57**	**3.98**	6.10	8.36
		thr1	**1.16**	**0.81**	**0.74**	0.72	0.38	0.21	**3.98**	5.62	7.73
		thr2	**1.18**	**0.98**	**1.11**	0.74	0.47	0.37	**4.02**	5.31	7.38
		thr3	**1.22**	**1.19**	**1.23**	0.75	0.64	0.45	**4.19**	4.91	**7.25**
		thr4	**1.26**	**1.22**	**1.21**	**0.76**	0.65	0.43	**4.38**	5.01	**7.25**
		thr5	**1.28**	**1.28**	**1.18**	**0.76**	0.71	0.42	**4.51**	4.90	**7.17**
λE	2003	control	0.81	0.88	1.11	0.78	0.78	0.72	50.62	48.96	69.06
		thr0	0.75	0.16	0.16	**0.78**	0.70	0.70	54.85	130.37	130.35
		thr1	0.75	0.52	0.66	**0.78**	0.38	0.35	54.65	98.04	101.65
		thr2	0.76	0.59	0.80	**0.78**	0.44	0.46	53.89	90.39	89.40
		thr3	0.77	0.79	**0.96**	**0.79**	0.64	0.57	52.34	66.06	80.40
		thr4	0.79	0.86	**1.03**	**0.79**	0.74	0.64	51.25	53.76	75.44
		thr5	0.80	0.87	**0.96**	**0.79**	0.77	0.58	50.81	50.52	79.63
	2004	control	0.78	0.85	1.01	0.76	0.72	0.68	55.09	57.48	68.07
		thr0	0.71	0.15	0.15	**0.76**	0.62	0.62	59.31	131.53	131.50
		thr1	0.71	0.47	0.57	**0.76**	0.33	0.31	59.24	105.06	106.25
		thr2	0.72	0.58	0.82	**0.76**	0.41	0.5	58.23	94.79	85.85
		thr3	0.74	0.75	0.91	**0.76**	0.59	0.58	57.14	73.14	76.91
		thr4	0.75	0.78	0.9	**0.76**	0.62	0.56	56.25	69.24	78.96
		thr5	0.77	0.82	0.88	**0.76**	0.68	0.56	55.45	62.09	78.83

Table 13 - Linear correlations between modelled versus measured GPP and λE for each season on the year 2003 under different ozone thresholds. Slope, R-squared and RMSE values are marked in bold where ozone corrections ameliorates or provide the same values of the control run simulation (no ozone effect). Values marked in red indicates the best values. For all the regressions both Slope (t-test) and model (Ftest) pValues resulted to be statistically significant (pValues <0.05).

Year	season	Run	GPP O_3 > 40 ppb									λE O_3 > 40 ppb								
			β			R^2			RMSE			*β*			R^2			RMSE		
			BWB	MD	JV	BWB	MD	JV	BWB	MD	JV	BWB	MD	JV	BWB	MD	JV	BWB	MD	JV
2003	Winter	Control	0.99	1.11	0.53	0.87	0.86	0.86	1.46	1.84	3.02	0.55	0.64	0.38	0.77	0.68	0.66	30.71	29.04	40.08
		thr0	0.91	0.57	0.21	**0.87**	0.76	0.69	**1.46**	2.91	4.87	0.50	0.14	0.14	**0.77**	0.67	**0.67**	33.09	53.44	53.44
		thr1	0.94	0.88	0.47	**0.88**	0.67	0.75	**1.43**	2.54	3.41	0.53	0.41	0.34	**0.77**	0.41	0.62	31.98	42.35	42.70
		thr2	0.98	**1.11**	**0.53**	**0.88**	**0.86**	**0.86**	**1.45**	**1.84**	**3.02**	**0.55**	**0.64**	**0.38**	0.76	**0.68**	**0.66**	30.87	**29.03**	**40.08**
		thr3	**0.99**	**1.11**	**0.53**	**0.87**	**0.86**	**0.86**	**1.46**	**1.84**	**3.02**	**0.55**	**0.64**	**0.38**	**0.77**	**0.68**	**0.66**	**30.71**	**29.03**	**40.08**
		thr4	**0.99**	**1.11**	**0.53**	**0.87**	**0.86**	**0.86**	**1.46**	**1.84**	**3.02**	**0.55**	**0.64**	**0.38**	**0.77**	**0.68**	**0.66**	**30.71**	**29.03**	**40.08**
		thr5	**0.99**	**1.11**	**0.53**	**0.87**	**0.86**	**0.86**	**1.46**	**1.84**	**3.02**	**0.55**	**0.64**	**0.38**	**0.77**	**0.68**	**0.66**	**30.71**	**29.03**	**40.08**
	Spring	Control	1.17	1.21	0.97	0.74	0.80	0.46	3.48	3.33	4.69	0.75	0.69	0.73	0.75	0.70	0.52	42.08	47.84	59.41
		thr0	**1.06**	0.46	0.16	0.70	0.67	0.59	**3.12**	5.25	7.76	0.69	0.12	0.12	**0.75**	0.69	**0.69**	45.63	101.65	101.65
		thr1	**1.06**	**0.91**	0.76	0.71	0.48	0.29	**3.10**	4.33	5.73	0.69	0.50	0.58	**0.75**	0.39	0.36	45.57	72.53	73.92
		thr2	**1.08**	**1.02**	0.92	0.73	0.59	0.41	**3.02**	3.84	4.95	0.70	0.54	0.70	**0.76**	0.47	0.47	44.42	66.89	63.33
		thr3	**1.10**	**1.13**	0.96	0.73	0.71	0.45	**3.15**	3.49	4.76	0.72	0.62	**0.73**	**0.77**	0.59	0.51	43.14	57.48	60.24
		thr4	**1.15**	**1.21**	0.85	0.73	**0.80**	0.40	**3.39**	3.34	4.85	0.74	**0.69**	0.60	**0.76**	**0.70**	0.43	42.24	48.29	67.73
		thr5	**1.17**	**1.21**	**0.97**	**0.74**	**0.80**	**0.46**	**3.45**	**3.33**	**4.69**	**0.75**	**0.69**	**0.73**	**0.76**	**0.70**	**0.52**	**42.05**	**47.84**	59.47
	Summer	Control	1.12	1.12	1.57	0.51	0.62	0.63	5.20	4.38	10.49	0.82	0.88	1.22	0.64	0.68	0.65	68.91	60.82	94.76
		thr0	**0.99**	0.27	0.11	0.42	0.58	0.55	**5.15**	11.53	14.16	0.76	0.15	0.15	0.63	0.60	0.60	75.55	188.46	188.46
		thr1	**0.99**	0.66	**0.81**	0.43	0.15	0.08	**5.10**	8.80	12.48	0.76	0.52	0.69	0.63	0.21	0.18	75.56	140.74	148.71
		thr2	**0.98**	0.75	**1.05**	0.39	0.18	0.14	5.42	8.00	11.55	0.76	0.57	**0.82**	0.63	0.25	0.25	75.38	131.60	133.15
		thr3	**1.00**	**1.00**	**1.36**	0.40	0.35	0.30	5.37	5.93	10.89	0.77	0.77	**1.05**	**0.65**	0.45	0.42	72.59	93.35	111.91
		thr4	**1.04**	**1.09**	**1.44**	0.46	0.50	0.38	**5.04**	5.00	10.70	0.79	0.86	**1.13**	**0.65**	0.60	0.51	70.44	70.47	104.16
		thr5	**1.06**	**1.11**	**1.28**	0.45	0.57	0.24	5.21	4.56	10.92	0.80	0.87	**1.01**	**0.65**	0.65	0.39	69.39	64.40	115.23
	Fall	Control	1.27	1.30	1.16	0.77	0.75	0.59	3.91	4.20	4.29	0.88	1.07	1.11	0.71	0.76	0.71	44.29	44.57	54.43
		thr0	**1.07**	0.42	0.16	0.58	0.63	0.57	**3.90**	5.73	8.02	0.80	0.21	0.21	**0.71**	0.64	0.64	46.03	105.35	105.35
		thr1	**1.07**	0.86	0.70	0.57	0.37	0.23	3.93	4.82	6.10	0.81	0.63	0.71	**0.71**	0.35	0.35	45.52	80.18	79.91
		thr2	**1.14**	**0.95**	**1.00**	0.65	0.41	0.44	**3.71**	4.83	4.66	0.83	0.72	0.95	**0.73**	0.39	0.55	**43.94**	76.47	62.51
		thr3	**1.18**	**1.24**	**0.90**	0.67	0.67	0.34	**3.85**	4.32	5.33	0.84	**1.02**	0.89	**0.72**	0.67	0.45	**43.76**	52.13	72.99
		thr4	**1.25**	**1.27**	**1.08**	**0.77**	0.71	0.50	**3.75**	4.26	4.53	0.86	**1.04**	1.05	**0.72**	0.72	0.63	**43.89**	48.30	59.12
		thr5	**1.26**	**1.29**	**1.06**	**0.77**	0.74	0.49	**3.85**	4.22	4.54	0.87	**1.07**	**1.02**	**0.71**	**0.76**	0.60	**44.15**	45.12	61.41

Table 14 - Linear correlations between modelled versus measured GPP and λE for each season on the year 2004 under different ozone thresholds. Slope, R-squared and RMSE values are marked in bold where ozone corrections ameliorates or provide the same values of the control run simulation (no ozone effect). Values marked in red indicates the best values. For all the regressions both Slope (t-test) and model (Ftest) pValues resulted to be statistically significant (pValues <0.05).

Year	season	Run	GPP O_3 > 40 ppb									λE O_3 > 40 ppb								
			β			R^2			RMSE			*β*			R^2			RMSE		
			BWB	MD	JV	BWB	MD	JV	BWB	MD	JV	BWB	MD	JV	BWB	MD	JV	BWB	MD	JV
2004	Winter	Control	1.05	1.23	0.58	0.85	0.86	0.81	1.43	1.95	2.27	0.60	0.59	0.36	0.60	0.53	0.46	23.41	25.07	30.97
		thr0	**0.97**	0.70	0.26	**0.85**	0.74	0.61	**1.30**	1.99	3.73	0.54	0.14	0.14	**0.60**	**0.57**	**0.57**	24.52	38.61	38.61
		thr1	**0.99**	**0.95**	0.50	**0.85**	0.70	0.69	**1.34**	2.00	2.72	0.56	0.35	0.27	**0.61**	**0.57**	0.39	24.04	30.35	33.95
		thr2	**1.05**	**1.23**	**0.58**	**0.85**	**0.86**	**0.81**	1.44	**1.95**	**2.27**	**0.60**	**0.59**	**0.36**	**0.60**	**0.53**	**0.46**	23.47	25.07	30.97
		thr3	**1.05**	**1.23**	**0.58**	**0.85**	**0.86**	**0.81**	**1.43**	**1.95**	**2.27**	**0.60**	**0.59**	**0.36**	**0.60**	**0.53**	**0.46**	**23.41**	**25.07**	**30.97**
		thr4	**1.05**	**1.23**	**0.58**	**0.85**	**0.86**	**0.81**	**1.43**	**1.95**	**2.27**	**0.60**	**0.59**	**0.36**	**0.60**	**0.53**	**0.46**	**23.41**	**25.07**	**30.97**
		thr5	**1.05**	**1.23**	**0.58**	**0.85**	**0.86**	**0.81**	**1.43**	**1.95**	**2.27**	**0.60**	**0.59**	**0.36**	**0.60**	**0.53**	**0.47**	**23.33**	**25.00**	**30.91**
	Spring	Control	1.15	1.13	0.87	0.80	0.84	0.59	3.31	2.83	3.91	0.69	0.65	0.59	0.79	0.75	0.71	51.97	57.25	64.32
		thr0	**1.06**	0.41	0.15	**0.80**	0.71	**0.64**	**2.76**	6.00	8.43	0.63	0.12	0.12	**0.79**	0.71	**0.71**	57.07	120.68	120.68
		thr1	**1.06**	0.83	0.59	**0.80**	0.49	0.32	**2.76**	4.60	5.98	0.63	0.42	0.39	**0.79**	0.40	0.40	57.02	90.24	92.16
		thr2	**1.08**	**0.96**	0.63	**0.81**	0.62	0.38	**2.82**	3.82	5.49	0.65	0.51	0.42	**0.80**	0.53	0.46	55.16	78.29	87.76
		thr3	**1.11**	**1.07**	0.79	**0.81**	0.76	0.52	**2.95**	3.11	4.37	0.66	0.60	0.53	**0.80**	0.66	0.65	53.72	65.12	72.13
		thr4	**1.14**	**1.13**	0.85	**0.80**	**0.84**	0.57	**3.19**	**2.83**	4.03	0.68	**0.65**	0.58	**0.79**	**0.75**	0.69	52.53	**57.25**	65.70
		thr5	**1.15**	**1.13**	0.84	**0.80**	**0.84**	0.55	**3.28**	**2.83**	4.18	0.68	**0.65**	0.58	**0.79**	**0.75**	0.67	52.08	**57.20**	66.88
	Summer	Control	1.37	1.37	1.81	0.74	0.75	0.67	5.76	5.80	11.46	0.77	0.87	1.15	0.66	0.70	0.68	74.77	64.00	84.26
		thr0	**1.21**	0.34	0.13	0.63	0.59	0.51	**4.81**	8.32	**10.82**	0.71	0.15	0.15	0.65	0.55	0.55	82.16	189.14	189.06
		thr1	**1.21**	**0.73**	**0.87**	0.63	0.19	0.11	**4.80**	7.44	**11.24**	0.71	0.45	0.61	0.65	0.20	0.19	82.09	151.13	152.04
		thr2	**1.23**	**0.89**	**1.47**	0.66	0.25	0.32	**4.74**	6.92	**11.00**	0.72	0.54	0.94	**0.66**	0.26	0.40	81.03	136.56	112.91
		thr3	**1.26**	**1.20**	**1.65**	0.70	0.46	0.47	**4.87**	6.17	**11.14**	0.73	0.75	**1.05**	**0.67**	0.47	0.52	79.07	96.44	98.97
		thr4	**1.30**	**1.20**	**1.55**	0.73	0.45	0.37	**5.11**	6.40	**11.17**	0.75	0.77	**1.00**	**0.66**	0.49	0.45	77.16	93.38	107.80
		thr5	**1.33**	**1.31**	**1.49**	**0.75**	0.60	0.33	**5.36**	6.08	**11.01**	0.76	0.84	0.96	**0.67**	0.61	0.43	75.56	75.45	108.60
	Fall	Control	1.55	1.62	1.21	0.55	0.55	0.40	6.07	6.47	4.97	1.02	1.27	1.21	0.65	0.61	0.58	42.38	64.05	62.43
		thr0	**1.33**	0.56	0.21	0.46	**0.64**	**0.56**	**5.26**	**3.44**	5.69	0.93	0.24	0.24	**0.66**	0.53	0.53	**39.28**	75.96	75.96
		thr1	**1.32**	**1.16**	**0.87**	0.46	0.35	0.24	**5.27**	**5.31**	5.11	0.94	**0.83**	0.88	**0.66**	0.33	0.36	**39.22**	68.85	67.97
		thr2	**1.39**	**1.37**	**1.07**	0.49	0.43	0.33	**5.42**	**5.84**	**4.93**	0.97	**1.03**	**1.06**	**0.67**	0.42	0.47	**39.38**	68.51	64.97
		thr3	**1.51**	**1.50**	**1.01**	**0.56**	0.49	0.32	**5.76**	**6.19**	**4.76**	**1.00**	**1.17**	**1.00**	**0.66**	0.51	0.43	**40.68**	67.83	65.89
		thr4	**1.53**	**1.58**	**1.18**	**0.55**	0.52	**0.40**	**5.95**	**6.43**	**4.84**	**1.01**	**1.24**	**1.18**	**0.65**	0.58	0.55	**41.97**	64.85	**62.26**
		thr5	**1.53**	**1.62**	**1.21**	**0.55**	**0.55**	**0.40**	**5.99**	**6.47**	**4.96**	**1.01**	**1.27**	**1.21**	**0.66**	**0.61**	**0.58**	**42.06**	64.06	**62.40**

3.3.2 AIRTREE

3.3.2.1 Ozone correction impact on *Quercus ilex* and *Pinus ponderosa*

The same approach used for the FORCAsT model was applied to AIRTREE to both CPZ and BLD sites (Table 15 and 16). The model "Control" run (i.e. the model parameterization resulting from the calibration procedure using data collected at all ozone concentrations) for CPZ showed a good linear correlation with observed GPP (R^2=0.63) and λE (R^2=0.64). The application of the BWB_{FO3} correction at critical ozone thresholds between 3 to 5 nmol m^{-2} s^{-1}, (thr3 to thr5 resulted to be the most appropriate thresholds to simulate ozone sensitivity in CPZ with the FORCAsT model), did not worsen the linear correlation between observed and simulated GPP and λE (same slope and R^2, RMSE reduced by 0.1%), while simulation at thr0 increased model accuracy (R^2=0.65 RMSE reduced by 18%) for λE. The control run for BLD showed a good linear correlation with observed GPP (R^2=0.66) while a poor correlation was found with λE (R^2=0.40). The application of the BWB_{FO3} correction at critical ozone thresholds between thr0 to thr2 (thr0 and thr1 resulted to be the most appropriate thresholds to simulate ozone sensitivity in BLD with the FORCAsT model) resulted to be the best thresholds to simulate the ozone impact on GPP (R^2=0.7, RMSE reduced by 4.7%) while no improvement were found for λE (Table 15). Linear regressions on data filtered at high ozone concentrations (above 40 ppb) provided similar results (not shown).

To better focus on ozone effects, regressions between modelled and measured values after filtering the hourly dataset for ozone concentration which exceeded 40 ppb were performed, since the AIRTREE model was calibrated on data collected at ozone concentration below 40 ppb. The application of the BWB_{FO3} correction at different critical ozone thresholds improved model accuracy at the seasonal level in both study sites (table 16). Focusing on CPZ, high threshold (thr4 to thr5) resulted to be appropriate to simulate both GPP and λE in Winter (same slope and R^2 and RMSE of the control run). In Spring thr5 provided the best results for both GPP (same slope, R^2 and RMSE of the control run) and λE (R^2=0.7, RMSE reduced by 0.3%). In Summer, thr1 improved the model accuracy for GPP (R^2=0.59, RMSE reduced by 10%) while thr0 improved λE simulation (R^2=0.54, RMSE reduced by 15.4%). In Fall thr1 improved the model accuracy for GPP (R^2=0.65, RMSE reduced by 5.9%) while thr0 improved λE simulation (R^2=0.59, RMSE reduced by 27.9%). Similar results were observed in regressions performed on the whole dataset (not shown).

Focusing on BLD site, low thresholds (thr1 and thr2) resulted to be appropriate to simulate GPP (R^2=0.74 and RMSE reduced by 3%) and λE (R^2=0.32, RMSE reduced by 2%) in Winter. Differences between threshold ameliorating model performance in simulating GPP and λE were found in Spring, when thr1 and thr2 resulted to be more appropriate for GPP (R^2=0.7, RMSE reduced by 12%), while thr3 to thr5 resulted to be appropriate to simulate λE (same slope, R^2 and RMSE of the control run). In Summer the best thresholds for both GPP and λE were found in thr3 to thr5 (same slope, R^2 and RMSE of the control run). Finally, in Fall, thr0 performed better for GPP (R^2=0.68, RMSE reduced by 15.6%), while thr3 to thr5 resulted to be more appropriate to simulate λE (same slope, R^2 and RMSE of the control run). Similar results were found in regression performed on the whole dataset (not shown).

Table 15 - The table shows linear correlations between modelled versus measured GPP and λE under different ozone thresholds for the year 2013 and 2003 for Castelporziano and Blodgett sites, respectively. Thresholds (thri) are critical ozone fluxes above 0, 1, 2, 3, 4, 5 nmol m^{-2} s^{-1}. Thr 0 to thr 5 = high to low sensitivity to ozone. Model was calibrated by excluding ambient ozone concentrations above 40 ppb. The correlation have been performed for GPP and λE values above 40 ppb. Intercept was forced to zero. Slope and R-squared values are marked in bold where ozone corrections ameliorates the correlation between measured and modelled GPP. For all the regressions both Slope (t-test) and model (Ftest) pValues resulted to be statistically significant (pValues <0.05).

Site	Data	Run	GPP			λE		
			Coeff.	R^2	RMSE	Coeff.	R^2	RMSE
Castelporziano	Unfiltered	control	0.88	0.63	4.46	1.03	0.64	48.87
		thr0	0.69	0.62	4.90	0.86	**0.65**	**41.39**
		thr1	0.74	0.60	4.84	0.88	0.63	**43.67**
		thr2	0.83	0.61	4.65	**1.01**	0.63	48.88
		thr3	0.87	**0.63**	**4.46**	**1.03**	**0.64**	**48.85**
		thr4	**0.88**	**0.63**	**4.46**	**1.03**	**0.64**	**48.84**
		thr5	**0.88**	**0.63**	**4.46**	**1.03**	**0.64**	**48.82**
	O_3 > 40 ppb	control	0.87	0.66	4.34	1.01	0.58	57.18
		thr0	0.69	0.65	**4.08**	0.84	**0.59**	**49.49**
		thr1	0.69	**0.66**	4.81	0.83	**0.59**	**49.52**
		thr2	0.79	0.63	**3.74**	0.98	0.57	**57.01**
		thr3	**0.87**	**0.66**	**4.14**	**1.01**	**0.58**	**57.14**
		thr4	**0.87**	**0.66**	5.00	**1.01**	**0.58**	**57.15**
		thr5	**0.87**	**0.66**	5.65	**1.01**	**0.58**	**57.15**
Blodgett	Unfiltered	control	0.82	0.66	76.27	0.33	0.40	7.30
		thr0	**0.93**	**0.70**	**74.30**	0.29	**0.40**	7.55
		thr1	**0.86**	**0.69**	**72.68**	0.31	**0.41**	7.38
		thr2	**0.86**	**0.69**	**72.68**	0.31	**0.41**	7.38
		thr3	**0.82**	**0.66**	**76.01**	**0.33**	**0.40**	**7.30**
		thr4	**0.82**	**0.66**	**76.23**	**0.33**	**0.40**	**7.30**
		thr5	**0.82**	**0.66**	**76.25**	**0.33**	**0.40**	**7.30**
	O_3 > 40 ppb	control	0.82	0.64	80.22	0.33	0.39	7.83
		thr0	**0.93**	**0.68**	**77.17**	0.29	0.39	8.12
		thr1	**0.86**	**0.67**	**75.96**	0.31	**0.41**	7.93
		thr2	**0.86**	**0.67**	**75.96**	0.31	**0.41**	7.93
		thr3	**0.82**	**0.64**	**79.92**	**0.33**	**0.39**	**7.83**
		thr4	**0.82**	**0.64**	**80.18**	**0.33**	**0.39**	**7.83**
		thr5	**0.82**	**0.64**	**80.21**	**0.33**	**0.39**	**7.83**

Table 16 - Linear correlations between modelled versus measured GPP and λE under different ozone thresholds for each season of the year 2013 and 2003 for Castelporziano and Blodgett sites, respectively. Slope, R-squared and RMSE values are marked in bold where ozone corrections ameliorates or provide the same values of the control run simulation (no ozone effect). Values marked in red indicates the best values. For all the regressions both Slope (t-test) and model (Ftest) pValues resulted to be statistically significant (pValues <0.05).

Season	Run	Castelporziano 2013						Blodgett 2003					
		GPP O_3>40 ppb			λE O_3>40 ppb			GPP O_3>40 ppb			λE O_3>40 ppb		
		Slope	R2adj	RMSE	Slope	R2adj	RMSE	Slope	R2adj	RMSE	Slope	R2adj	RMSE
Winter	Control	0.74	0.75	4.08	0.82	0.77	20.45	0.76	0.72	59.02	0.76	0.32	2.91
	thr0	0.58	**0.75**	5.65	0.70	**0.79**	23.42	**0.81**	**0.73**	59.70	0.67	**0.32**	**2.82**
	thr1	0.59	**0.76**	5.60	0.70	**0.79**	23.45	**0.79**	**0.74**	**57.29**	0.71	**0.32**	**2.85**
	thr2	0.71	0.73	4.45	0.79	**0.77**	21.23	**0.79**	**0.74**	**57.29**	0.71	**0.32**	**2.85**
	thr3	**0.74**	**0.75**	**4.08**	**0.82**	**0.77**	20.46	**0.76**	**0.72**	**59.01**	**0.76**	**0.32**	**2.91**
	thr4	**0.74**	**0.75**	**4.08**	**0.82**	**0.77**	**20.45**	**0.76**	**0.72**	59.04	**0.76**	**0.32**	**2.91**
	thr5	**0.74**	**0.75**	**4.08**	**0.82**	**0.77**	**20.45**	0.75	**0.72**	59.16	**0.76**	**0.32**	2.92
Spring	Control	0.82	0.66	4.81	0.83	0.69	38.12	0.73	0.64	84.87	0.54	0.31	5.32
	thr0	0.64	**0.66**	6.17	0.68	**0.70**	41.50	**0.83**	**0.70**	**75.43**	0.47	**0.31**	5.52
	thr1	0.65	**0.66**	6.10	0.69	**0.70**	41.10	**0.82**	**0.70**	**74.77**	0.48	**0.31**	5.46
	thr2	0.73	0.64	5.47	0.77	0.68	39.65	**0.82**	**0.70**	**74.77**	0.48	**0.31**	5.46
	thr3	**0.82**	**0.66**	**4.81**	0.82	**0.69**	**38.07**	**0.74**	**0.65**	**83.58**	0.53	**0.31**	5.33
	thr4	**0.82**	**0.66**	**4.81**	0.82	**0.70**	**38.01**	**0.73**	**0.64**	**84.77**	0.53	**0.31**	5.33
	thr5	**0.82**	**0.66**	**4.81**	0.82	**0.70**	**37.99**	**0.73**	**0.64**	**84.84**	0.53	**0.31**	5.33
Summer	Control	0.98	0.58	3.74	1.05	0.53	81.66	1.02	0.70	71.05	0.26	0.51	10.55
	thr0	0.89	0.57	**3.53**	0.90	**0.54**	**69.11**	1.13	**0.71**	80.44	0.23	**0.52**	10.91
	thr1	0.84	**0.59**	**3.37**	0.88	**0.53**	**69.55**	1.05	**0.72**	71.14	0.25	**0.51**	10.66
	thr2	**0.99**	**0.58**	**3.73**	**1.05**	**0.53**	81.76	1.05	**0.72**	71.14	0.25	**0.51**	10.66
	thr3	**0.98**	**0.58**	**3.74**	**1.05**	**0.53**	**81.66**	**1.02**	**0.70**	71.15	**0.26**	**0.51**	**10.55**
	thr4	**0.98**	**0.58**	**3.74**	**1.05**	**0.53**	81.67	**1.02**	**0.70**	71.08	**0.26**	**0.51**	**10.55**
	thr5	**0.98**	**0.58**	**3.74**	**1.05**	**0.53**	81.67	**1.02**	**0.70**	71.08	**0.26**	**0.51**	**10.55**
Fall	Control	1.01	0.65	4.14	1.31	0.60	58.29	0.65	0.60	93.15	0.37	0.46	5.85
	thr0	0.77	0.64	**3.95**	**1.02**	0.59	**41.98**	**0.77**	**0.68**	**78.63**	0.33	**0.46**	6.14
	thr1	0.78	**0.65**	**3.90**	**1.02**	0.59	**42.00**	**0.68**	**0.64**	**87.73**	0.36	**0.47**	5.91
	thr2	0.91	0.61	4.22	**1.25**	0.58	**55.96**	**0.68**	**0.64**	**87.73**	0.36	**0.47**	5.91
	thr3	**1.01**	**0.65**	4.15	**1.31**	**0.60**	**58.20**	**0.65**	**0.60**	**93.09**	**0.37**	**0.46**	**5.85**
	thr4	**1.01**	**0.65**	4.15	**1.31**	**0.60**	**58.29**	**0.65**	**0.60**	**93.06**	**0.37**	**0.46**	**5.85**
	thr5	**1.01**	**0.65**	4.15	**1.31**	**0.60**	**58.29**	**0.65**	**0.60**	**93.06**	**0.37**	**0.46**	**5.85**

3.3.2.2 Dynamic critical ozone threshold

A strong seasonality of the critical ozone threshold was found in both CPZ and BLD by both the AIRTREE and FORCAsT models. Correlations between daily THR (eq.64) and daily mean environmental variables were evaluated.

In CPZ (Figure 18), the Spearman correlation index (r_s) showed a negative correlation between THR and VPD (r_s= -0.58 $p<0.05$), air temperature (r_s= -0.68 $p<0.05$) and PAR (r_s= -0.33 $p<0.05$), a positive correlation between THR and SWC (r_s= 0.57 $p<0.05$)while no correlation was found with O_3 concentration.

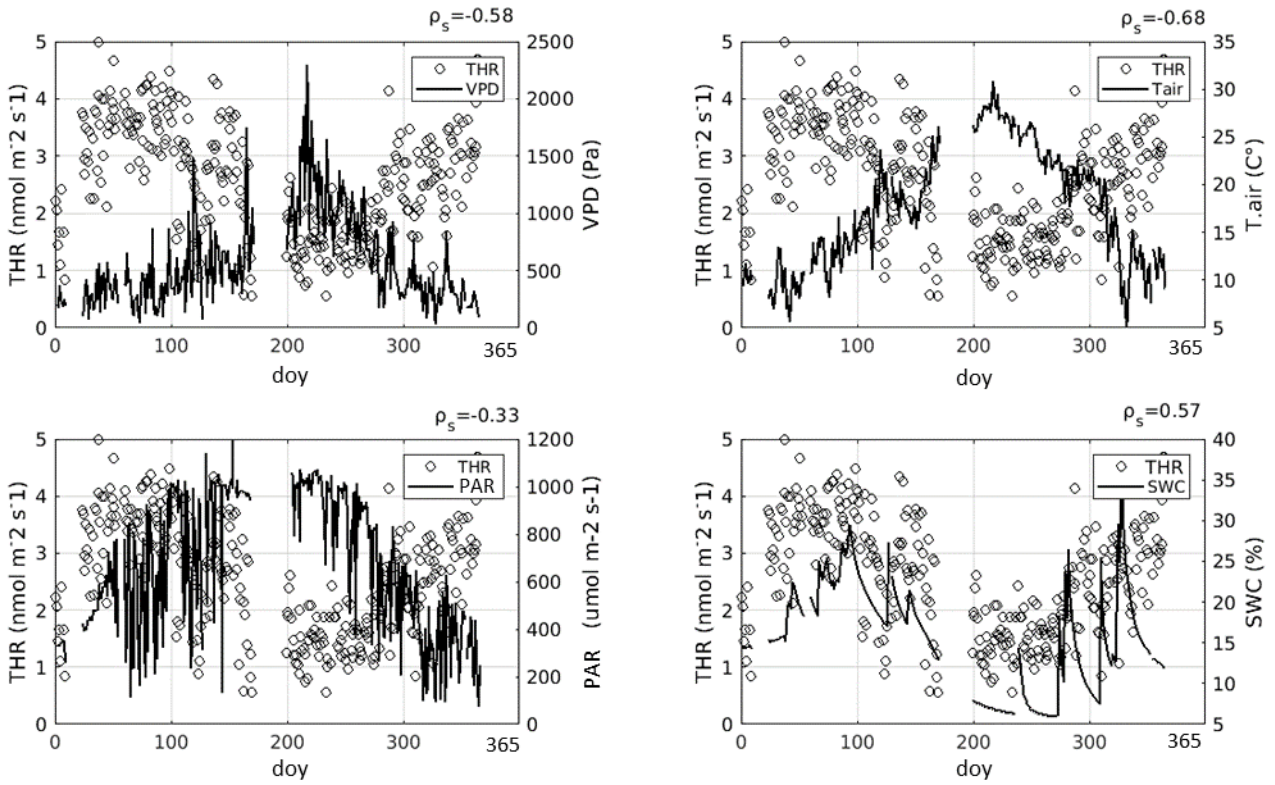

Figure 18 - Correlation values between THR (empty circles) and VPD (top left), Air temperature (Top right), PAR (bottom left) and SWC (Bottom right) for CPZ site for the year 2013.

Response functions of THR to these variables were developed and a multiplicative algorithm to simulate a dynamic ozone threshold was developed (Figure 19, eq.65).

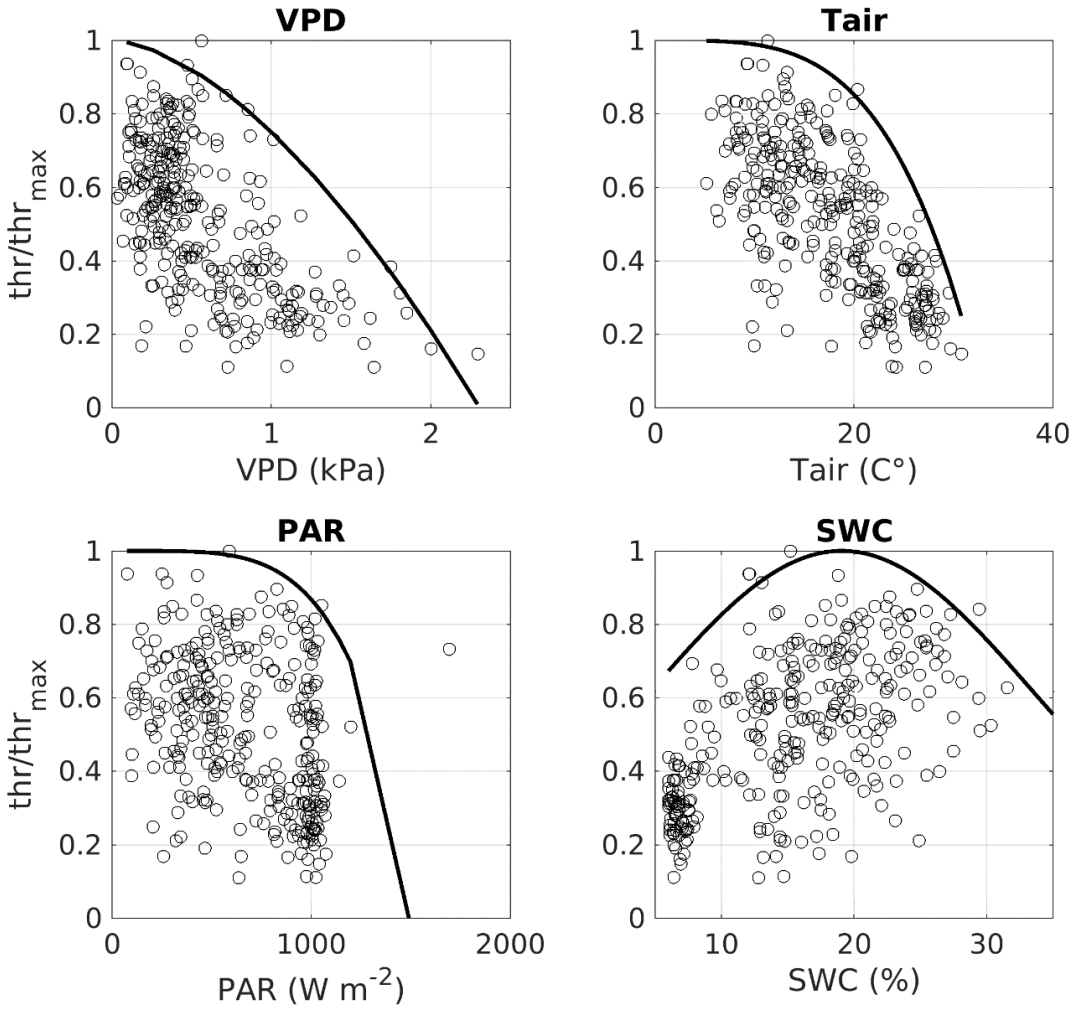

Figure 19 – response function of THR, derived by the boundary line analysis, to environmental parameters for which correlations were observed

Based on the analysis, the resulting models are:

$$THRp_{CPZ}=THR_{max}*fT*fVPD*fSWC*flight*\ fO_3; \quad \text{eq.65}$$

Where THR_{max} is the maximum threshold for ozone tolerance (5 nmol m^{-2} s^{-1}), fT, fVPD, fSWC, fO_3 (set = 1), and flight are the relationships between THR and changes

in air temperature (°C), vapor pressure deficit (kPa), soil water content (%), ozone concentrations (ppb), and photosynthetically active radiation (µmol photons m^{-2} s^{-1}).

With:

$$fVPD = a \cdot VPD^{b+c} \quad \text{eq.66}$$

Where a (-0.2493), b (1.661) and c (0.96) are the coefficients describing the power function describing THR response to VPD (R^2 = 0.88, RMSE = 0.083).

$$fSWC = a \cdot e^{-(\frac{x-b}{c})^2} \quad \text{eq.67}$$

Where a (0.96), b (19.07) and c (20.77) are the coefficients describing the nonlinear gaussian function describing THR response to SWC (R^2 = 0.6, RMSE = 0.072).

$$fT = a \cdot Tair^{b+c} \quad \text{eq.68}$$

Where a (-1.8e-06), b (3.8) and c (0.9) are the coefficients describing the nonlinear gaussian function describing THR response to SWC (R^2 = 0.82, RMSE = 0.068).

$$flight = a \cdot PAR^{b+c} \quad \text{eq.69}$$

Where a (-2.278e-15), b (4.59) and c (0.91) are the coefficients describing the power function describing THR response to PAR (R^2 = 0.52, RMSE = 0.069).

In BLD (Figure 20), a positive correlation between THR and VPD (r_s= 0.43 p<0.05), air temperature (r_s=0.42 p<0.05), ozone concentration (r_s= 0.37 p<0.05) and PAR (r_s= 0.51 p<0.05) was found, while no correlation was found with SWC.

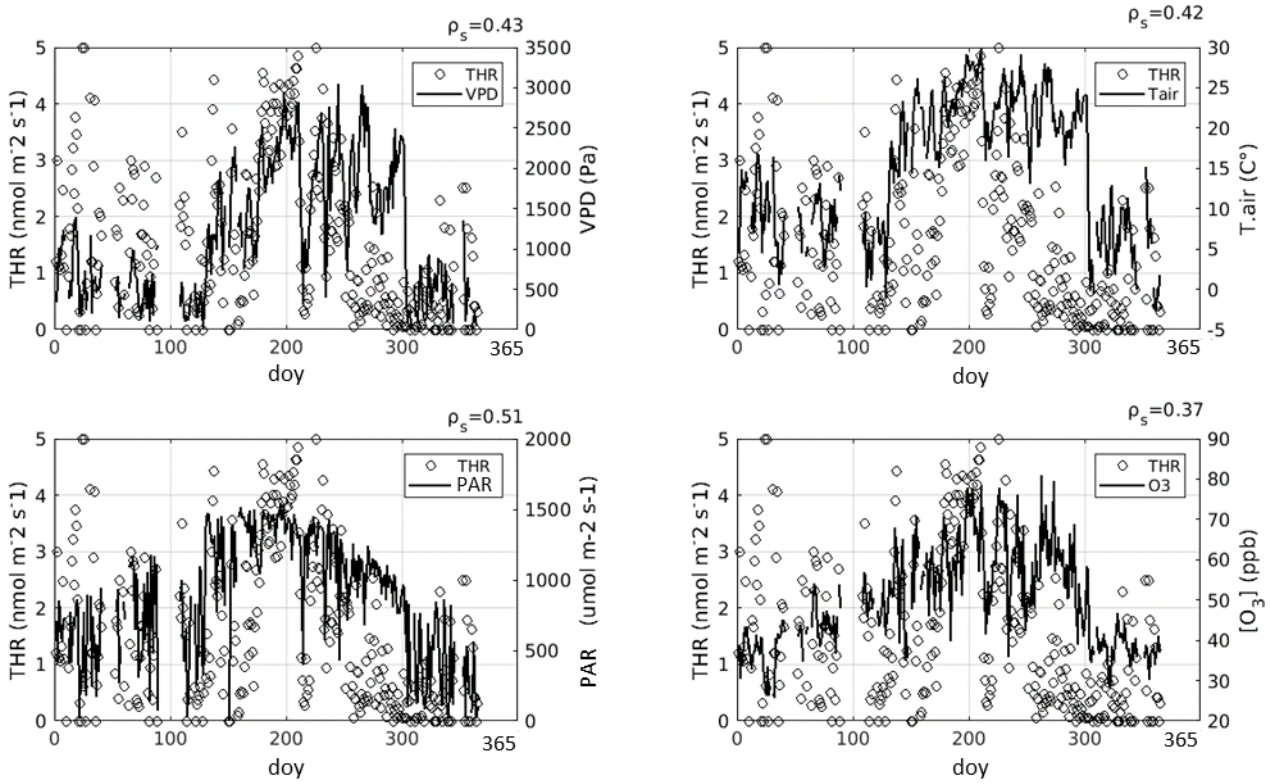

Figure 20 - Correlation values between THR (empty circles) and the environmental variables VPD (top left), Air Temperature (Top right), PAR (bottom left) and ozone concentrations (Bottom right) for BLD site for the year 2003.

Response functions of THR to these variables were developed in a multiplicative algorithm scheme to simulate a dynamic ozone threshold (Figure 21, eq. 70).

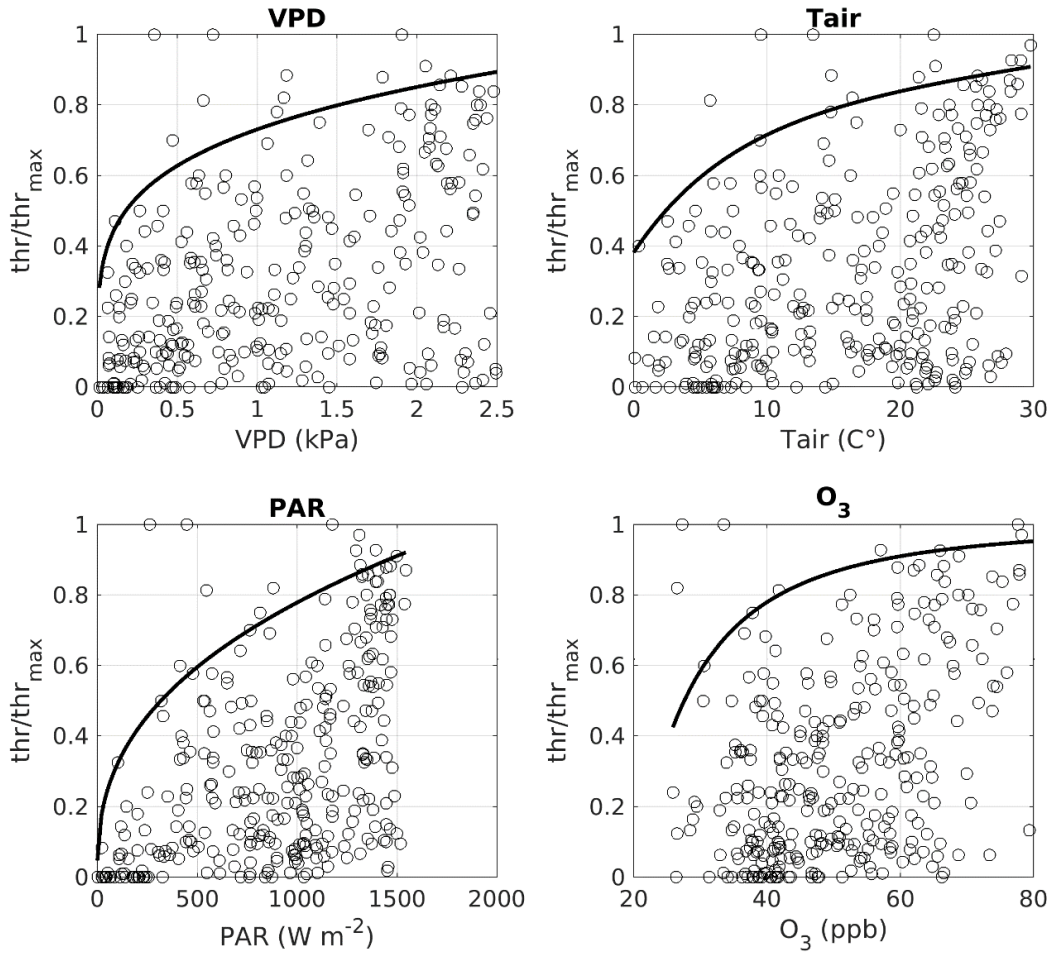

Figure 21 - response function of THR derived by the boundary line analysis to environmental parameters for which correlations were observed

$$THR_{pBLD} = THR_{max} * fT * fVPD * fSWC * flight * fO_3; \quad \text{eq.70}$$

Where THR_{max} is the maximum threshold for ozone tolerance (5 nmol m^{-2} s^{-1}), fT, fVPD, fSWC (set =1), fO_3, and flight are the relationships between THR and changes

in air temperature (°C), vapor pressure deficit (kPa), soil water content (%), ozone concentrations (ppb), and photosynthetically active radiation (µmol photons m^{-2} s^{-1}).

With:

$$flight = a \cdot PAR^{b} \quad \text{eq.71}$$

Where a (0.053), b (0.39) are the coefficients describing the power function describing THR response to PAR (R^2 = 0.45, RMSE =0.2).

$$fO_3 = a \cdot [O_3]^{b+c} \quad \text{eq.72}$$

Where a (-738), b (-2.2) and c (0.99) are the coefficients describing the power function describing THR response to ozone *(R^2 = 0.8,* RMSE= 0.049*).*

$$fT = a \cdot e^{(-b \cdot Tair)+c} \quad \text{eq.73}$$

Where a (0.77), b (0.006) and c (0.38) are the coefficients describing the nonlinear function describing THR response to Tair (R^2 = 0.58, RMSE= 0.155).

$$fVPD = a \cdot VPD^{b} \quad \text{eq.75}$$

Where a (0.79), b (0.16) are the coefficients describing the power function describing THR response to Tair (R^2 = 0.97, RMSE = 0.031).

Linear correlation between *THR* and THR_p (Figure 22) was observed for both CPZ (R^2 =0.57 $p<0.05$) and BLD sites (R^2 =0.3 $p<0.05$).

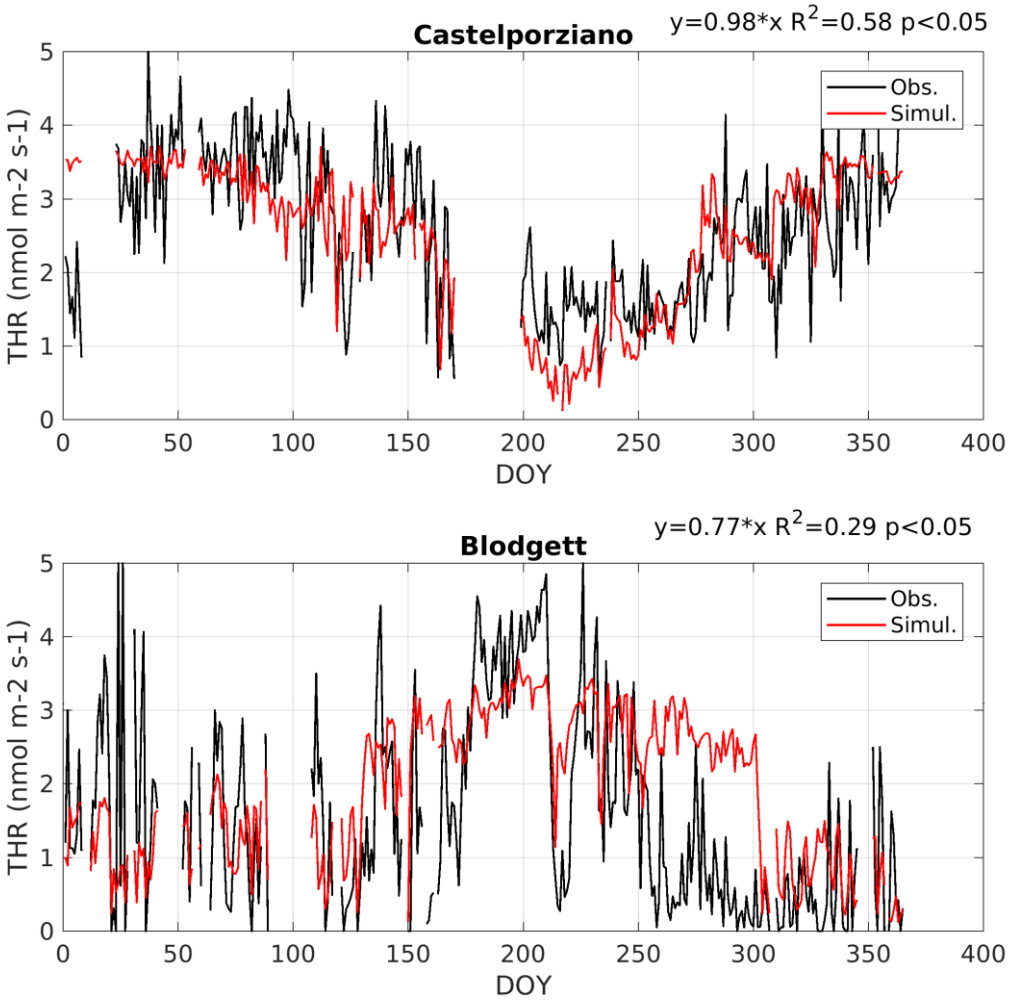

Figure 22 –Correlation between observed THR (in black), derived from simulation, eq. 64) and the simulated THRp (in red) derived from the multiplicative model.

4. Discussion

4.1 Ozone correction factors

Deriving ozone corrections from manipulative experiments data on the studied species provided interesting results. The slope of the regression lines between g_s and ozone concentrations to derive the multiplicative correction factor fO_3 for the Jarvis model (Hoshika et al., 2018) from manipulative studies was higher for *Q. ilex* than *P. ponderosa* (Figure 15), thus suggesting a higher effect of ozone on stomatal aperture (typical of avoidance strategies). Similarly, for the BWB model which includes two different correction factors for g_s and A_n (F_{cO3} and $F_{pO3,}$ eq.61, table 7) respectively (Lombardozzi et al., 2013, 2015), the lower intercept (0.8572 for *Q.ilex* and 1.067 for *P.ponderosa*) and the higher slope (-0.0009 for *Q.ilex* and -0.0007 for *P.ponderosa*) of the regression line between % change from control and CUO lead to a higher correction factor for g_s in *Q. ilex*. Vice versa, we obtained higher F_{pO3} for *P. ponderosa* (table 7) which showed a higher decoupling between g_s and A_n. This feature reveals higher ozone damage to the photosynthetic apparatus in this ozone sensitive species. If we assume that high correction factors for A_n translate into a higher sensitivity to ozone, these results are in line with the initial hypothesis that *Q. ilex* is an ozone tolerant species and *P. ponderosa* is a more ozone sensitive species. F_{cO3} and F_{pO3} extracted in this study seem to be related to different species-specific strategies to face ozone stress which suggest that *Q. ilex* is a more avoidant species compared with *P. ponderosa*. Indeed, while reductions of g_s and A_n were clearly reported in literature studies on *Q. ilex* (Alonso et al., 2014; Fusaro et al., 2016; Vitale et al., 2008), a lower effect on g_s was found in studies on *P. ponderosa* (Beyers et al., 1991; Coyne and Bingham, 1981). This response of *P. ponderosa* to ozone exposure was observed in several studies in which g_s even increased in plants under short-term elevated ozone exposure while only long-term ozone-exposure led to a reduction in g_s (Beyers et al., 1992; Bytnerowicz and Grulke, 2013). The ability to match observations of models used in this study to reproduce photosynthetic performances increased by adopting lower thresholds in *P. ponderosa* compared with *Q. ilex*, thus confirming initial hypothesis on different ozone sensitivities between the two studied species. This suggests that sensitivity to ozone is coupled to correction factors, and F_{cO3} and F_{pO3} should both concur to build phytotoxic thresholds.

4.2 FORCAsT - g_s models inter-comparison

4.2.1 Control Run simulations

The "control" run represents the model simulation resulting from a basic configuration, in which ozone effect on g_s is not taken into account (i.e. ozone corrections deactivated in the model run). In broad terms, it represents the model predictive capacity before this study. This simulation is the reference output to evaluate the impact of the ozone corrections on model predictive capacity. In FORCAsT, the statistical analysis identified the Medlyn A_n-g_s model (Medlyn et al., 2011) as the best configuration to simulate GPP and λE in both CPZ and BLD sites. This parameterization is based on the optimal stomatal behavior theory (Cowan and Farquhar, 1977). This theory postulates that plants regulate stomata to maximize carbon gain while minimizing water loss. Such behavior is in line with the "isohydric" water use strategy, consisting in a constant stomatal regulation to control water loss within a certain range to avoid damages due to water deficits (Buckley, 2005). Such strategy was observed both in *Quercus ilex* (Aguadé et al., 2015; Garcia-Forner et al., 2017) and *Pinus Ponderosa* (Anderegg and HilleRisLambers, 2016). The BWB A_n-g_s model parameterization provided good results as well, thus suggesting that coupled A_n-g_s models developed to account for g_s response to external conditions and to internal feedbacks with A_n (Wong et al., 1979) best describe the regulatory mechanisms of ecosystems characterized by a Mediterranean climate. Conversely to the other two models, the JV model has the limitation to be affected by environmental variables only, lacking of any internal regulatory signal (Gerosa et al., 2012). This lack may explain the lower predictive capacity observed in both sites, when compared to the other two A_n-g_s models (Tables 9 and 12). Such regulatory feedbacks are particularly important for forest growing in the Mediterranean area, where the optimization of water loss per carbon gain seems to be crucial for plant growth during drought periods (Tenhunen et al., 1980). Similar results were found by Misson *et al.* (2004) in a comparative study on g_s-model in BLD site. The authors found the Jarvis model to be unsuitable to describe g_s for BLD site vegetation, while better results were provided by the BWB model. The authors related the lower performance of the Jarvis model to an incorrect simulation of stomatal response to changes in VPD. Such issue made the Jarvis model unable to reproduce the change of the intrinsic water-use efficiency observed at the end of the Spring (low VPD and

high SWC), during which a non-conservative water use of stomata turned into a conservative water use as soil–water content become limited in Summer (high VPD and low SWC). In this condition, it is reasonable that a coupled A_n-g_s model, developed to simulate an optimized stomatal control would result to be more appropriate than an empirical model.

4.2.1.2 The MD_K ozone correction

The implementation of the optimal stomatal behavior "MD_K" proposed by Hoshika et al. (2013) did not provide as good results as the MD model in the control run inter-comparison. In their study, Hoshika et al. (2013) proposed a range of values for the K parameter ($0.1 \times 1.6\ D/[O_3] < K < 1.6\ D/[O_3]$) to account for the drought/ozone response ratio. This ratio can be interpreted as an indicator of plant's responsiveness to ozone, since at low K values (K=0 indicates no ozone effect) stomatal regulation is driven by drought and when K is different from zero the plant is responding also to ozone stress by regulating stomata (i.e. ozone stress avoidance) to maximize A_n while minimizing the $F_{st}O_3$ and ET. Since this work was focused on ozone stress, the same responsiveness (1:1 ratio) of stomata to ET (λ) and to ozone ($\lambda°$) was assumed (i.e. $K = 1.6\ D/\ [O_3]$) for the whole year. Such assumption might have led to overestimate the impact of ozone on A and g_s. Indeed, it has been observed that drought stress can protect plants from ozone injury by inducing stomatal closure (Beyers et al., 1992; Reiner et al., 1996; Tingey and Hogsett, 1985), thus overruling the response to ozone that would be observed under non limiting moisture conditions (Löw et al., 2006). In their study, Hoshika et al. (2018) observed also that the K factor increased at the end of the growing season, suggesting that the leaves exposed to enhanced ozone concentration began to lose stomatal control, thus reducing plants capacity to perform avoidance vs ozone stress (Hoshika et al., 2013). Taking into account the seasonal variation of the drought/ozone responsiveness (k) could help to increase the model accuracy by correctly assessing the dominating stressor between drought and ozone in stomatal regulation. Furthermore, since the Hoshika MD_K model was developed to take in account the avoidance (i.e. the reduction of ozone flux by stomatal closure) of ozone stress alone, the ozone tolerance (i.e. repair and detoxification) needed to be considered. For this reason, critical ozone thresholds (thr_i) were applied to the Hoshika formulation as well. The results indicate low tolerance (thr0 and thr1) for

CPZ for both the whole year and at seasonal level in simulating GPP, while no improvements were found for λE, thus indicating that a possible decoupling between A (GPP) and ET (λE) occurred. These results suggest that in CPZ the main mechanism to face ozone stress was avoidance. However, this correction factor did not ameliorate model accuracy in BLD (Tables 12-14) even if the control run displayed the best results using this approach. Therefore, we cannot speculate on different levels of ozone tolerance between the two sites and further improvements taking account simultaneous and dynamic effects of ozone and drought during the year are needed.

4.2.1.3 The JV_{fO3} ozone correction

The JV_{fO3} correction proposed by Hoshika et al. (2018) ameliorated the model accuracy in CPZ when applying thresholds 4 and 5, thus suggesting low sensitivity to ozone for the holm oak forest, as expected for an ozone tolerant species. However, as the MD_K, this correction factor did not increase model accuracy for both GPP and λE in BLD site. While rejecting the hypothesis that *P. ponderosa* is not an ozone tolerant species, this unexpected low performance of the model can be ascribed to the fact that this correction factor represents a concentration-based approach that (as previously discussed) might have not correctly taken into account the amount of ozone directly entered through stomata (Emberson et al., 2000). Another explanation may be found in Hoshika et al. (2018) who implemented the JV model hypothesizing that in addition to the fO_3 parameter, an ozone-induced stomatal sluggishness parameter "S" (i.e. S=r*POD) to reproduce the impact of ozone on the responsiveness of stomata to each environmental variable of the multiplicative model should be taken into account (e.g. f_{VPD}, f_{light}, f_{SWC}). This formulation was not considered in this study, since it would have needed a POD to simulate g_s and a further iterative approach to identify a second empirical unknown "r" (Hoshika et al., 2018). Accounting for this sluggishness effect which is indirectly accounted for in the BWB model (by an impaired response between stomatal conductance and photosynthesis) might have led to better results in BLD site. Indeed, sluggish responses of stomata at elevated oxidant concentrations have been observed in coniferous species (Grulke, 1999; Patterson and Rundel, 1989; Reich and Lassoie, 1984; Tjoelker et al., 1995).

4.2.1.4 The BWB_{FO3} ozone correction

The application of the ozone correction factors for the BWB model (BWB_{FO3}) provided the best results in both the study sites when compared to the other models. A possible reason behind the successful application of this approach could be that, differently to both JV and MD formulations the BWB_{FO3} correction factors were derived from the response of both g_s and A_n to a cumulated stomatal ozone flux (CUO). This is in line with the growing consensus for the use of flux-based metric in ozone risk assessment studies as rather than concentration-based metrics (Emberson et al., 2000; Fares et al., 2018; Gina Mills, Pleijel, et al., 2011). The most important aspect of this method is that it takes in account two distinct responses of g_s and A_n to ozone, thus accounting for the decoupling of the two processes observed in many experiments (Lombardozzi et al., 2012; Paoletti, 2005; Tjoelker et al., 1995). Such decoupling describes ozone induced impairment of the A_n/ET ratio (λ) that plants stomatal regulation would maintain constant under ideal conditions (Cowan and Farquhar, 1977). This approach allowed to identify species-specific response to ozone in both sites (providing answer to the scientific questions of this PhD work). Indeed, model accuracy was higher for *Q. ilex* when adopting a high critical ozone dose threshold (3 to 5 nmol O_3 m^{-2} s^{-1}) which translates into a high tolerance to ozone. This feature may be due to species-specific capacity to detoxify ozone with for instance antioxidant production or with unaccounted amount of ozone scavenged by non-stomatal reactions between monoterpenes and ozone (Fares *et al.* 2008). On the contrary, *P. ponderosa* resulted to be characterized by a lower detoxification capacity (best thresholds between 0 to 2 nmol O_3 m^{-2} s^{-1}) that seems to be appropriate for a species considered to be ozone sensitive (Anderson et al., 2001; Coyne and Bingham, 1982). Focusing on cumulative values (Figure 23), in CPZ the application of a threshold corresponding to 4 nmol m^{-2} s^{-1} reduced the model overestimation up to 12.7% for GPP and up to 9% for λE. In BLD, the application of threshold corresponding to 1 nmol m^{-2} s^{-1} reduced the model “control" run overestimation by 11.8% for GPP but worsened model simulation by increasing the underestimation of λE by 6.4%.

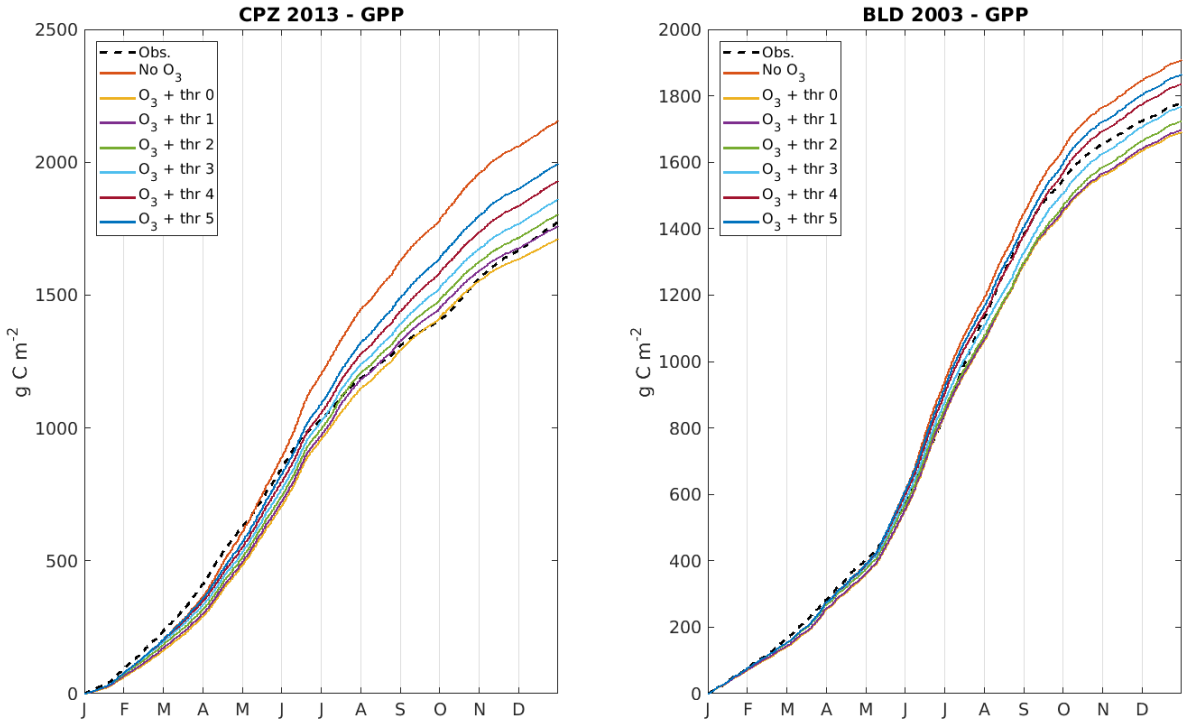

Figure 23 - Cumulative values of Gross Primary Productivity (GPP)) simulated for the Castelporziano (CPZ) and Blodgett (BLD) sites by applying the BWB_{FO3} corrections. O3 + thr_i = Modelled values when considering thresholds of ozone exposure of 1 to 5 nmol m^{-2} s^{-1}.

However, the application of a fixed critical ozone dose threshold for the whole year might lead to unrealistic results, in particular for ozone tolerant species or for species characterized by dormancy periods (e.g. conifers) when ozone might not represent a threat for the vegetation in certain seasons (Bytnerowicz and Grulke, 1992). The importance of identifying the correct threshold for each season is particularly evident in Figure 24, in which the differences and the % deviation from cumulated observations of each simulation compared to the control run is shown for each site. By considering seasonal cumulative values, the application of high thresholds strongly affected the impact of ozone on g_s and A_n. Indeed, in this study the thresholds depend on the occurrence (frequency) of ozone corrections (and therefore ambient ozone concentrations), thus compensating for possible overestimation of ozone impact when it had not relevant role (e.g. in Winter). It is also evident that if

the model control run would underestimate observations, the application of ozone corrections (Thr_i) would worsen the results. A possible solution would be to apply the highest threshold since it would lead to results closer or equal to the control run, thus excluding ozone impact from simulations. Therefore, the study of the impact of the BWB_{FO3} corrections at seasonal scale (Table 16) allowed to evaluate "if" and "when" these corrections would be useful (by ameliorating the model accuracy), worsening (by reducing the model accuracy), or unnecessary (same accuracy as control run). Linear regressions between the observed and simulated values identified different trends in ozone tolerance for the two sites. In CPZ the critical ozone thresholds providing the best results in simulating GPP and λE shifted from high values (thr3 to thr5) in Winter and Spring, to low values (thr0 and thr1) in Summer and Fall. An opposite trend was observed for BLD site, in which the ozone critical thresholds shifted from lower values in Winter (thr1-thr2 for GPP and λE), to higher values in Spring (thr2 for GPP and thr5 for λE) and Summer (thr4-thr5 for GPP and λE), decreasing in Fall (thr3-4 for GPP and λE). The shift of thresholds through seasons suggests that a variable capacity to detoxify ozone can be expected for forests, as previously observed on crops (Sitch et al., 2007).

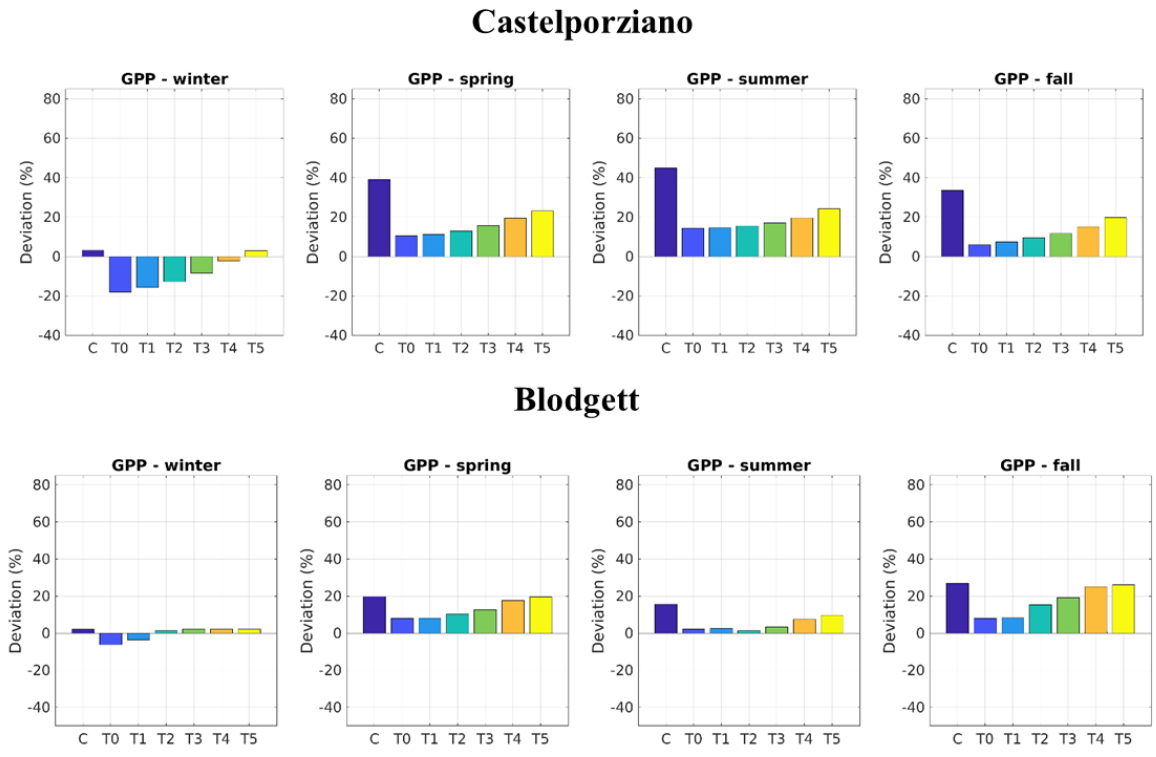

Figure 24 - For each season, bars show percent deviation from measured values of Gross Primary Productivity (GPP). Coloured bars refer to different threshold (thr_i) values adopted to correct modelled values in response to different levels of ozone fluxes. Control (C) represents differences between measured and calibrated values when ozone correction was not applied.

4.3 AIRTREE

The application of BWB model was used to estimate ozone damage with the AIRTREE multi-layer canopy model. The choice to use AIRTREE was driven by both the necessity to evaluate the reproducibility of this approach and to account for possible differences between a model parametrized with measurements and literature data, and a site-specific calibrated model.

Indeed, to obtain the most representative parameterization for the two sites, the AIRTREE model was specifically calibrated by excluding data collected at high ozone concentrations. The resulting "control" runs were so unaffected by ozone assuming no memory effects in the long term, and suitable to account for ozone effects on model predictive capacity (Fares et al., 2019) through the application of the BWB_{FO3} correction (Lombardozzi et al. 2013, 2015).

Results obtained by this approach confirmed what found with the FORCAsT model in both the study sites. Indeed, CPZ showed a general best fit with measured EC values when critical ozone thresholds of 3-5 nmol m^{-2} s^{-1} were applied, suggesting low ozone sensitivity for this species (Table 15). The holm oak forest (dominated by *Quercus ilex*) is considered to be an ozone tolerant species (Paoletti, 2006), suggesting that high critical ozone thresholds should be appropriate for CPZ site. Results agree with the manipulative experiments in open-top chambers performed by Gerosa *et al.* (2015). The authors found that a threshold of 1 nmol m^{-2} s^{-1} was the most appropriate to explain ozone damages in terms of canopy loss, but also threshold of 4 nmol m^{-2} s^{-1} was found to be appropriate to explain biomass losses including roots for *Q. ilex*. However, either thresholds of 0 and 1 nmol O_3 m^{-2} s^{-1} improved the agreement between the estimated value of λE and measured values, thus suggesting that evapotranspiration was more sensitive to ozone than A_n. Such a difference in ozone thresholds for GPP and evapotranspiration can be explained as a decoupling between photosynthesis and stomatal conductance by diffusive limitations (Lombardozzi et al., 2012). The decoupling between A_n and g_s has been observed in many experiments (Francini et al., 2007; Tjoelker et al., 1995; Wittig et al., 2007) under chronic ozone exposure. Indeed, ozone can induce stomatal sluggishness leading to a delay in stomatal responses that may change the carbon (by enhanced ozone stress) and water balance (due to water loss) of forests (Hoshika et al., 2015, 2018b).

Results confirmed what found with the FORCAsT model for the BLD site as well. Critical ozone thresholds of 0 and 1 nmol m^{-2} s^{-1} resulted to best fit with observed GPP, confirming high sensitivity to ozone.
Focusing on cumulative values, for CPZ the inclusion of ozone corrections reduced the "control" model overestimation of GPP and evapotranspiration by 5% and 14%, respectively, in line with previous findings (Fares et al., 2013) reporting a reduction in carbon assimilation by 5% by exposure to ozone (Figure 25). For BLD, the inclusion of ozone corrections reduced the "control" run overestimation of GPP by 5.8%, while no amelioration was observed on λE simulations.

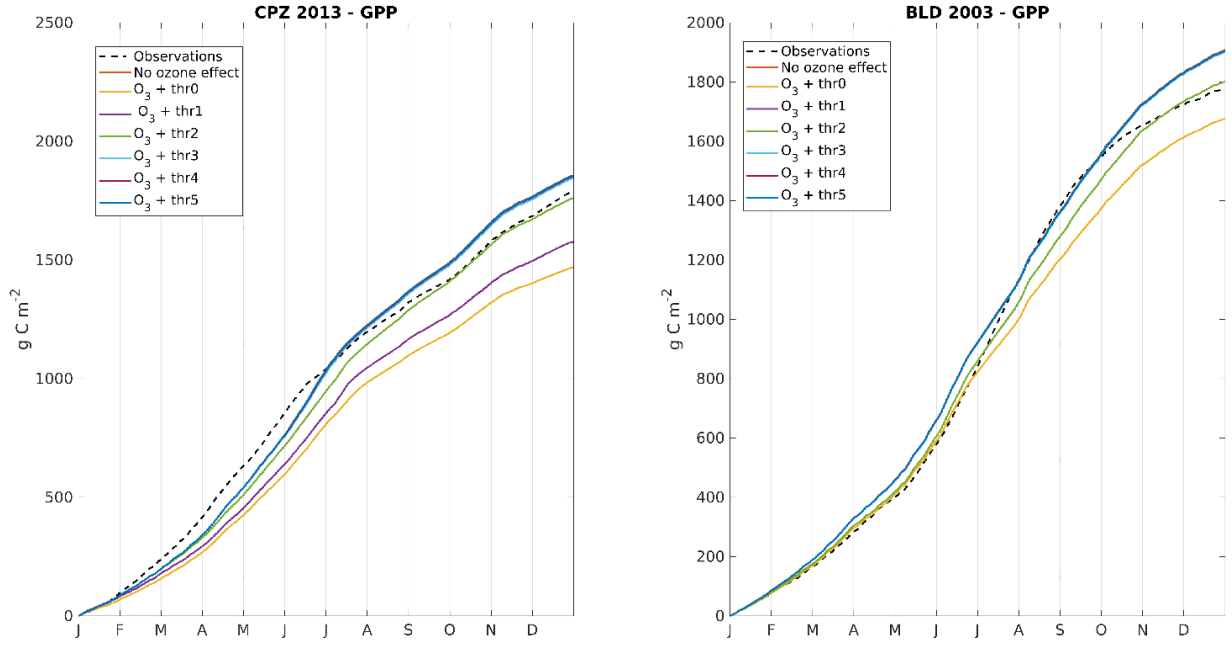

Figure 25 - Cumulative values of Gross Primary Productivity (GPP) and Latent heat flux (λE) simulated for the Castelporziano (CPZ) and Blodgett (BLD) sites by applying the BWB_{FO3} corrections. $O_3 + thr_i$ = Modelled values when considering thresholds of ozone exposure of 1 to 5 nmol m^{-2} s^{-1}.

Seasonal regressions confirmed the existence of a seasonality of thresholds in both sites. An example of such shifts in can be observed in CPZ (Table 16). In Summer, for high ozone concentration, when low thresholds (close to 1 nmol m^{-2} s^{-1}) were applied and ozone limitation to GPP was accounted for, higher (minimally but statistically significant) R-squares and slopes of the linear regression between modelled versus measured GPP were obtained. Similar results were observed for λE,

where application of a threshold of 0 nmol m^{-2} s^{-1} produced higher R^2 between modelled and measured values in Summer. The reduction of ozone tolerance in Summer is reasonable especially in the central hours of the days and the early afternoon, when ozone concentration reaches the highest levels, the stomatal uptake is maximum (Gerosa et al., 2009), and the antioxidant defense mechanism is less responsive since most antioxidants have been scavenged during the day (Dizengremel et al., 2008). On the contrary, BLD forest showed an increase in ozone tolerance during Summer, when highest ozone concentrations and drought stress are concurrent and stomatal closure and allows to avoid ozone stress (Kurpius *et al.* 2002). In addition, several authors observed that after a period of active Summer growth, conifers undergo to a dormancy phase during which anti-oxidant levels increase and accumulate in leaf tissues (Hausladen et al., 1990; Kurpius et al., 2002), but it was unclear whether the antioxidant pools could be maintained through the Winter due to lowered metabolism of dormant trees (Öquist et al., 1978).

The UNECE manual for assessing the impact of ozone on vegetation (Mills et al., 2010) suggests the adoption of a threshold for forest vegetation of 1 nmol O_3 m^{-2} s^{-1} to evaluate the Phytotoxic Ozone Dose (i.e. POD1), thus assuming a high sensitivity to ozone for all tree species. Conversely, the results of this study suggest that such a low threshold would lead to unrealistic estimation of ozone effects on tolerant species such as *Q. ilex* and that a "dynamic" rather than a "fixed" threshold is necessary to understand plant strategies to face ozone stress through the growing season.

4.3.1 Towards adoption of a dynamic threshold

The idea that plant detoxification capacity could be described by an empirical model arose when significative correlations between daily thresholds and environmental parameters were found (Figure 17, 19). Therefore, if a correlation exists it should be possible to derive a function to predict the thresholds variation to changes in environmental conditions.
For each day of the year, the best daily thresholds were identified from simulations and collected into a new "dynamic" threshold variable (THR). To simulate this dynamic variable a multiplicative empirical approach was tested. Although the weak points of a multiplicative approach have been already evidenced, the choice of an empirical approach for this exercise was driven by data availability and the formulation simplicity. Indeed, since the final scope of deriving this function was to

avoid the iterative approach used in this study, this formulation needed to be based on model's input data only. Therefore, a simple multiplicative model based on response functions to changes in environmental parameters seemed perfect for that scope.

Relatively low but statistically significant linear correlations (R^2 =0.51 and 0.3, for CPZ and BLD, respectively) between the "observed" (THR) and the simulated (THR_p) THR were obtained (Figure 22). Such a poor fit can be explained by the fact that in this work only six thresholds were used, while intermediate values could best represent shifts in ozone tolerance during the day. Another possible explanation is that other important variables might not have been included in the analysis. Interestingly, as observed from regressions, the observed THR variables for CPZ and BLD sites (Fig 17,19) showed opposite trends. There are several possible explanations for that difference. A possible reason may be found in the different water availability (precipitation and SWC) between the two study sites. Indeed, although both sites are characterized by a summer drought period typical of the Mediterranean climate, it resulted to be more extended in CPZ, probably because of the lower precipitations observed in Spring compared to BLD site (Figure 11). Therefore, in CPZ oxidative stress due to drought might be enhanced by ozone (Alonso et al., 2014). Conversely, in BLD site during Summer high solar irradiation and high temperatures might have favored the emission of monoterpenes leading to non-stomatal ozone scavenging reactions (Dindorf et al., 2006; Fares et al., 2010; Tingey et al., 1980) that reduce ozone impact since ozone is scavenged in the gas-phase before entering stomata. Another hypothesis is that the vegetation has developed an antioxidant pool during Winter to avoid photooxidation, which also enhance ozone tolerance during the growing season (Anderson et al., 1992).

A third hypothesis that may be drawn is that differences in ozone tolerance between the two study sites could be related to site specific trends of ozone concentration through the year. Indeed, as shown in Figure 14, ozone concentrations were higher in BLD site than in CPZ all year long. Such a difference is probably due to different elevation of the two study sites.

Indeed, CPZ is located in a rural area few meters (17 m) above the sea level. In this area, ozone concentrations increase rapidly in the central hours of the day, when the intensity of solar radiation is at maximum and decrease during the late afternoon and early evening hours, reaching a steady state. Conversely, high elevations sites such as BLD forest have a different daily pattern (Figure 26), in which ozone concentrations remain relatively steady through day and night (Krupa et al., 2001). At BLD, the effect of source areas is also relevant, with high loads of ozone and ozone precursors advected to the study site from the urban areas nearby.

Such different patterns indicate that vegetation in CPZ has to face higher and faster changes in ozone concentrations than BLD site. Therefore, while BLD vegetation may be acclimatized to a high ozone environment, accumulating antioxidant all year long, the CPZ Holm oak forest might be more susceptible to Summer peaks in ozone concentrations, thus lacking of an antioxidant reserve to scavenge oxidative stress.

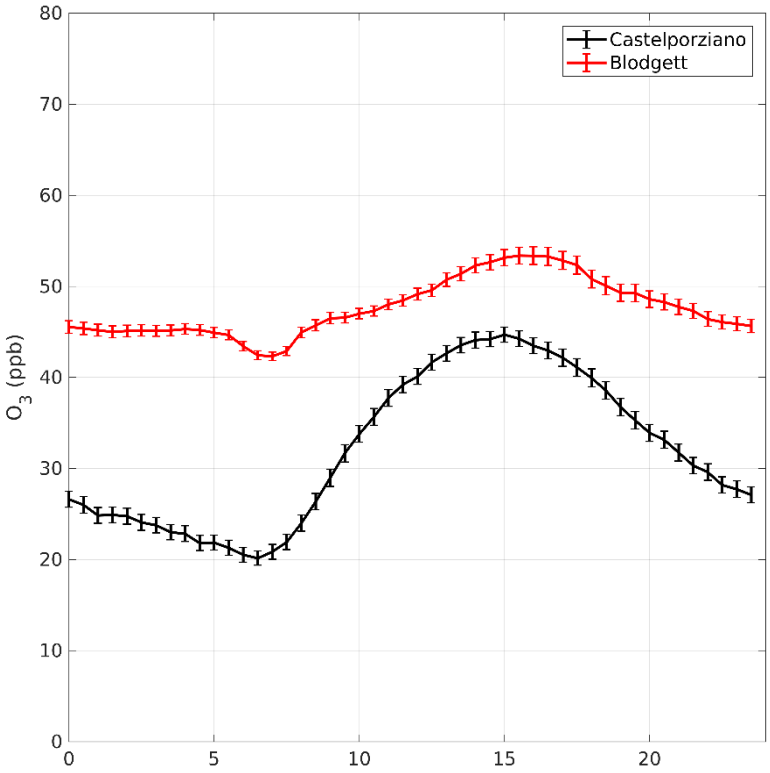

Figure 26 - Daily patterns of hourly mean ozone concentrations measured in both study sites at the top of the canopies. Comparison of a lower elevation (in black, 13 m a.s.l) monitoring site and a higher elevation (in red, 1,315 m a.s.l) site.

The opposite trends observed in this study in THR made not possible to derive a unique generalized multiplicative model for both sites. The limited number of sites and years of study used in this work don't allow to understand if a generalized rather than site-specific or PFTs models are necessary to correctly simulate the thresholds' variations between seasons. Extending this study to other sites might help to clarify this point. The cumulated values (Figure 27) resulting from the application of the simulated mobile THR provided promising results. GPP values corresponding to simulated THR led to a cumulative GPP close to observations (-3.3% in CPZ and 4.4% in BLD site) and to the fixed threshold that have been identified after this

iterative approach, confirming the hypothesis that it is necessary to find a way to account for shifts in ozone tolerance during the year to improve ozone metrics for risk assessment.

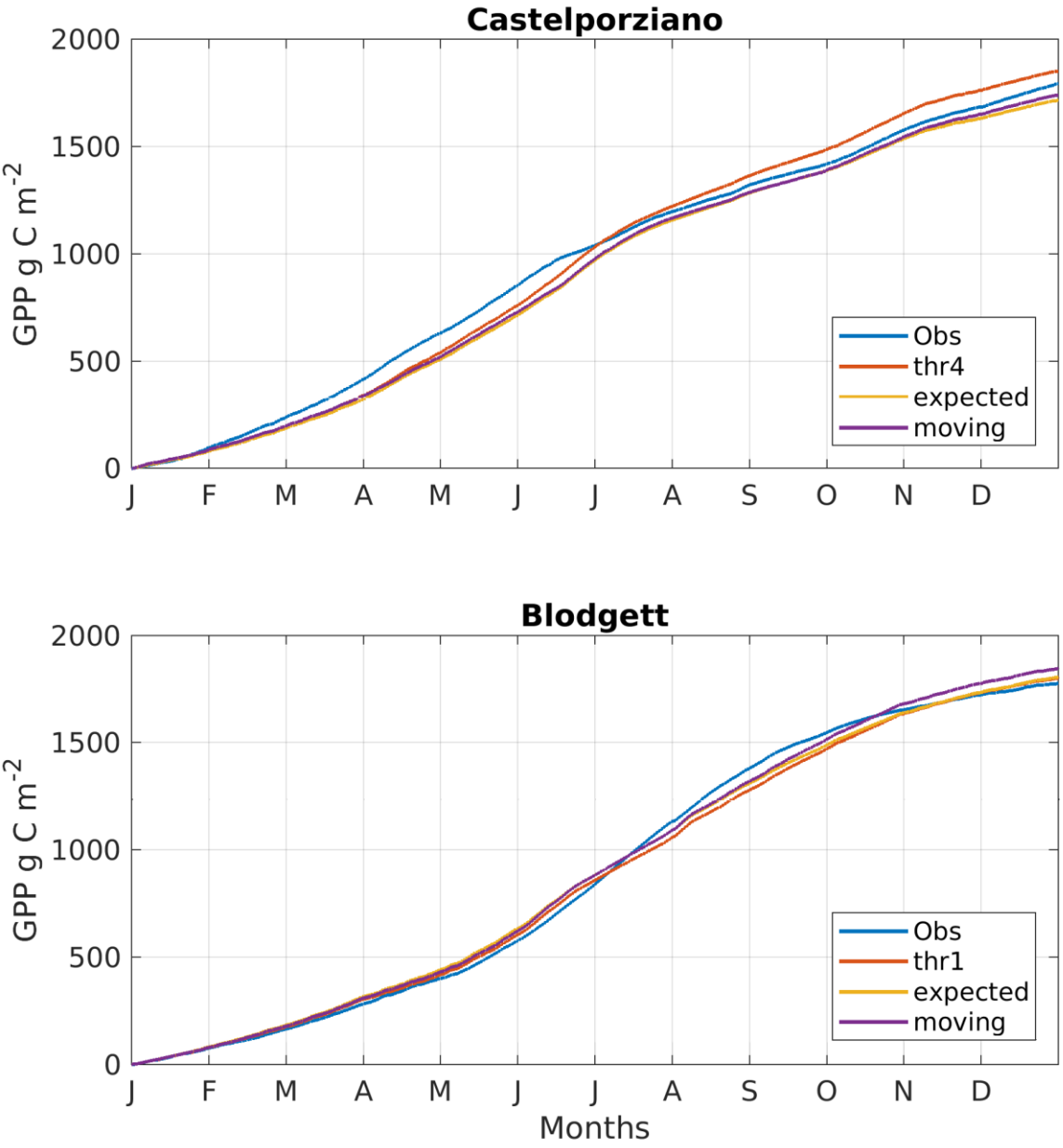

Figure 27 – Cumulative values of Gross Primary Productivity (GPP) for the Castelporziano (top) and Blodgett (bottom) sites by applying the BWB_{FO3} corrections. $O_3 + thr_i$. The blue line represent Observations (Obs.) The orange line represents the modelled values when considering thresholds of ozone exposure of 1 (for BLD) and 4 (for CPZ) nmol m^{-2} s^{-1}. The yellow line (expected) represent the best modelled values observed at each model time step (i.e. observed THR). The violet line represents modelled values identified by the dynamic threshold at each model time step (i.e. THR_{pCPZ} and THR_{pBLD}, respectively).

5. Conclusion and future perspectives

In this PhD thesis, a bottom-up approach to evaluate the effect of ozone exposure on plant ecophysiological processes was used. This approach gathered the state of the art of methods to quantify the effects of ozone using empirical (Jarvis, 1976), semi-empirical (Ball et al., 1987) and theoretical (Medlyn et al. 2011) models, to simulate leaf level photosynthesis and stomatal conductance. By integrating leaf level measurements of gas exchange, meteorological data from eddy covariance monitoring towers and multi-layer canopy models it has been possible to upscale these effects to the canopy level and compare them with EC fluxes of carbon (GPP) and evapotranspiration. Since plants have different capacity to resist the oxidative stress, two eddy covariance forest sites, whose vegetation is characterized by different ozone sensitivity were compared to:

A) Evaluate if a multi-layer model could represent a useful tool as accurate to estimate even small reductions in GPP due to ozone.

B) Evaluate if through this approach it would be possible to define a threshold of phytotoxic ozone dose for trees with known differences in ozone sensitivity.

Although testing and comparing three of the most widely used stomatal conductance models was not a novel methodology *per sé*, it allowed to propose different ways to approach the study of ozone damage on forests, providing answer to each of these scientific questions. The implementation of ozone corrections into the FORCAsT and the AIRTREE models improved (minimally but statistically significant) the accuracy of their simulations of GPP and ET, allowing to identify which stomatal conductance model would be more appropriate for a *Holm oak* and a *Ponderosa pine* forest growing in a Mediterranean climate, both characterized by different levels of ozone sensitivity. Methods accounting for decoupling between photosynthesis and stomatal conductance (Lombardozzi et al., 2013, 2015) provided the best results for both the studied species. This approach allowed to quantify a reduction in carbon sequestration due to ozone exposure of 5-12%, confirming that the study of its impact through a multi-layer canopy model is a feasible option and represents a useful tool for both ozone tolerant and sensitive species. Finally, the identification of site-specific critical stomatal ozone fluxes (i.e. critical ozone thresholds) resulted to be crucial for a realistic quantification of its impact on plants ecophysiological

processes. These results, describing plant's responsiveness to oxidative stress, identified higher thresholds for ozone tolerant species such as *Q. ilex*, and lower thresholds for ozone sensitive species such as *P. ponderosa*, but not on a seasonal basis. Changes in efficacy of threshold corrections during different seasons in this study was observed in both the FORCAsT and the AIRTREE model, suggesting that a possible way to implement metrics for ozone-risk assessment could be to derive a dynamic threshold which takes into account possible changes in ozone sensitivity at different time scales during the vegetative period. This may be plausible, as described in previous works showing different responses to oxidative stress according to the hour of the day and the season (Dizengremel et al., 2008; Luwe and Heber, 1995; Sitch et al., 2007) and may represent a possible future work. Following this hypothesis, a simple empirical model to predict changes in ozone tolerance was developed, providing interesting results. A recent study by Agathokleous et al., (2019) supports the hypothesis that an hormetic-like biphasic dose-response function would be more representative of the plant's adaptive responses to ozone exposure, including a compensation phase. These studies suggest that the development of new non-linear dose response functions could represent a key for improving metrics for ozone risk assessment. Although promising, this approach was not object of this thesis, since more data and specific manipulative experiments would be necessary to identify the entire dose (time) – response continuum.

A few research questions arise after my work for this thesis:

1) How site-specific these formulation for variable thresholds would be? Results support the idea that developing functions to describe dynamic thresholds is necessary. This approach could be replicated for many other forest types by integrating manipulative experiments of ozone fumigation and dose-response studies, eddy covariance monitoring site data and multi-layer modeling, up to estimate new so-called "Critical Levels" for broader scales. However, there is actually only a limited number of eddy covariance sites measuring ozone concentrations and fluxes. While the scientific community has moved to establishing long-term Ecosystem Research Infrastructures to measure carbon assimilation in response to climate changes (i.e. the ICOS infrastructure in Europe), these results demonstrate that the use of relatively low-cost ozone sensors deployed at the measurement sites may constitute a valuable effort to help understanding of carbon assimilation in response to environmental stresses. This

will be object of my future research with access to a broader range of ecosystem data.

2) May future Mapping manuals take into account for my results? This depends on how feasible will be to replicate my approach to a broader range of crops and forest ecosystems. In particular, since the is a wide number of regional models using different approaches to simulate stomatal conductance, the other two approaches (MD_K and JV_{fO3}) need to be ameliorated.

3) What is the role of chemical reactive species in the canopy such as VOC or Nitrogen Oxides? Can these reactive species represent a sort of barrier against ozone? This will be part of my future research activities, which I plan to carry out in collaboration with both CREA, the University of Tuscia, and Lancaster University thanks to the chemistry box model incorporated in the FORCAsT model.

Main symbols and abbreviations

Variable.	Description	Units
A_c	photosynthetic rate limited by CO_2	µmol m^{-2} s^{-1}
A_j	photosynthetic rate limited by electron transport	µmol m^{-2} s^{-1}
An	net photosynthesis	µmol m^{-2} s^{-1}
$a_p;\ a_c$	A-CUO and g_s-CUO slope	-
AOT40	Accumulated dose of ozone Over a Threshold of 40 ppb	ppb h^{-1}
$b_p;\ b_c$	A-CUO and g_s-CUO intercept	-
BLD	Blodgett Ponderosa pine forest	-
BWB_{FO3}	BWB model implemented with the $F_{PO_3} and\ F_{cO_3}$ ozone corrections	-
C_a	ambient CO_2 concentration	ppm
C_c	chloroplastic CO_2 concentration	ppm
C_i	internal CO_2 concentration	ppm
CEO_3	cumulative O_3 exposure	nmol mol^{-1} h^{-1}
CPZ	Castelporziano Holm oak forest	-
CUO	cumulative uptake of O_3	mmol m^{-2}
D	vapor pressure deficit	kPa
E	transpiration rate	J
$F_{PO_3}\ ;\ F_{cO_3}$	correction factor for ozone effect on A_n and g_s	%
f_{phen}	response function of g_s to plant's phenology	-
f_{light}	response function to light intensity (PPFD)	-
fO_3	response function to ozone concentrations	-
f_{swc}	response function to soil water content	-
f_{temp}	response function to leaf temperature	-
f_{vpd}	response function to leaf level vapour pressure deficit	-
F_{st}	stomatal ozone flux	nmol m^{-2} s^{-1}
g_0	residual stomatal conductance when *A* tends to zero	mol m^{-2} s^{-1}

$g1$	slope parameter for the BWB and the Medlyn model	-
g_{max}	maximum stomatal conductance to water	mol H_2O m^{-2} s^{-1}
GPP	gross primary productivity	g CO_2 ha^{-1} y^{-1}
$g_{s\,;}$	stomatal conductance to water vapour	mol m^{-2} s^{-1}
J_{max}	light-saturated rate of electron transport	
JV_{fO3}	JV model implemented with the fO_3ozone correction	-
k	ratio of λ/λº	mol H_2O mol^{-1} O_3
K_o	Vcmax scaling factor	-
LAI	leaf area index	m^2 m^{-2}
MD_K	Optimal stomatal model (MD) for ozone avoidance	-
$[O_3]$	O_3 concentration	ppb
$PPFD$	photosynthetic photon flux density	µmol m^{-2} s^{-1}
R_d	dark respiration rate of CO_2	µmol m^{-2} s^{-1}
R_{eco}	ecosystem respiration	Kg CO_2 ha^{-1} y^{-1}
RH	relative humidity	%
r_s	stomatal resistance	s m^{-1}
THR	dynamic critical stomatal ozone flux threshold	nmol m^{-2} s^{-1}
THR_p	simulated dynamic critical stomatal ozone flux threshold	nmol m^{-2} s^{-1}
T_a	air temperature	°C
T_l	leaf temperature	°C
V_{cmax}	carboxylation rate of CO_2	µmol m^{-2} s^{-1}
VPD	vapor pressure deficit	kPa
$Y,\ thr_i$	critical stomatal ozone flux (i.e. detoxification threshold)	nmol m^{-2} s^{-1}
λ	Lagrange multiplier that represents the marginal water cost of plant carbon gain	mol H_2O mol^{-1} CO_2
λ^o	Lagrange multiplier that represents the marginal ozone damage of plant carbon gain	mol O_3 mol^{-1} CO_2
λE	latent heat flux	W m^{-2}

Acknowledgments

The PhD research was made possible by a grant co-financed by the Department for Innovation in Biological, Agro-Food and Forest Systems (DIBAF) – University of Tuscia, Viterbo, and the Council for Agricultural Research and Economics – Forestry and Woods (CREA - FL), Rome.
The research was also made possible thanks to the Scientific Commission of Castelporziano, the Multi-disciplinary Centre for the Study of Coastal Mediterranean Ecosystems and the Directorate of Castelporziano Estate.
Thanks to the UE LIFE financial instrument *SMART4Action* - Sustainable Monitoring And Reporting To Inform Forest - and *Environmental* Awareness and Protection. (LIFE13 ENV/IT/000813) and the national grant CASTEL4.
Thanks also to Professor. Elena Paoletti and to Dr. Yasutomo Hoshika and to the UE LIFE financial instrument project MOTTES "MOnitoring ozone injury for seTTing new critical LEvelS" (LIFE15 ENV/IT/000183).
This work is the result of the fruitful cooperation between CREA-FL, the University of Tuscia and the Lancaster University, that hosted me for a short-term visit to learn the basis of modelling and to parametrize the FORCAsT model with the help of the PhD student Frederik Out-Larbi and his supervisor, Professor Kirsti Ashworth.

Bibliography

Aasamaa, K., Sober, A., Hartung, W., Niinemets, U., 2002. Rate of stomatal opening, shoot hydraulic conductance and photosynthetic characteristics in relation to leaf abscisic acid concentration in six temperate deciduous trees. Tree Physiol. 22, 267–276. https://doi.org/10.1093/treephys/22.4.267

Agathokleous, E., Belz, R.G., Calatayud, V., De Marco, A., Hoshika, Y., Kitao, M., Saitanis, C.J., Sicard, P., Paoletti, E., Calabrese, E.J., 2019. Predicting the effect of ozone on vegetation via linear non-threshold (LNT), threshold and hormetic dose-response models. Sci. Total Environ. 649, 61–74. https://10.1016/j.scitotenv.2018.08.264

Aguadé, D., Poyatos, R., Rosas, T., Martínez-Vilalta, J., 2015. Comparative Drought Responses of Quercus ilex L. and Pinus sylvestris L. in a Montane Forest Undergoing a Vegetation Shift. Forests 6, 2505–2529. https://doi.org/10.3390/f6082505

Ainsworth, E. a, Yendrek, C.R., Sitch, S., Collins, W.J., Emberson, L.D., 2012. The Effects of Tropospheric Ozone on Net Primary Productivity and Implications for Climate Change*. Annu. Rev. Plant Biol. 63, 637–661. https://doi.org/doi:10.1146/annurev-arplant-042110-103829

Ainsworth, E.A., Rogers, A., 2007. The response of photosynthesis and stomatal conductance to rising [CO 2]: Mechanisms and environmental interactions. Plant, Cell Environ. 30, 258–270. https://doi.org/10.1111/j.1365-3040.2007.01641.x

Alonso, R., Elvira, S., González-Fernández, I., Calvete, H., García-Gómez, H., Bermejo, V., 2014. Drought stress does not protect Quercus ilex L. from ozone effects: Results from a comparative study of two subspecies differing in ozone sensitivity. Plant Biol. 16, 375–384. https://doi.org/10.1111/plb.12073

Anderegg, L.D.L., HilleRisLambers, J., 2016. Drought stress limits the geographic ranges of two tree species via different physiological mechanisms. Glob. Chang. Biol. 22, 1029–1045. https://doi.org/10.1111/gcb.13148

Anderson, C.P., Hogsett, W.E., Plocher, M., Rodecap, K., Lee, E.H., 2001. Blue wild-rye grass competition increases the effect of ozone on ponderosa pine seedlings. Tree Physiol. 21, 319–327. https://doi.org/10.1093/treephys/21.5.319

Anderson, J. V, Chevone, B.I., Hess, J.L., 1992. Seasonal variation in the antioxidant system of eastern white pine needles: evidence for thermal dependence. Plant Physiol. 98, 501–508. https://doi.org/10.1104/pp.98.2.501.

Anenberg, S.C., Horowitz, L.W., Tong, D.Q., West, J.J., 2010. An estimate of the global burden of anthropogenic ozone and fine particulate matter on premature human mortality using atmospheric modeling. Environ. Health Perspect. 118, 1189–95. https://doi.org/10.1289/ehp.0901220

Arneth, A., Lloyd, J., Šantrůčková, H., Bird, M., Grigoryev, S., Kalaschnikov, Y.N., Gleixner, G., Schulze, E.-D., 2002. Response of central Siberian Scots pine to soil water deficit and long-term trends in atmospheric CO 2 concentration . Global Biogeochem. Cycles 16, 5-1-5–13. https://doi.org/10.1029/2000gb001374

Ashmore, M.R., 2005. Assessing the future global impacts of ozone on vegetation. Plant, Cell Environ. 28, 949–964. https://doi.org/10.1111/j.1365-3040.2005.01341.x

Ashworth, K., Chung, S.H., Griffin, R.J., Chen, J., Forkel, R., Bryan, A.M., Steiner, A.L., 2015. FORest Canopy Atmosphere Transfer (FORCAsT) 1.0: a 1-D model of biosphere–atmosphere chemical exchange. Geosci. Model Dev. 8, 3765–3784. https://doi.org/10.5194/gmd-8-3765-2015

Ashworth, K., Chung, S.H., McKinney, K.A., Liu, Y., Munger, J.W., Martin, S.T., Steiner, A.L., 2016. Modelling bidirectional fluxes of methanol and acetaldehyde with the FORCAsT canopy exchange model. Atmos. Chem. Phys. 16, 15461–15484. https://doi.org/10.5194/acp-16-15461-2016

Aubinet, M., 2008. Eddy covariance CO2 flux measurements in nocturnal conditions: An analysis of the problem. Ecol. Appl. 18, 1368–1378. https://doi.org/10.1890/06-1336.1

Aubinet, M., Vesala, T., Papale, D., Kb, D.P.D.F., William, J.M., Loescher, H.W., Luo, H., Rebmann, C., Kolle, O., Heinesch, B., Queck, R., Ibrom, A., Foken, T., Leuning, R., Oncley, S.R., M, M., Aubinet, M., Aubinet, M., Feigenwinter, C., Heinesch, B., Laffineur, Q., Papale, D., 2012. Eddy Covariance: A Practical Guide to Measurement and Data Analysis. p. 460. https://doi.org/10.1007/978-94-007-2351-1

Baldocchi, D., 1994. An analytical solution for coupled leaf photosynthesis and stomatal conductance models. Tree Physiol. 14, 1069–1079. https://doi.org/10.1093/treephys/14.7-8-9.1069

Ball, J.T., Woodrow, I.E., Berry, J.A., 1987. A Model Predicting Stomatal Conductance and its Contribution to the Control of Photosynthesis under Different Environmental Conditions, in: Progress in Photosynthesis Research. Springer Netherlands, Dordrecht, pp. 221–224. https://doi.org/10.1007/978-94-017-0519-6_48

Bernstein, L., Bosch, P., Canziani, O., Chen, Z., Christ, R., Riahi, K., 2008. IPCC, 2007: climate change 2007: synthesis report.

Beyers, J., Reichers, G., Temple, P., 1991. Photosynthetic capacity of ponderosa pine seedlings exposed to different levels of atmospheric ozone and drought stress. Bull. Ecol. Soc. Am. 72, 69.

Beyers, J.L., Riechers, G.H., Temple, P.J., 1992. Effects of long-term ozone exposure and drought on the photosynthetic capacity of ponderosa pine (Pinus ponderosa Laws.). New Phytol. 122, 81–90. https://doi.org/10.1111/j.1469-8137.1992.tb00055.x

Bičárová, S., Sitková, Z., Pavlendová, H., Fleischer Jr., P., Fleischer Sr., P., Dalstein-Richier, L., Ciriani, M.-L., Bytnerowicz, A., 2017. How does soil water availability control phytotoxic O_3 dose to montane pines? Modelling and experimental study from two contrasting climatic regions in Europe. Atmos. Chem. Phys. Discuss. 1–18. https://doi.org/10.5194/acp-2017-1005

Biondi, F.A., Downgiallo, G., Gisotti, G., Tinelli, A., Figliolia, A., Scarascia Mugnozza, G., 2001. Memoria illustrativa alla carta dei suoli della Tenuta di Castelporziano. Sist. Ambient. della Tenuta Pres. di Castelporziano, Accad. Naz. delle Sci. Detta dei XL Roma (ed), Scr. e Doc. 26.

Bombelli, A., Gratani, L., 2003. Interspecific differences of leaf gas exchange and water relations of three evergreen Mediterranean shrub species. Photosynthetica 41, 619–625. https://doi.org/10.1023/B:PHOT.0000027529.82395.86

Bonan, G.B., Lawrence, P.J., Oleson, K.W., Levis, S., Jung, M., Reichstein, M., Lawrence, D.M., Swenson, S.C., 2011. Improving canopy processes in the Community Land Model version 4 (CLM4) using global flux fields empirically inferred from FLUXNET data. J. Geophys. Res. 116, G02014. https://doi.org/10.1029/2010JG001593

Bonan, G.B., Williams, M., Fisher, R.A., Oleson, K.W., 2014. Modeling stomatal conductance in the earth system: linking leaf water-use efficiency and water transport along the soil–plant–atmosphere continuum. Geosci. Model Dev. 7, 2193–2222. https://doi.org/10.5194/gmd-7-2193-2014

Bortier, K., Ceulemans, R., De Temmerman, L., 1999. Effects of tropospheric ozone on woody plants. Environ. Pollut. plant responses 153–173.

Bryan, A.M., Bertman, S.B., Carroll, M.A., Dusanter, S., Edwards, G.D., Forkel, R., Griffith, S., Guenther, A.B., Hansen, R.F., Helmig, D., Jobson, B.T., Keutsch, F.N., Lefer, B.L., Pressley, S.N., Shepson, P.B., Stevens, P.S., Steiner, A.L., 2012. In-canopy gas-phase chemistry during CABINEX 2009: Sensitivity of a 1-D canopy model to vertical mixing and isoprene chemistry. Atmos. Chem. Phys. 12, 8829–8849. https://doi.org/10.5194/acp-12-8829-2012

Buckley, T.N., 2005. The control of stomata by water balance. New Phytol. 168, 275–292. https://doi.org/10.1111/j.1469-8137.2005.01543.x

Büker, P., Emberson, L.D., Ashmore, M.R., Cambridge, H.M., Jacobs, C.M.J., Massman, W.J., Müller, J., Nikolov, N., Novak, K., Oksanen, E., Schaub, M., de la Torre, D., 2007. Comparison of different stomatal conductance algorithms for ozone flux modelling. Environ. Pollut. 146, 726–735. https://doi.org/10.1016/j.envpol.2006.04.007

Büker, P., Feng, Z., Uddling, J., Briolat, A., Alonso, R., Braun, S., Elvira, S., Gerosa, G., Karlsson, P.E., Le Thiec, D., Marzuoli, R., Mills, G., Oksanen, E., Wieser, G., Wilkinson, M., Emberson, L.D., 2015. New flux based dose–response relationships for ozone for European forest tree species. Environ. Pollut. 206, 163–174. https://doi.org/10.1016/J.ENVPOL.2015.06.033

Bussotti, F., 2008. Functional leaf traits, plant communities and acclimation processes in relation to oxidative stress in trees: A critical overview. Glob. Chang. Biol. https://doi.org/10.1111/j.1365-2486.2008.01677.x

Bytnerowicz, A., Grulke, N.E., 2013. Physiological Effects of Air Pollutants on Western Trees, in: The Response of Western Forests to Air Pollution. Springer, pp. 183–233. https://doi.org/10.1007/978-1-4612-2960-5_6

Caird, M.A., Richards, J.H., Donovan, L.A., 2007. Nighttime stomatal conductance and transpiration in C3 and C4 plants. Plant Physiol. 143, 4–10. https://doi.org/10.1104/pp.106.092940

Calatayud, V., Cerveró, J., Sanz, M.J., 2007. Foliar, Physiologial and Growth Responses of Four Maple Species Exposed to Ozone. Water. Air. Soil Pollut. 185, 239–254. https://doi.org/10.1007/s11270-007-9446-5

Carriero, G., Emiliani, G., Giovannelli, A., Hoshika, Y., Manning, W.J., Traversi, M.L., Paoletti, E., 2015. Effects of long-term ambient ozone exposure on biomass and wood traits in poplar treated with ethylenediurea (EDU). Environ. Pollut. 206, 575–581. https://doi.org/10.1016/J.ENVPOL.2015.08.014

Castagna, A., Ranieri, A., 2009. Detoxification and repair process of ozone injury: from O3 uptake to gene expression adjustment. Environ. Pollut. 157, 1461–9.

https://doi.org/10.1016/j.envpol.2008.09.029

Castell, C., Terradas, J., 1995. Water relations, gas exchange and growth of dominant and suppressed shoots of Arbutus unedo L. Tree Physiol. 15, 405–409. https://doi.org/10.1093/treephys/15.6.405

Castillo, F.J., Greppin, H., 1988. Extracellular ascorbic acid and enzyme activities related to ascorbic acid metabolism in Sedum album L. leaves after ozone exposure. Environ. Exp. Bot. 28, 231–238. https://doi.org/10.1016/0098-8472(88)90033-0

CCAC Scientific Advisory Panel, 2014. Time to act to reduce Short-Lived Climate Pollutants, Unep-Cca.

Chen, J., Griffin, R.J., 2005. Modeling secondary organic aerosol formation from oxidation of α-pinene, β-pinene, and d-limonene. Atmos. Environ. 39, 7731–7744. https://doi.org/10.1016/j.atmosenv.2005.05.049

Chevalier, A., Gheusi, F., Delmas, R., Ordóñez, C., Sarrat, C., Zbinden, R., Thouret, V., Athier, G., Cousin, J.-M., 2007. Influence of altitude on ozone levels and variability in the lower troposphere: a ground-based study for western Europe over the period 2001–2004. Atmos. Chem. Phys. 7, 4311–4326.

Chevone, B., 1991. Seasonal changes in components of the antioxidant system in eastern white pine and ozone effects on antioxidant metabolism, in: Air & Waste Management Association (Ed.), . pp. 91–142.

Cieslik, S.A., 2004. Ozone uptake by various surface types: a comparison between dose and exposure. Atmos. Environ. 38, 2409–2420. https://doi.org/10.1016/j.atmosenv.2003.10.063

Conklin, P.L., Williams, E.H., Last, R.L., 2002. Environmental stress sensitivity of an ascorbic acid-deficient Arabidopsis mutant. Proc. Natl. Acad. Sci. 93, 9970–9974. https://doi.org/10.1073/pnas.93.18.9970

Conte, A., Fares, S., Salvati, L., … Montagnani, L., 2019. Ecophysiological Responses to Rainfall Variability in Grassland and Forests Along a Latitudinal Gradient in Italy. *Frontiers in Forests and Global Change*, **2**, 16.

Contran, N., Paoletti, E., 2007. Visible Foliar Injury and Physiological Responses to Ozone in Italian Provenances of Fraxinus excelsior and F. ornus . Sci. World J. 7, 90–97. https://doi.org/10.1100/tsw.2007.10

Cowan, I.R., 1978. Stomatal Behaviour and Environment. Adv. Bot. Res. 4, 117–228. https://doi.org/10.1016/S0065-2296(08)60370-5

Cowan, I.R., Farquhar, G.D., 1977. Stomatal function in relation to leaf metabolism and environment. Symp. Soc. Exp. Biol. 31, 471–505.

Coyne, P.I., Bingham, G.E., 1982. Variation in photosynthesis and stomatal conductance in an ozone-stressed ponderosa pine stand: light response. For. Sci. 28, 257–273.

Coyne, P.I., Bingham, G.E., 1981. Comparative Ozone Dose Response of Gas Exchange in a Ponderosa Pine Stand Exposed to Long-Term Fumigations. J. Air Pollut. Control Assoc. 31, 38–41. https://doi.org/10.1080/00022470.1981.10465184

Damour, G., Simonneau, T., Cochard, H., Urban, L., 2010. An overview of models of stomatal conductance at the leaf level. Plant, Cell Environ. https://doi.org/10.1111/j.1365-3040.2010.02181.x

Danielsson, H., Karlsson, G.P., Karlsson, P.E., Pleijel, H.H., 2003. Ozone uptake modelling and flux-response relationships—an assessment of ozone-induced yield loss in spring wheat. Atmos. Environ. 37, 475–485.

Darcy, H. P. G. (1856). *Les Fontaines publiques de la ville de Dijon. Exposition et application des principes à suivre et des formules à employer dans les questions de distribution d'eau, etc*, V. Dalamont.

De Kauwe, M.G., Kala, J., Lin, Y.S., Pitman, A.J., Medlyn, B.E., Duursma, R.A., Abramowitz, G., Wang, Y.P., Miralles, D.G., 2015. A test of an optimal stomatal conductance scheme within the CABLE land surface model. Geosci. Model Dev. 8, 431–452. https://doi.org/10.5194/gmd-8-431-2015

De Lillis, M., Mirgone, E., 1994. Water relations of some Mediterranean evergreen sclerophylls: some considerations on sclerophylly and microphylly. Ecol. Mediterr. 20, 39–49.

De Lillis, M., Bianco, P.M., Loreto, F., 2009. The influence of leaf water content and isoprenoids on flammability of some Mediterranean woody species. Int. J. Wildl. Fire 18, 203–212.

De Marco, A., Sicard, P., Fares, S., Tuovinen, J.-P., Anav, A., Paoletti, E., 2016. Assessing the role of soil water limitation in determining the Phytotoxic Ozone Dose (PODY) thresholds. Atmos. Environ. 147, 88–97. https://doi.org/10.1016/J.ATMOSENV.2016.09.066

Demmig-Adams, B., Adams, W.W., 2006. Photoprotection in an ecological context: the remarkable complexity of thermal energy dissipation. New Phytol. 172, 11–21. https://doi.org/10.1111/j.1469-8137.2006.01835.x

Desai, A.R., Richardson, A.D., Moffat, A.M., Kattge, J., Hollinger, D.Y., Barr, A., Falge, E., Noormets, A., Papale, D., Reichstein, M., 2008. Cross-site evaluation of eddy covariance GPP and RE decomposition techniques. Agric. For. Meteorol. 148, 821–838.

Desario, P.A., Gray, K.A., 2012. Passive systems to improve air quality and reduce heat retention in the urban environment. Metrop. Sustain. 292–316. https://doi.org/10.1533/9780857096463.3.292

Di Carlo, P., Pitari, G., Mancini, E., Gentile, S., Pichelli, E., Visconti, G., 2007. Evolution of surface ozone in central Italy based on observations and statistical model. J. Geophys. Res. Atmos. 112.

Dindorf, T., Kuhn, U., Ganzeveld, L., Schebeske, G., Ciccioli, P., Holzke, C., Köble, R., Seufert, G., Kesselmeier, J., 2006. Significant light and temperature dependent monoterpene emissions from European beech (Fagus sylvatica L.) and their potential impact on the European volatile organic compound budget. J. Geophys. Res. Atmos. 111.

Dizengremel, P., Le Thiec, D., Bagard, M., Jolivet, Y., 2008. Ozone risk assessment for plants: Central role of metabolism-dependent changes in reducing power. Environ. Pollut. 156, 11–15. https://doi.org/10.1016/J.ENVPOL.2007.12.024

Drake, P.L., Froend, R.H., Franks, P.J., 2013. Smaller, faster stomata: scaling of stomatal size, rate of response, and stomatal conductance. J. Exp. Bot. 64, 495–505. https://doi.org/10.1093/jxb/ers347

Dumont, J., Cohen, D., Gérard, J., Jolivet, Y., Dizengremel, P., Le Thiec, D., 2014. Distinct responses to ozone of abaxial and adaxial stomata in three Euramerican poplar genotypes. Plant, Cell Environ. 37, 2064–2076. https://doi.org/10.1111/pce.12293

Duursma, R.A., 2015. Plantecophys - An R Package for Analysing and Modelling Leaf Gas Exchange Data. PLoS One 10, e0143346. https://doi.org/10.1371/journal.pone.0143346

Emberson, L.D., Ashmore, M.R., Cambridge, H.M., Simpson, D., Tuovinen, J.P., 2000. Modelling stomatal ozone flux across Europe. Environ. Pollut. 109, 403–413. https://doi.org/10.1016/S0269-7491(00)00043-9

Emberson, L.D.I., Massman, W.J., Bdkerl, P., Soja, G., 2004. The development , evaluation and application of 0 3 flux and flux-response models for additional agricultural crops, in: Critical Levels of Ozone: Further Applying and Developing the Flux-Based Concept. pp. 53–58.

Emberson, L.D., Büker, P., Ashmore, M.R., 2007. Assessing the risk caused by ground level ozone to European forest trees: A case study in pine, beech and oak across different climate regions. Environ. Pollut. 147, 454–466. https://doi.org/10.1016/J.ENVPOL.2006.10.026

Emberson, L.D., Büker, P., Ashmore, M.R., Mills, G., Jackson, L.S., Agrawal, M., Atikuzzaman, M.D., Cinderby, S., Engardt, M., Jamir, C., Kobayashi, K., Oanh, N.T.K., Quadir, Q.F., Wahid, A., 2009. A comparison of North American and Asian exposure–response data for ozone effects on crop yields. Atmos. Environ. 43, 1945–1953. https://doi.org/10.1016/j.atmosenv.2009.01.005

Erisman, J.W., Van Pul, A., Wyers, P., 1994. Parametrization of surface resistance for the quantification of atmospheric deposition of acidifying pollutants and ozone. Atmos. Environ. 28, 2595–2607. https://doi.org/10.1016/1352-2310(94)90433-2

Fanjul, L., Jones, H.G., 1982. Rapid stomatal responses to humidity. Planta 154, 135–138. https://doi.org/10.1007/BF00387906

Fares, S., Loreto, F., Kleist, E., Wildt, J., 2008. Stomatal uptake and stomatal deposition of ozone in isoprene and monoterpene emitting plants. Plant Biol. 10, 44–54. https://doi.org/10.1055/s-2007-965257

Fares, S., Goldstein, A., Loreto, F., 2010. Determinants of ozone fluxes and metrics for ozone risk assessment in plants. J. Exp. Bot. 61, 629–633. https://doi.org/10.1093/jxb/erp336

Fares, Silvano, McKay, M., Holzinger, R., Goldstein, A.H., 2010. Ozone fluxes in a Pinus ponderosa ecosystem are dominated by non-stomatal processes: Evidence from long-term continuous measurements. Agric. For. Meteorol. 150, 420–431. https://doi.org/10.1016/j.agrformet.2010.01.007

Fares, S., Matteucci, G., Scarascia Mugnozza, G., Morani, A., Calfapietra, C., Salvatori, E., Fusaro, L., Manes, F., Loreto, F., 2013. Testing of models of stomatal ozone fluxes with field measurements in a mixed Mediterranean forest. Atmos. Environ. 67, 242–251. https://doi.org/10.1016/j.atmosenv.2012.11.007

Fares, Silvano, Vargas, R., Detto, M., Goldstein, A.H., Karlik, J., Paoletti, E., Vitale, M., 2013. Tropospheric ozone reduces carbon assimilation in trees: Estimates from analysis of continuous flux measurements. Glob. Chang. Biol. 19, 2427–2443. https://doi.org/10.1111/gcb.12222

Fares, S., Savi, F., Muller, J., Matteucci, G., Paoletti, E., 2014. Simultaneous measurements of above and below canopy ozone fluxes help partitioning ozone deposition between its various sinks in a Mediterranean Oak Forest. Agric. For. Meteorol. 198, 181–191. https://doi.org/10.1016/j.agrformet.2014.08.014

Fares, S., Conte, A., Chabbi, A., 2018. Ozone flux in plant ecosystems: new opportunities for long-term monitoring networks to deliver ozone-risk assessments. Environ. Sci. Pollut. Res. 25, 8240–8248. https://doi.org/10.1007/s11356-017-0352-0

Fares, S., Alivernini, A., Conte, A., Maggi, F., 2019. Ozone and particle fluxes in a Mediterranean forest predicted by the AIRTREE model. Sci. Total Environ. https://doi.org/10.1016/J.SCITOTENV.2019.05.109

Farquhar, G.D., Dubbe, D.R., Raschke, K., 1978. Gain of the feedback loop involving carbon dioxide and stomata: theory and measurement. Plant Physiol. 62, 406–12. https://doi.org/10.1104/PP.62.3.406

Farquhar, G.D., Sharkey, T.D., 1982. Stomatal Conductance and Photosynthesis. Annu. Rev. Plant Physiol. 33, 317–345. https://doi.org/10.1146/annurev.pp.33.060182.001533

Farquhar, G.D., von Caemmerer, S., Berry, J.A., 1980. A biochemical model of photosynthetic CO2 assimilation in leaves of C3 species. Planta 149, 78–90. https://doi.org/10.1007/BF00386231

Feigenwinter, C., Bernhofer, C., Vogt, R., 2004. The influence of advection on the short term CO2-budget in and above a forest canopy. Boundary-Layer Meteorol. 113, 201–224. https://doi.org/10.1023/B:BOUN.0000039372.86053.ff

Felzer, B.S., Cronin, T., Reilly, J.M., Melillo, J.M., Wang, X., 2007. Impacts of ozone on trees and crops. Comptes Rendus - Geosci. 339, 784–798. https://doi.org/10.1016/j.crte.2007.08.008

Feng, Z., Büker, P., Pleijel, H., Emberson, L., Karlsson, P.E., Uddling, J., 2018. A unifying explanation for variation in ozone sensitivity among woody plants. Glob. Chang. Biol. 24, 78–84. https://doi.org/10.1111/gcb.13824

Fiscus, E.L., Booker, F.L., Burkey, K.O., 2005. Crop responses to ozone: Uptake, modes of action, carbon assimilation and partitioning. Plant, Cell Environ. 28, 997–1011. https://doi.org/10.1111/j.1365-3040.2005.01349.x

Forkel, R., Klemm, O., Graus, M., Rappenglück, B., Stockwell, W.R., Grabmer, W., Held, A., Hansel, A., 2006. Trace gas exchange and gas phase chemistry in a Norway spruce forest: A study with a coupled 1-dimensional canopy atmospheric chemistry emission model. Atmos. Environ. 40, 28–42. https://doi.org/10.1016/J.ATMOSENV.2005.11.070

Forster, P., Ramaswamy, V., Artaxo, P., Berntsen, T., Betts, R., Fahey, D.W., Haywood, J., Lean, J., Lowe, D.C., Myhre, G., Nganga, J., Prinn, R., Raga, G., Schulz, M., Van Dorland, R., 2007. Changes in Atmospheric Constituents and in Radiative Forcing. Chapter 2.

Fowler, D., Flechard, C., Cape, J.N., Storeton-West, R.L., Coyle, M., 2001. Measurements of Ozone Deposition to Vegetation Quantifying the Flux, the Stomatal and Non-Stomatal Components. Water. Air. Soil Pollut. 130, 63–74. https://doi.org/10.1023/A:1012243317471

Foyer, C.H., Halliwell, B., 1976. The presence of glutathione and glutathione reductase in chloroplasts: A proposed role in ascorbic acid metabolism. Planta 133, 21–25. https://doi.org/10.1007/BF00386001

Foyer, C.H., Noctor, G., 2011. Ascorbate and Glutathione: The Heart of the Redox Hub. Plant Physiol. 155, 2–18. https://doi.org/10.1104/pp.110.167569

Francini, A., Nali, C., Picchi, V., Lorenzini, G., 2007. Metabolic changes in white clover clones exposed to ozone. Environ. Exp. Bot. 60, 11–19. https://doi.org/10.1016/J.ENVEXPBOT.2006.06.004

Fredericksen, T.S., Kolb, T.E., Skelly, J.M., Steiner, K.C., Joyce, B.J., Savage, J.E., 1996. Light environment alters ozone uptake per net photosynthetic rate in black cherry trees. Tree Physiol. 16, 485–490. https://doi.org/10.1093/treephys/16.5.485

Fuhrer, J., Skärby, L., Ashmore, M.R., 1997. Critical levels for ozone effects on vegetation in Europe. Environ. Pollut. 97, 91–106. https://doi.org/10.1016/S0269-7491(97)00067-5

Furukawa, A., Park, S.Y., Fujinuma, Y., 1990. Hybrid poplar stomata unresponsive to changes in environmental conditions. Trees 4, 191–197. https://doi.org/10.1007/BF00225315

Fusaro, L., Gerosa, G., Salvatori, E., Marzuoli, R., Monga, R., Kuzminsky, E., Angelaccio, C., Quarato, D., Fares, S., 2016. Early and late adjustments of the photosynthetic traits and stomatal density in Quercus ilex L. grown in an ozone-enriched environment. Plant Biol. 18, 13–21. https://doi.org/10.1111/plb.12383

Galvagno, M., Wohlfahrt, G., 2015. On Extrapolating Nighttime Ecosystem Respiration To Daytime Conditions and Implications for Gross Primary Productivity Estimation. Am. Geophys. Union, Fall Meet. 2015, Abstr. id. B22E-08.

Gao, W., Wesely, M.L., Doskey, P. V., 1993. Numerical modeling of the turbulent diffusion and chemistry of NOx, O3, isoprene, and other reactive trace gases in and above a forest canopy. J. Geophys. Res. Atmos. 98, 18339–18353. https://doi.org/10.1029/93JD01862

Garcia-Forner, N., Biel, C., Savé, R., Martínez-Vilalta, J., 2017. Isohydric species are not necessarily more carbon limited than anisohydric species during drought. Tree Physiol. 37, 441–455. https://doi.org/10.1093/treephys/tpw109

Gerosa, G., Finco, A., Mereu, S., Vitale, M., Manes, F., Denti, A.B., 2009. Comparison of seasonal variations of ozone exposure and fluxes in a Mediterranean Holm oak forest between the exceptionally dry 2003 and the following year. Environ. Pollut. 157, 1737–44. https://doi.org/10.1016/j.envpol.2007.11.025

Gerosa, G., Fusaro, L., Monga, R., Finco, A., Fares, S., Manes, F., Marzuoli, R., 2015. A flux-based assessment of above and below ground biomass of Holm oak (Quercus ilex L.) seedlings after one season of exposure to high ozone concentrations. Atmos. Environ. 113, 41–49. https://doi.org/10.1016/J.ATMOSENV.2015.04.066

Gerosa, G., Mereu, S., Finco, A., Marzuoli, R., 2012. Stomatal Conductance Modeling to Estimate the Evapotranspiration of Natural and Agricultural Ecosystems, in: Evapotranspiration - Remote Sensing and Modeling. InTech. https://doi.org/10.5772/21825

Gerosa, G., Vitale, M., Finco, A., Manes, F., Denti, A.B., Cieslik, S., 2005. Ozone uptake by an evergreen Mediterranean Forest (Quercus ilex) in Italy. Part I: Micrometeorological flux measurements and flux partitioning. Atmos. Environ. 39, 3255–3266. https://doi.org/10.1016/j.atmosenv.2005.01.056

Gimenez, C., Gallardo, M., Thompson, R.B., 2005. PLANT–WATER RELATIONS. Encycl. Soils Environ. 231–238. https://doi.org/10.1016/B0-12-348530-4/00459-8

Glick, R.E., Schlagnhaufer, C.D., Arteca, R.N., Pell, E.J., 1995. Ozone-induced ethylene emission accelerates the loss of ribulose-1, 5-bisphosphate carboxylase/oxygenase and nuclear-encoded mRNAs in senescing potato leaves. Plant Physiol. 109, 891–898.

Gomez-Aparicio, L., Valladares, F., Zamora, R., 2006. Differential light responses of Mediterranean tree saplings: linking ecophysiology with regeneration niche in four co-occurring species. Tree Physiol. 26, 947–958. https://doi.org/10.1093/treephys/26.7.947

Goulden, M.L., 1998. Sensitivity of Boreal Forest Carbon Balance to Soil Thaw. Science (80-.). 279, 214–217. https://doi.org/10.1126/science.279.5348.214

Goudriaan, J., Van Laar, H.H., 1994. Modelling crop growth processes. Kluwer, Amsterdam. https://doi.org/10.1016/s0304-4238(96)00923-5

Grantz, D.A., 1990. Plant response to atmospheric humidity. Plant. Cell Environ. 13, 667–679. https://doi.org/10.1111/j.1365-3040.1990.tb01082.x

Griffin, R.J., Dabdub, D., Seinfeld, J.H., 2005. Development and initial evaluation of a dynamic species-resolved model for gas phase chemistry and size-resolved gas/particle partitioning associated with secondary organic aerosol formation. J. Geophys. Res. D Atmos. 110, 1–16. https://doi.org/10.1029/2004JD005219

Griffin, R.J., Dabdub, D., Seinfeld, J.H., 2002. Secondary organic aerosol 1. Atmospheric chemical mechanism for production of molecular constituents. J. Geophys. Res. Atmos. 107, AAC 3-1-AAC 3-26. https://doi.org/10.1029/2001JD000541

Griffin, R.J., Nguyen, K., Dabdub, D., Seinfeld, J.H., 2003. A Coupled Hydrophobic-Hydrophilic Model for Predicting Secondary Organic Aerosol Formation. J. Atmos. Chem. https://doi.org/10.1023/A:1022436813699

Grulke, N.E., 1999. Physiological responses of ponderosa pine to gradients of environmental stressors, in: Oxidant Air Pollution Impacts in the Montane Forests of Southern California. Springer, pp. 126–163. https://doi.org/10.1007/978-1-4612-1436-6_7

Grünhage, L., Pleijel, H., Mills, G., Bender, J., Danielsson, H., Lehmann, Y., Castell, J.F., Bethenod, O., 2012. Updated stomatal flux and flux-effect models for wheat for quantifying effects of ozone on grain yield, grain mass and protein yield, in: Environmental Pollution. pp. 147–157. https://doi.org/10.1016/j.envpol.2012.02.026

Guardia, M., Fernandez, J., Elena, G., Fleck, I., 2012. Stomatal patchiness in the Mediterranean holm oak (Quercus ilex L.) under water stress in the nursery and in the forest. Tree Physiol. 32, 829–838. https://doi.org/10.1093/treephys/tps035

Guerrero, C.C., Günthardt-Goerg, M.S., Vollenweider, P., 2013. Foliar Symptoms Triggered by Ozone Stress in Irrigated Holm Oaks from the City of Madrid, Spain. PLoS One 8, e69171. https://doi.org/10.1371/journal.pone.0069171

Guidi, L., Degl'Innocenti, E., Soldatini, G.F., 2002. Assimilation of CO2, enzyme activation and photosynthetic electron transport in bean leaves, as affected by high light and ozone. New Phytol. 156, 377–388. https://doi.org/10.1046/j.1469-8137.2002.00533.x

Gupta, H. V., Kling, H., Yilmaz, K.K., Martinez, G.F., 2009. Decomposition of the mean squared error and NSE performance criteria: Implications for improving hydrological modelling. J. Hydrol. 377, 80–91. https://doi.org/10.1016/J.JHYDROL.2009.08.003

Hartung, W., Radin, J.W., Hendrix, D.L., 2008. Abscisic Acid Movement into the Apoplastic solution of Water-Stressed Cotton Leaves: Role of Apoplastic pH. PLANT Physiol. 86, 908–913. https://doi.org/10.1104/pp.86.3.908

Hassan, I.A., Ashmore, M.R., Bell, J.N.B., 1994. Effects of O3 on the stomatal behaviour of Egyptian varieties of radish (Raphanus sativus L. cv. Baladey) and turnip (Brassica rapa L. cv. Sultani). New Phytol. 128, 243–249. https://doi.org/10.1111/j.1469-8137.1994.tb04008.x

Hausladen, A., Madamanchi, N.R., Fellows, S., Alscher, R.G., Amundson, R.G., 1990. Seasonal

changes in antioxidants in red spruce as affected by ozone. New Phytol. 115, 447–458. https://doi.org/10.1111/j.1469-8137.1990.tb00470.x

Heagle, A.S., Reinert, R.A., Miller, J.E., 2010. Response of White Clover to Ozone in Different Environments. J. Environ. Qual. 25, 273. https://doi.org/10.2134/jeq1996.00472425002500020010x

Heath, R.L., 1988. Biochemical Mechanisms of Pollutant Stress, in: Assessment of Crop Loss From Air Pollutants. Springer Netherlands, Dordrecht, pp. 259–286. https://doi.org/10.1007/978-94-009-1367-7_12

Heath, R.L., Taylor, G.E., 1997. Physiological processes and plant responses to ozone exposure, in: Forest Decline and Ozone. Springer, pp. 317–368.

Heimann, M., Reichstein, M., 2008. Terrestrial ecosystem carbon dynamics and climate feedbacks. Nature 451, 289–92. https://doi.org/10.1038/nature06591

Hendrey, G.R., Ellsworth, D.S., Lewin, K.F., Nagy, J., 1999. A free-air enrichment system for exposing tall forest vegetation to elevated atmospheric CO2. Glob. Chang. Biol. 5, 293–309. https://doi.org/10.1046/j.1365-2486.1999.00228.x

Herman, F., Smidt, S., Huber, S., Englisch, M., Knoflacher, M., 2001. Evaluation of pollution-related stress factors for forest ecosystems in Central Europe. Environ. Sci. Pollut. Res. 8, 231–242. https://doi.org/10.1007/BF02987399

Hetherington, A.M., Woodward, F.I., 2003. The role of stomata in sensing and driving environmental change. Nature 424, 901–908. https://doi.org/10.1038/nature01843

Hicks, B.B., Baldocchi, D.D., Meyers, T.P., Hosker, R.P., Matt, D.R., 1987. A preliminary multiple resistance routine for deriving dry deposition velocities from measured quantities. Water. Air. Soil Pollut. 36, 311–330. https://doi.org/10.1007/BF00229675

Hippeli, S., Elstner, E.F., 1996. Mechanisms of oxygen activation during plant stress: Biochemical effects of air pollutants. J. Plant Physiol. 148, 249–257. https://doi.org/10.1016/S0176-1617(96)80250-1

Hoffmann, B., Flanker, R., Mengel, K., 1992. Measurements of pH in the apoplast of sunflower leaves by means of fluorescence. Physiol. Plant. 84, 146–153. https://doi.org/10.1111/j.1399-3054.1992.tb08777.x

Hom, J.L., Riechers, G.H., 1991. Carbon assimilation, allocation, and nutrient use efficiency of ponderosa pine as a compensatory response to ozone fumigation and water stress. Ecol. Soc. Am. Bull. 72, 144.

Hoshika, Y., De Marco, A., Materassi, A., Paoletti, E., 2016. Light Intensity Affects Ozone-Induced Stomatal Sluggishness in Snapbean. Water. Air. Soil Pollut. 227, 419. https://doi.org/10.1007/s11270-016-3127-1

Hoshika, Y., Fares, S., Savi, F., Gruening, C., Goded, I., De Marco, A., Sicard, P., Paoletti, E., 2017. Stomatal conductance models for ozone risk assessment at canopy level in two Mediterranean evergreen forests. Agric. For. Meteorol. 234–235, 212–221. https://doi.org/10.1016/j.agrformet.2017.01.005

Hoshika, Y., Katata, G., Deushi, M., Watanabe, M., Koike, T., Paoletti, E., 2015. Ozone-induced stomatal sluggishness changes carbon and water balance of temperate deciduous forests. Sci. Rep. 5, 9871. https://doi.org/10.1038/srep09871

Hoshika, Yasutomo, Moura, B., Paoletti, E., 2018. Ozone risk assessment in three oak species as affected by soil water availability. Environ. Sci. Pollut. Res. 25, 8125–8136. https://doi.org/10.1007/s11356-017-9786-7

Hoshika, Y., Omasa, K., Paoletti, E., 2013a. Both ozone exposure and soil water stress are able to induce stomatal sluggishness. Environ. Exp. Bot. 88, 19–23. https://doi.org/10.1016/j.envexpbot.2011.12.004

Hoshika, Y., Pecori, F., Conese, I., Bardelli, T., Marchi, E., Manning, W.J., Badea, O., Paoletti, E., 2013b. Effects of a three-year exposure to ambient ozone on biomass allocation in poplar using ethylenediurea. Environ. Pollut. 180, 299–303. https://doi.org/10.1016/J.ENVPOL.2013.05.041

Hoshika, Y., Watanabe, M., Carrari, E., Paoletti, E., Koike, T., 2018. Ozone-induced stomatal sluggishness changes stomatal parameters of Jarvis-type model in white birch and deciduous oak. Plant Biol. 20, 20–28. https://doi.org/10.1111/plb.12632

Hoshika, Y., Watanabe, M., Inada, N., Koike, T., 2013c. Model-based analysis of avoidance of ozone stress by stomatal closure in Siebold's beech (Fagus crenata). Ann. Bot. 112, 1149–1158. https://doi.org/10.1093/aob/mct166

Hoshika, Y., Watanabe, M., Inada, N., Koike, T., 2012. Modeling of Stomatal Conductance for Estimating Ozone Uptake of Fagus crenata Under Experimentally Enhanced Free-air Ozone Exposure. Water, Air, Soil Pollut. 223, 3893–3901. https://doi.org/10.1007/s11270-012-1158-9

Hoshika Y., Fares S., Pellegrini E., Conte A., Paoletti E., (2019). Water use strategy affects avoidance of ozone stress by stomatal closure in Mediterranean trees –A modelling analysis–. *Plant, Cell & Environment. - submitted*

Jarvis, P.G., 1976. The Interpretation of the Variations in Leaf Water Potential and Stomatal Conductance Found in Canopies in the Field. Philos. Trans. R. Soc. B Biol. Sci. 273, 593–610. https://doi.org/10.1098/rstb.1976.0035

Journet, A.R.P., Etherington, J.R., 2006. Plant Physiological Ecology. Bryologist 82, 508. https://doi.org/10.2307/3242233

Kangasjärvi, J., Jaspers, P., Kollist, H., 2005. Signalling and cell death in ozone-exposed plants. Plant, Cell Environ. https://doi.org/10.1111/j.1365-3040.2005.01325.x

Kärenlampi, L., Skarby, L., 1996. Critical Levels for Ozone in Europe: Testing and Finalising the Concepts (A UNECE Workshop Report). Dep. Ecol. Environ. Sci.

Karlsson, P.E., Braun, S., Broadmeadow, M., Elvira, S., Emberson, L., Gimeno, B.S., Le Thiec, D., Novak, K., Oksanen, E., Schaub, M., Uddling, J., Wilkinson, M., 2007. Risk assessments for forest trees: The performance of the ozone flux versus the AOT concepts. Environ. Pollut. 146, 608–616. https://doi.org/10.1016/J.ENVPOL.2006.06.012

Karlsson, P.E., Uddling, J., Braun, S., Broadmeadow, M., Elvira, S., Gimeno, B.S., Le Thiec, D., Oksanen, E., Vandermeiren, K., Wilkinson, M., Emberson, L., 2004. New critical levels for ozone effects on young trees based on AOT40 and simulated cumulative leaf uptake of ozone. Atmos. Environ. 38, 2283–2294. https://doi.org/10.1016/J.ATMOSENV.2004.01.027

Karnosky, D.F., Skelly, J.M., Percy, K.E., Chappelka, A.H., 2007. Perspectives regarding 50 years of research on effects of tropospheric ozone air pollution on US forests. Environ. Pollut. 147, 489–506. https://doi.org/10.1016/J.ENVPOL.2006.08.043

Karsenty, A., Blanco, C., Dufour, T., 2003. Instruments related to the United Nations framework convention on climate change and their potential for sustainable forest management in Africa.

Katul, G.G., Palmroth, S., Oren, R., 2009. Leaf stomatal responses to vapour pressure deficit under current and CO 2 -enriched atmosphere explained by the economics of gas exchange. Plant. Cell Environ. 32, 968–979. https://doi.org/10.1111/j.1365-3040.2009.01977.x

Keenan, T., Sabate, S., Gracia, C., 2010. Soil water stress and coupled photosynthesis–conductance models: Bridging the gap between conflicting reports on the relative roles of stomatal, mesophyll conductance and biochemical limitations to photosynthesis. Agric. For. Meteorol. 150, 443–453. https://doi.org/10.1016/J.AGRFORMET.2010.01.008

Killus, J., Meyer, J., Durran, D., Anderson, G., 1984. Continued research in mesoscale air pollution simulation modeling. Volume 5. Refinements in numerical analysis, transport, chemistry, and pollutant.

Kolb, T.., Matyssek, R., 2001. Limitations and perspectives about scaling ozone impacts in trees. Environ. Pollut. 115, 373–393. https://doi.org/10.1016/S0269-7491(01)00228-7

Kouvarakis, G., Vrekoussis, M., Mihalopoulos, N., Kourtidis, K., Rappenglueck, B., Gerasopoulos, E., Zerefos, C., 2002. Spatial and temporal variability of tropospheric ozone (O3) in the boundary layer above the Aegean Sea (eastern Mediterranean). J. Geophys. Res. Atmos. 107, PAU-4.

Krupa, S., McGrath, M.T., Andersen, C.P., Booker, F.L., Burkey, K.O., Chappelka, A.H., Chevone, B.I., Pell, E.J., Zilinskas, B.A., 2001. Ambient ozone and plant health. Plant Dis. 85, 4–12.

Kurpius, M.R., McKay, M., Goldstein, A.H., 2002. Annual ozone deposition to a Sierra Nevada ponderosa pine plantation. Atmos. Environ. 36, 4503–4515. https://doi.org/10.1016/S1352-2310(02)00423-5

Laisk, A., Kull, O., Moldau, H., 1989. Ozone concentration in leaf intercellular air spaces is close to zero. Plant Physiol. 90, 1163–7. https://doi.org/10.1104/PP.90.3.1163

Lasslop, G., Reichstein, M., Papale, D., Richardson, A., Arneth, A., Barr, A., Stoy, P., Wohlfahrt, G., 2010. Separation of net ecosystem exchange into assimilation and respiration using a light response curve approach: Critical issues and global evaluation. Glob. Chang. Biol. 16, 187–208. https://doi.org/10.1111/j.1365-2486.2009.02041.x

Law, B.E., Williams, M., Anthoni, P.M., Baldocchi, D.D., Unsworth, M.H., 2000. Measuring and modelling seasonal variation of carbon dioxide and water vapour exchange of a Pinus ponderosa forest subject to soil water deficit. Glob. Chang. Biol. 6, 613–630. https://doi.org/10.1046/j.1365-2486.2000.00339.x

Lawson, T., Blatt, M.R., 2014. Stomatal Size, Speed, and Responsiveness Impact on Photosynthesis and Water Use Efficiency. Plant Physiol. 164, 1556–1570. https://doi.org/10.1104/PP.114.237107

Leadley, P.W., Niklaus, P., Stocker, R., Korner, C., 1997. Screen-aided CO2 control (SACC): A middle ground between FACE and open-top chambers. Acta Oecologica 18, 207–219. https://doi.org/10.1016/S1146-609X(97)80007-0

Lelieveld, J., Berresheim, H., Borrmann, S., Crutzen, P.J., Dentener, F.J., Fischer, H., Feichter, J., Flatau, P.J., Heland, J., Holzinger, R., 2002. Global air pollution crossroads over the Mediterranean. Science (80-.). 298, 794–799.

Leisner, C.P., Ainsworth, E.A., 2012. Quantifying the effects of ozone on plant reproductive growth and development. Glob. Chang. Biol. 18, 606–616. https://doi.org/10.1111/j.1365-2486.2011.02535.x

Lhomme, J.P., 1988. Extension of Penman's formulae to multi-layer models. Boundary-Layer Meteorol. 42, 281–291. https://doi.org/10.1007/BF00121587

Li, P., Calatayud, V., Gao, F., Uddling, J., Feng, Z., 2016. Differences in ozone sensitivity among woody species are related to leaf morphology and antioxidant levels. Tree Physiol. 36, 1105–1116.

Lim, S.S., Vos, T., Flaxman, A.D., Danaei, G., Shibuya, K., Adair-Rohani, H., AlMazroa, M.A., Amann, M., Anderson, H.R., Andrews, K.G., Aryee, M., Atkinson, C., Bacchus, L.J., Bahalim, A.N., Balakrishnan, K., Balmes, J., Barker-Collo, S., Baxter, A., Bell, M.L., Blore, J.D., Blyth, F., Bonner, C., Borges, G., Bourne, R., Boussinesq, M., Brauer, M., Brooks, P., Bruce, N.G., Brunekreef, B., Bryan-Hancock, C., Bucello, C., Buchbinder, R., Bull, F., Burnett, R.T., Byers, T.E., Calabria, B., Carapetis, J., Carnahan, E., Chafe, Z., Charlson, F., Chen, H., Chen, J.S., Cheng, A.T.-A., Child, J.C., Cohen, A., Colson, K.E., Cowie, B.C., Darby, S., Darling, S., Davis, A., Degenhardt, L., Dentener, F., Des Jarlais, D.C., Devries, K., Dherani, M., Ding, E.L., Dorsey, E.R., Driscoll, T., Edmond, K., Ali, S.E., Engell, R.E., Erwin, P.J., Fahimi, S., Falder, G., Farzadfar, F., Ferrari, A., Finucane, M.M., Flaxman, S., Fowkes, F.G.R., Freedman, G., Freeman, M.K., Gakidou, E., Ghosh, S., Giovannucci, E., Gmel, G., Graham, K., Grainger, R., Grant, B., Gunnell, D., Gutierrez, H.R., Hall, W., Hoek, H.W., Hogan, A., Hosgood, H.D., Hoy, D., Hu, H., Hubbell, B.J., Hutchings, S.J., Ibeanusi, S.E., Jacklyn, G.L., Jasrasaria, R., Jonas, J.B., Kan, H., Kanis, J.A., Kassebaum, N., Kawakami, N., Khang, Y.-H., Khatibzadeh, S., Khoo, J.-P., Kok, C., Laden, F., Lalloo, R., Lan, Q., Lathlean, T., Leasher, J.L., Leigh, J., Li, Y., Lin, J.K., Lipshultz, S.E., London, S., Lozano, R., Lu, Y., Mak, J., Malekzadeh, R., Mallinger, L., Marcenes, W., March, L., Marks, R., Martin, R., McGale, P., McGrath, J., Mehta, S., Memish, Z.A., Mensah, G.A., Merriman, T.R., Micha, R., Michaud, C., Mishra, V., Hanafiah, K.M., Mokdad, A.A., Morawska, L., Mozaffarian, D., Murphy, T., Naghavi, M., Neal, B., Nelson, P.K., Nolla, J.M., Norman, R., Olives, C., Omer, S.B., Orchard, J., Osborne, R., Ostro, B., Page, A., Pandey, K.D., Parry, C.D., Passmore, E., Patra, J., Pearce, N., Pelizzari, P.M., Petzold, M., Phillips, M.R., Pope, D., Pope, C.A., Powles, J., Rao, M., Razavi, H., Rehfuess, E.A., Rehm, J.T., Ritz, B., Rivara, F.P., Roberts, T., Robinson, C., Rodriguez-Portales, J.A., Romieu, I., Room, R., Rosenfeld, L.C., Roy, A., Rushton, L., Salomon, J.A., Sampson, U., Sanchez-Riera, L., Sanman, E., Sapkota, A., Seedat, S., Shi, P., Shield, K., Shivakoti, R., Singh, G.M., Sleet, D.A., Smith, E., Smith, K.R., Stapelberg, N.J., Steenland, K., Stöckl, H., Stovner, L.J., Straif, K., Straney, L., Thurston, G.D., Tran, J.H., Van Dingenen, R., van Donkelaar, A., Veerman, J.L., Vijayakumar, L., Weintraub, R., Weissman, M.M., White, R.A., Whiteford, H., Wiersma, S.T., Wilkinson, J.D., Williams, H.C., Williams, W., Wilson, N., Woolf, A.D., Yip, P., Zielinski, J.M., Lopez, A.D., Murray, C.J., Ezzati, M., 2012. A comparative risk assessment of burden of disease and injury attributable to 67 risk factors and risk factor clusters in 21 regions, 1990–2010: a systematic analysis for the Global Burden of Disease Study 2010. Lancet 380, 2224–2260. https://doi.org/10.1016/S0140-6736(12)61766-8

Lloyd, J., Taylor, J.A., 1994. On the Temperature Dependence of Soil Respiration. Funct. Ecol. 8, 315. https://doi.org/10.2307/2389824

Lombardozzi, D., Levis, S., Bonan, G., Hess, P.G., Sparks, J.P., Lombardozzi, D., Levis, S., Bonan, G., Hess, P.G., Sparks, J.P., 2015. The Influence of Chronic Ozone Exposure on Global

Carbon and Water Cycles. J. Clim. 28, 292–305. https://doi.org/10.1175/JCLI-D-14-00223.1

Lombardozzi, D., Levis, S., Bonan, G., Sparks, J.P., 2012. Predicting photosynthesis and transpiration responses to ozone: decoupling modeled photosynthesis and stomatal conductance. Biogeosciences 9, 3113–3130. https://doi.org/10.5194/bg-9-3113-2012

Lombardozzi, D., Sparks, J.P., Bonan, G., 2013. Integrating O3 influences on terrestrial processes: photosynthetic and stomatal response data available for regional and global modeling. Biogeosciences Discuss. 10, 6973–7012. https://doi.org/10.5194/bgd-10-6973-2013

Löw, M., Herbinger, K., Nunn, A.J., Häberle, K.-H., Leuchner, M., Heerdt, C., Werner, H., Wipfler, P., Pretzsch, H., Tausz, M., Matyssek, R., 2006. Extraordinary drought of 2003 overrules ozone impact on adult beech trees (Fagus sylvatica). Trees 20, 539–548. https://doi.org/10.1007/s00468-006-0069-z

Lowman, M., Rinker, H.B., 2004. Forest canopies. Elsevier Academic Press.

Luwe, M., Heber, U., 1995. Ozone detoxification in the apoplasm and symplasm of spinach, broad bean and beech leaves at ambient and elevated concentrations of ozone in air. Planta. https://doi.org/10.2307/23383610

Macháčová, K., 2010. Open top chamber and free air CO2 Enrichment - approaches to investigate tree responses to elevated CO2. IForest 3, 102–105. https://doi.org/10.3832/ifor0544-003

Mächler, F., Wasescha, M.R., Krieg, F., Oertli, J.J., 1995. Damage by Ozone and Protection by Ascorbic Acid in Barley Leaves. J. Plant Physiol. 147, 469–473. https://doi.org/10.1016/S0176-1617(11)82185-1

Maier-Maercker, U., Kock, W., 1991. Experiments on the control capacity of stomata of Picea abies (L.) Karst. after fumigation with ozone and in environmentally damaged material. Plant. Cell Environ. 14, 175–184. https://doi.org/10.1111/j.1365-3040.1991.tb01334.x

Manes, F., Vitale, M., Donato, E., Paoletti, E., 1998. O3 and O3 + CO2 effects on a Mediterranean evergreen broadleaf tree, holm oak (Quercus ilex L.), in: Chemosphere. pp. 801–806. https://doi.org/10.1016/S0045-6535(97)10127-8

Manes, F., Vitale, M., Fabi, A.M., De Santis, F., Zona, D., 2007. Estimates of potential ozone stomatal uptake in mature trees of Quercus ilex in a Mediterranean climate. Environ. Exp. Bot. 59, 235–241.

Manes, F., Silli, V., Salvatori, E., Incerti, G., Galante, G., Fusaro, L., Perrino, C., 2014. Urban ecosystem services: tree diversity and stability of PM10 removal in the metropolitan area of Rome. Ann. di Bot. https://doi.org/10.4462/annbotrm-11746

Matyssek, R., Bytnerowicz, A., Karlsson, P.E., Paoletti, E., Sanz, M., Schaub, M., Wieser, G., 2007. Promoting the O3 flux concept for European forest trees. Environ. Pollut. 146, 587–607. https://doi.org/10.1016/j.envpol.2006.11.011

Matyssek, R., Günthardt-Goerg, M.S., Keller, T., Scheidegger, C., 1991. Impairment of gas exchange and structure in birch leaves (Betula pendula) caused by low ozone concentrations. Trees 5, 5–13. https://doi.org/10.1007/BF00225329

Matyssek, R., Sandermann, H., Wieser, G., Booker, F., Cieslik, S., Musselman, R., Ernst, D., 2008. The challenge of making ozone risk assessment for forest trees more mechanistic. Environ. Pollut. https://doi.org/10.1016/j.envpol.2008.04.017

Medlyn, B.E., Duursma, R.A., Eamus, D., Ellsworth, D.S., Prentice, I.C., Barton, C.V.M., Crous, K.Y., De Angelis, P., Freeman, M., Wingate, L., 2011. Reconciling the optimal and empirical approaches to modelling stomatal conductance. Glob. Chang. Biol. 17, 2134–2144. https://doi.org/10.1111/j.1365-2486.2010.02375.x

Mehlhorn, H., Cottam, D.A., Lucas, P.W., Wellburn, A.R., 1987. Induction of Ascorbate Peroxidase and Glutathione Reductase Activities by Interactions of Mixtures of Air Pollutants. Free Radic. Res. Commun. 3, 193–197. https://doi.org/10.3109/10715768709069784

Mehlhorn, H., Seufert, G., Schmidt, A., Kunert, K.J., 1986. Effect of SO2 and O3 on Production of Antioxidants in Conifers. Plant Physiol. 82, 336–8. https://doi.org/10.1104/pp.82.1.336

Mehlhorn, H., Wellburn, A.R., 1987. Stress ethylene formation determines plant sensitivity to ozone. Nature 327, 417–418. https://doi.org/10.1038/327417a0

Mészáros, R., Horváth, L., Weidinger, T., Neftel, A., Nemitz, E., Dämmgen, U., Cellier, P., Loubet, B., 2009. Measurement and modelling ozone fluxes over a cut and fertilized grassland. Biogeosciences 6, 1987–1999. https://doi.org/10.5194/bg-6-1987-2009

Meyers, T.P., Baldocchi, D.D., 1988. A comparison of models for deriving dry deposition fluxes of O3 and SO2 to a forest canopy. Tellus B 40 B, 270–284. https://doi.org/10.1111/j.1600-0889.1988.tb00297.x

Millán, M.M., Mantilla, E., Salvador, R., Carratalá, A., Sanz, M.J., Alonso, L., Gangoiti, G., Navazo, M., Millán, M.M., Mantilla, E., Salvador, R., Carratalá, A., Sanz, M.J., Alonso, L., Gangoiti, G., Navazo, M., 2000. Ozone Cycles in the Western Mediterranean Basin: Interpretation of Monitoring Data in Complex Coastal Terrain. J. Appl. Meteorol. 39, 487–508. https://doi.org/10.1175/1520-0450(2000)039<0487:OCITWM>2.0.CO;2

Mills, G., Hayes, F., Simpson, D., Emberson, L., Norris, D., Harmens, H., Büker, P., 2011a. Evidence of widespread effects of ozone on crops and (semi-)natural vegetation in Europe (1990-2006) in relation to AOT40- and flux-based risk maps. Glob. Chang. Biol. 17, 592–613. https://doi.org/10.1111/j.1365-2486.2010.02217.x

Mills, G., Hayes, F., Wilkinson, S., Davies, W.J., 2009. Chronic exposure to increasing background ozone impairs stomatal functioning in grassland species. Glob. Chang. Biol. 15, 1522–1533. https://doi.org/10.1111/j.1365-2486.2008.01798.x

Mills, G., Pleijel, H., Braun, S., Büker, P., Bermejo, V., Calvo, E., Danielsson, H., Emberson, L., Fernández, I.G., Grünhage, L., Harmens, H., Hayes, F., Karlsson, P.-E., Simpson, D., 2011b. New stomatal flux-based critical levels for ozone effects on vegetation. Atmos. Environ. 45, 5064–5068. https://doi.org/10.1016/J.ATMOSENV.2011.06.009

Mills, G., Pleijel, H., Büker, P., Braun, S., Emberson, L., 2010. Chapter 3: mapping critical levels for vegetation. Mapping manual. Manual on methodologies and criteria for modelling and mapping critical loads and.

Misson, L., Panek, J.A., Goldstein, A.H., 2004. A comparison of three approaches to modeling leaf gas exchange in annually drought-stressed ponderosa pine forests. Tree Physiol. 24, 529–541. https://doi.org/10.1093/treephys/24.5.529

Misson, L., Tu, K.P., Boniello, R.A., Goldstein, A.H., 2006. Seasonality of photosynthetic parameters in a multi-specific and vertically complex forest ecosystem in the Sierra Nevada of California. Tree Physiol. 26, 729–741.

Mittler, R., Vanderauwera, S., Gollery, M., Van Breusegem, F., 2004. Reactive oxygen gene

network of plants. Trends Plant Sci. 9, 490–498. https://doi.org/10.1016/J.TPLANTS.2004.08.009

Moldau, H., Bichele, I., Hüve, K., 1998. Dark-induced ascorbate deficiency in leaf cell walls increases plasmalemma injury under ozone. Planta 207, 60–66. https://doi.org/10.1007/s004250050455

Møller, I.M., Jensen, P.E., Hansson, A., 2007. Oxidative Modifications to Cellular Components in Plants. Annu. Rev. Plant Biol. 58, 459–481. https://doi.org/10.1146/annurev.arplant.58.032806.103946

Monks, P.S., Archibald, A.T., Colette, A., Cooper, O., Coyle, M., Derwent, R., Fowler, D., Granier, C., Law, K.S., Mills, G.E., Stevenson, D.S., Tarasova, O., Thouret, V., von Schneidemesser, E., Sommariva, R., Wild, O., Williams, M.L., 2015. Tropospheric ozone and its precursors from the urban to the global scale from air quality to short-lived climate forcer. Atmos. Chem. Phys. 15, 8889–8973. https://doi.org/10.5194/acp-15-8889-2015

Monteith, J.L., 1995. A reinterpretation of stomatal responses to humidity. Plant. Cell Environ. 18, 357–364. https://doi.org/10.1111/j.1365-3040.1995.tb00371.x

Morgan, P.W., Drew, M.C., 1997. Ethylene and plant responses to stress. Physiol. Plant. 100, 620–630. https://doi.org/10.1111/j.1399-3054.1997.tb03068.x

Mott, K.A., Parkhurst, D.F., 1991. Stomatal responses to humidity in air and helox. Plant, Cell Environ. 14, 509–515. https://doi.org/10.1111/j.1365-3040.1991.tb01521.x

Mühling, K.H., Plieth, C., Hansen, U.P., Sattelmacher, B., 1995. Apoplastic ph of intact leaves of Vicia faba as influenced by light. J. Exp. Bot. 46, 377–382. https://doi.org/10.1093/jxb/46.4.377

Müller, J.-F., Stavrakou, T., Wallens, S., De Smedt, I., Van Roozendael, M., Potosnak, M.J., Rinne, J., Munger, B., Goldstein, A., Guenther, A.B., 2008. Global isoprene emissions estimated using MEGAN, ECMWF analyses and a detailed canopy environment model. Atmos. Chem. Phys. 8, 1329–1341. https://doi.org/10.5194/acp-8-1329-2008

Musselman, R.C., Lefohn, A.S., Massman, W.J., Heath, R.L., 2006. A critical review and analysis of the use of exposure- and flux-based ozone indices for predicting vegetation effects. Atmos. Environ. 40, 1869–1888. https://doi.org/10.1016/J.ATMOSENV.2005.10.064

Musselman, R.C., Massman, W.J., 1998. Ozone flux to vegetation and its relationship to plant response and ambient air quality standards. Atmos. Environ. 33, 65–73. https://doi.org/10.1016/S1352-2310(98)00127-7

Musselman, R.C., Minnick, T.J., 2000. Nocturnal stomatal conductance and ambient air quality standards for ozone. Atmos. Environ. 34, 719–733. https://doi.org/10.1016/S1352-2310(99)00355-6

Nali, C., Paoletti, E., Marabottini, R., Della Rocca, G., Lorenzini, G., Paolacci, A.., Ciaffi, M., Badiani, M., 2004. Ecophysiological and biochemical strategies of response to ozone in Mediterranean evergreen broadleaf species. Atmos. Environ. 38, 2247–2257. https://doi.org/10.1016/J.ATMOSENV.2003.11.043

Neirynck, J., Gielen, B., Janssens, I.A., Ceulemans, R., 2012. Insights into ozone deposition patterns from decade-long ozone flux measurements over a mixed temperate forest. J. Environ. Monit. 14, 1684. https://doi.org/10.1039/c2em10937a

Noctor, G., Foyer, C.H., 2002. ASCORBATE AND GLUTATHIONE: Keeping Active Oxygen

Under Control. Annu. Rev. Plant Physiol. Plant Mol. Biol. 49, 249–279. https://doi.org/10.1146/annurev.arplant.49.1.249

Noormets, A., Sober, A., Pell, E.J., Dickson, R.E., Podila, G.K., Sober, J., Isebrands, J.G., Karnosky, D.F., 2001. Stomatal and non-stomatal limitation to photosynthesis in two trembling aspen (Populus tremuloides Michx.) clones exposed to elevated CO2 and/or O3. Plant, Cell Environ. 24, 327–336. https://doi.org/10.1046/j.1365-3040.2001.00678.x

Norman, J.M., 1982. Simulation of microclimates. Biometeorol. Integr. pest Manag. 65–99.

Norman, J.M., 1979. " Modelling the complete crop canopy",'Modification of the Aerial Environment of Plants'. Am. Soc. Agr. Eng. Monogr. 2, 249–277.

Norman, J.M., Campbell, G., 1983. Application of a Plant-Environment Model to Problems in Irrigation. Adv. Irrig. 2, 155–188. https://doi.org/10.1016/B978-0-12-024302-0.50011-4

Nunn, A.J., Wieser, G., Reiter, I.M., Häberle, K.H., Grote, R., Havranek, W.M., Matyssek, R., 2006. Testing the unifying theory of ozone sensitivity with mature trees of Fagus sylvatica and Picea abies. Tree Physiol. 26, 1391–1403. https://doi.org/10.1093/treephys/26.11.1391

Oksanen, E., Kontunen-Soppela, S., Riikonen, J., Peltonen, P., Uddling, J., Vapaavuori, E., 2007. Northern environment predisposes birches to ozone damage. Plant Biol. https://doi.org/10.1055/s-2006-924176

Ollinger, S., Aber, J., Reich, P., 1997. Simulation ozone effects on forest productivitiy: interactions among leaf, canopy, and stand-level processes. Ecol. Appl. 7, 1237–1251. https://doi.org/10.1890/1051-0761(1997)007[1237:SOEOFP]2.0.CO;2

Omasa, K., Abo, F., Natori, T., Totsuka, T., 2011. Studies of Air Pollutant Sorption by Plants. J. Agric. Meteorol. 35, 77–83. https://doi.org/10.2480/agrmet.35.77

Omasa, K., Takayama, K., 2002. Image instrumentation of chlorophyll a fluorescence for diagnosis photosynthetic injury. In "Air Pollution and Plant Biotechnology."

Öquist, G., Martin, B., Mårtensson, O., Christersson, L., Malmberg, G., 1978. Effects of Season and Low Temperature on Polypeptides from Thylakoids Isolated from Chloroplasts of Pinus silvestris. Physiol. Plant. 44, 300–306. https://doi.org/10.1111/j.1399-3054.1978.tb08636.x

Oren, R., Sperry, J.S., Katul, G.G., Pataki, D.E., Ewers, B.E., Phillips, N., Schäfer, K.V.R., 1999. Survey and synthesis of intra- and interspecific variation in stomatal sensitivity to vapour pressure deficit. Plant. Cell Environ. 22, 1515–1526. https://doi.org/10.1046/j.1365-3040.1999.00513.x

Outlaw, W.H., De Vlieghere-He, X., 2001. Transpiration rate. An important factor controlling the sucrose content of the guard cell apoplast of broad bean. Plant Physiol. 126, 1716–24. https://doi.org/10.1104/PP.126.4.1716

Outlaw, W.H., Manchester, J., Dicamelli, C.A., Randall, D.D., Rapp, B., Veith, G.M., 1979. Photosynthetic carbon reduction pathway is absent in chloroplasts of Vicia faba guard cells. Proc. Natl. Acad. Sci. U. S. A. 76, 6371–5. https://doi.org/10.1073/PNAS.76.12.6371

Pääkkönen, E., Metsärinne, S., Holopainen, T., Kärenlampi, L., 1996. The ozone sensitivity of birch (Betula pendula) in relation to the developmental stage of leaves. New Phytol. 132, 145–154. https://doi.org/10.1111/j.1469-8137.1996.tb04520.x

Pallardy, S.G., Kozlowski, T.T. (Theodore T., 2008. Physiology of woody plants. Elsevier.

Panek, J.A., 2004. Ozone uptake, water loss and carbon exchange dynamics in annually drought-

stressed Pinus ponderosa forests: measured trends and parameters for uptake modeling. Tree Physiol. 24, 277–290. https://doi.org/10.1093/treephys/24.3.277

Paoletti, E., 2007a. The effects of ozone on Mediterranen forests. For. - Riv. di Selvic. ed Ecol. For. 4, 478–487. https://doi.org/10.3832/efor0490-0040478

Paoletti, E., 2007b. Ozone impacts on forests. CAB Rev. Perspect. Agric. Vet. Sci. Nutr. Nat. Resour. 2. https://doi.org/10.1079/pavsnnr20072068

Paoletti, E., 2006. Impact of ozone on Mediterranean forests: A review. Environ. Pollut. 144, 463–474. https://doi.org/10.1016/J.ENVPOL.2005.12.051

Paoletti, E., 2005. Ozone slows stomatal response to light and leaf wounding in a Mediterranean evergreen broadleaf, Arbutus unedo. Environ. Pollut. 134, 439–445. https://doi.org/10.1016/J.ENVPOL.2004.09.011

Paoletti, E., Contran, N., Bernasconi, P., Günthardt-Goerg, M.S., Vollenweider, P., 2009. Structural and physiological responses to ozone in Manna ash (Fraxinus ornus L.) leaves of seedlings and mature trees under controlled and ambient conditions. Sci. Total Environ. 407, 1631–1643. https://doi.org/10.1016/J.SCITOTENV.2008.11.061

Paoletti, E., Grulke, N.E., 2005. Does living in elevated CO2 ameliorate tree response to ozone? A review on stomatal responses. Environ. Pollut. 137, 483–493. https://doi.org/10.1016/J.ENVPOL.2005.01.035

Paoletti, E., Materassi, A., Fasano, G., Hoshika, Y., Carriero, G., Silaghi, D., Badea, O., 2017. A new-generation 3D ozone FACE (Free Air Controlled Exposure). Sci. Total Environ. 575, 1407–1414. https://doi.org/10.1016/j.scitotenv.2016.09.217

Paoletti, E., Nali, C., Meeting, G.L., 2004, U., 2004. Gas exchange and ozone visibile injury in Mediterranean evergreen broadleaved seedlings. IUFRO Meet. (pp. 85-101). Oulu Univ. Press.

Paoletti, E., Ranieri, A., Lauteri, M., 2008. Moving toward effective ozone flux assessment. Environ. Pollut. 156, 16–19. https://doi.org/10.1016/j.envpol.2008.02.025

Parrish, D.D., Lamarque, J.-F., Naik, V., Horowitz, L., Shindell, D.T., Staehelin, J., Derwent, R., Cooper, O.R., Tanimoto, H., Volz-Thomas, A., Gilge, S., Scheel, H.-E., Steinbacher, M., Fröhlich, M., 2014. Long-term changes in lower tropospheric baseline ozone concentrations: Comparing chemistry-climate models and observations at northern midlatitudes. J. Geophys. Res. Atmos. 119, 5719–5736. https://doi.org/10.1002/2013JD021435

Patterson, M.T., Rundel, P.W., 1989. Seasonal physiological responses of ozone stressed Jeffrey pine in Sequoia National Park, California, in: Proceedings- 82 Nd A & WMA Annual Meeting, Anaheim, CA, USA, 06/25-30/89.

Patwardhan, S., Pavlick, R., Kleidon, A., 2006. Does the empirical Ball-Berry law of stomatal conductance emerge from maximization of productivity? Am. Geophys. Union, Fall Meet. 2006, Abstr. id. H51C-0498.

Pearson, M., Mansfield, T.A., 1993. Interacting effects of ozone and water stress on the stomatal resistance of beech (Fagus sylvatica L.). New Phytol. 123, 351–358. https://doi.org/10.1111/j.1469-8137.1993.tb03745.x

Pell, E.J., Eckardt, N.A., Glick, R.E., 1994. Biochemical and molecular basis for impairment of photosynthetic potential. Photosynth. Res. 39, 453–462.

Pelloux, J., Jolivet, Y., Fontaine, V., Banvoy, J., Dizengremel, P., 2001. Changes in Rubisco and

Rubisco activase gene expression and polypeptide content in Pinus halepensis M. subjected to ozone and drought. Plant, Cell Environ. 24, 123–131. https://doi.org/10.1046/j.1365-3040.2001.00665.x

Peñuelas, J., Llusià, J., 2002. Linking photorespiration, monoterpenes and thermotolerance in Quercus. New Phytol. 155, 227–237.

Peñuelas, J., Llusia, J., Asensio, D., Munné-Bosch, S., 2005. Linking isoprene with plant thermotolerance, antioxidants and monoterpene emissions. Plant. Cell Environ. 28, 278–286.

Pinzari, F., Trinchera, A., Benedetti, A., Sequi, P., 1999. Use of biochemical indices in the Mediterranean environment: comparison among soils under different forest vegetation. J. Microbiol. Methods 36, 21–28. https://doi.org/10.1016/S0167-7012(99)00007-X

Pleijel, H., Danielsson, H., Ojanperä, K., De Temmerman, L., Högy, P., Badiani, M., Karlsson, P.E., 2004. Relationships between ozone exposure and yield loss in European wheat and potato - A comparison of concentration- and flux-based exposure indices, in: Atmospheric Environment. Pergamon, pp. 2259–2269. https://doi.org/10.1016/j.atmosenv.2003.09.076

Pleijel, H., Danielsson, H., Vandermeiren, K., Blum, C., Colls, J., Ojanperä, K., 2002. Stomatal conductance and ozone exposure in relation to potato tuber yield - Results from the European CHIP programme. Eur. J. Agron. 17, 303–317. https://doi.org/10.1016/S1161-0301(02)00068-0

Plöchl, M., Lyons, T., Ollerenshaw, J., Barnes, J., 2000. Simulating ozone detoxification in the leaf apoplast through the direct reaction with ascorbate. Planta 210, 454–467. https://doi.org/10.1007/PL00008153

Pochanart, P., Akimoto, H., Maksyutov, S., Staehelin, J., 2001. Surface ozone at the Swiss Alpine site Arosa: the hemispheric background and the influence of large-scale anthropogenic emissions. Atmos. Environ. 35, 5553–5566.

Quiang, Y., Youngquiang, Z., Yunfen, L., Peili, S., 2004. Simulation of the Stomatal Conductance of Winter Wheat in Response to Light , Temperature and CO 2 Changes. Ann. Bot. 93, 435–441. https://doi.org/10.1093/aob/mch023

Rai, A., Kulshreshtha, K., Srivastava, P.K., Mohanty, C.S., 2009. Leaf surface structure alterations due to particulate pollution in some common plants. Environmentalist 30, 18–23. https://doi.org/10.1007/s10669-009-9238-0

Rapport, D., 1998. Assessing ecosystem health. Trends Ecol. Evol. 13, 397–402. https://doi.org/10.1016/S0169-5347(98)01449-9

Reich, P.B., 1987. Quantifying plant response to ozone: a unifying theory. Tree Physiol. 3, 63–91. https://doi.org/10.1093/treephys/3.1.63

Reich, P.B., Lassoie, J.P., 1984. Effects of low level O3 exposure on leaf diffusive conductance and water-use efficiency in hybrid poplar. Plant. Cell Environ. 7, 661–668. https://doi.org/10.1111/1365-3040.ep11571645

Reichenauer, T., Bolhàr-Nordenkampf, H.R., Ehrlich, U., Soja, G., Postl, W.F., Halbwachs, F., 1997. The influence of ambient and elevated ozone concentrations on photosynthesis in Populus nigra. Plant, Cell Environ. 20, 1061–1069. https://doi.org/10.1111/j.1365-3040.1997.tb00682.x

Reichstein, M., 2005. On the separation of net ecosystem exchange into assimilation and ecosystem respiration: review and improved algorithm. Glob. Chang. Biol. 11, 1424–1439.

https://doi.org/10.1111/j.1365-2486.2005.001002.x

Reiner, S., Wiltshire, J.J.J., Wright, C.J., Colls, J.J., 1996. The Impact of Ozone and Drought on the Water Relations of Ash Trees (Fraxinus excelsior L.). J. Plant Physiol. 148, 166–171. https://doi.org/10.1016/S0176-1617(96)80310-5

Ribas, À., Peñuelas, J., 2004. Temporal patterns of surface ozone levels in different habitats of the North Western Mediterranean basin. Atmos. Environ. 38, 985–992. https://doi.org/10.1016/j.atmosenv.2003.10.045

Rice-Evans, C., Miller, N., Paganga, G., 1997. Antioxidant properties of phenolic compounds. Trends Plant Sci. 2, 152–159. https://doi.org/10.1016/S1360-1385(97)01018-2

Richards, L. A. 193). Capillary conduction of liquids through porous mediums. *Physics*, **1**(5), 318–333.

Richardson, L. F. 2007. Weather prediction by numerical process, Cambridge university press.

Romane, F., Terradas, J., 2013. Quercus ilex L. ecosystems: function, dynamics and management. Springer Science & Business Media.

Rosa, E.A., Dietz, T., 2012. Human drivers of national greenhouse-gas emissions. Nat. Clim. Chang. 2, 581–586. https://doi.org/10.1038/nclimate1506

Salvati, L., Sabbi, A., and Carlucci, M., 2014. Exploring complex relationships using non-parametric principal components analysis: a case study with land-use data. Int. J. Ecol. Econ. Stat. 33, 90–97.

Saxe, H., Ellsworth, D.S., Heath, J., 1998. Tree and forest functioning in an enriched CO2 atmosphere. New Phytol. https://doi.org/10.1046/j.1469-8137.1998.00221.x

Savé, R., Castell, C., Terradas, J., 1999. Gas Exchange and Water Relations, in: Ecology of Mediterranean Evergreen Oak Forests. Springer, pp. 135–147. https://doi.org/10.1007/978-3-642-58618-7_10

Scholes, R.J., 1999. Will the terrestrial carbon sink saturate soon? Glob. Chang. Newsl. 37, 2–3.

Schuepbach, E., Friedli, T.K., Zanis, P., Monks, P.S., Penkett, S.A., 2001. State space analysis of changing seasonal ozone cycles (1988-1997) at Jungfraujoch (3580 m above sea level) in Switzerland. J. Geophys. Res. Atmos. 106, 20413–20427. https://doi.org/10.1029/2000JD900591

Sharma, P., Sober, A., Sober, J., Podila, G.P., Kubiske, M.E., Mattson, W.J., Isebrands, J.G., Karnosky, D.F., 2003. Moderation of [CO_2]-induced gas exchange responses by elevated tropospheric O_3 in trembling aspen and sugar maple. Ekol. 22(Supplement 1) 304-317. 22.

Shimazaki, K., 1989. Ribulosebisphosphate carboxylase activity and photosynthetic o(2) evolution rate in vicia guard-cell protoplasts. Plant Physiol. 91, 459–63. https://doi.org/10.1104/PP.91.2.459

Sitch, S., Cox, P.M., Collins, W.J., Huntingford, C., 2007. Indirect radiative forcing of climate change through ozone effects on the land-carbon sink. Nature 448, 791–794. https://doi.org/10.1038/nature06059

Stanners, D., Bourdeau, P., Agency, E.E., 1995. Europe's environment: the Dobrís assessment.

Sun, G., McLaughlin, S.B., Porter, J.H., Uddling, J., Mulholland, P.J., Adams, M.B., Pederson, N., 2012. Interactive influences of ozone and climate on streamflow of forested watersheds. Glob. Chang. Biol. 18, 3395–3409. https://doi.org/10.1111/j.1365-2486.2012.02787.x

Szarka, A., Tomasskovics, B., Bánhegyi, G., 2012. The ascorbate-glutathione-α-tocopherol triad in abiotic stress response. Int. J. Mol. Sci. 13, 4458–83. https://doi.org/10.3390/ijms13044458

Takahama, U., Oniki, T., 1992. Regulation of Peroxidase-Dependent Oxidation of Phenolics in the Apoplast of Spinach Leaves by Ascorbate. Plant Cell Physiol. 33, 379–387. https://doi.org/10.1093/oxfordjournals.pcp.a078265

Takahama, U., 1993. Redox state of ascorbic acid in the apoplast of stems of Kalanchoe daigremontiana. Physiol. Plant. 89, 791–798. https://doi.org/10.1111/j.1399-3054.1993.tb05286.x

Tanaka, K., Sugahara, K., 1980. Role of superoxide dismutase in defense against SO2 toxicity and an increase in superoxide dismutase activity with SO2 fumigation. Plant Cell Physiol. 21, 601–611. https://doi.org/10.1093/oxfordjournals.pcp.a076035

Tausz, M., Grulke, N.E., Wieser, G., 2007. Defense and avoidance of ozone under global change. Environ. Pollut. 147, 525–531. https://doi.org/10.1016/j.envpol.2006.08.042

Tenhunen, J.D., Lange, O.L., Braun, M., Meyer, A., Lösch, R., Pereira, J.S., 1980. Midday stomatal closure in Arbutus unedo leaves in a natural macchia and under simulated habitat conditions in an environmental chamber. Oecologia 47, 365–367. https://doi.org/10.1007/BF00398530

Teskey, R.O., Fites, J.A., Samuelson, L.J., Bongarten, B.C., 1986. Stomatal and nonstomatal limitations to net photosynthesis in Pinus taeda L. under different environmental conditions. Tree Physiol. 2, 131–142. https://doi.org/10.1093/treephys/2.1-2-3.131

Tingey, D.T., Hogsett, W.E., 1985. Water Stress Reduces Ozone Injury via a Stomatal Mechanism. Plant Physiol. 77, 944–7. https://doi.org/10.1104/pp.77.4.944

Tingey, D.T., Manning, M., Grothaus, L.C., Burns, W.F., 1980. Influence of light and temperature on monoterpene emission rates from slash pine. Plant Physiol. 65, 797–801.

Tjoelker, M.G., Volin, J.C., Oleskyn, J., Reich, P.B., 1995. Interaction of ozone pollution and light effects on photosynthesis in a forest canopy experiment. Plant. Cell Environ. 18, 895–905. https://doi.org/10.1111/j.1365-3040.1995.tb00598.x

Torsethaugen, G., Pell, E.J., Assmann, S.M., 2002. Ozone inhibits guard cell K+ channels implicated in stomatal opening. Proc. Natl. Acad. Sci. 96, 13577–13582. https://doi.org/10.1073/pnas.96.23.13577

Uddling, J., Günthardt-Goerg, M.., Matyssek, R., Oksanen, E., Pleijel, H., Selldén, G., Karlsson, P.., 2004. Biomass reduction of juvenile birch is more strongly related to stomatal uptake of ozone than to indices based on external exposure. Atmos. Environ. 38, 4709–4719. https://doi.org/10.1016/J.ATMOSENV.2004.05.026

Uddling, J., Hogg, A.J., Teclaw, R.M., Carroll, M.A., Ellsworth, D.S., 2010. Stomatal uptake of O3 in aspen and aspen-birch forests under free-air CO2 and O3 enrichment. Environ. Pollut. 158, 2023–31. https://doi.org/10.1016/j.envpol.2009.12.001

UNECE, 2004. Revised manual on methodologies and criteria for mapping critical levels/loads and geographical areas where they are exceeded., (February. ed.) http://icpmapping.org/cms/zeigeBereich/5/manual_und_downloads.html

UNECE, 2010. Manual on methodologies and criteria for modeling and mapping critical loads and levels, and air pollution effects, trends and risks. Chapter 3: mapping critical levels for vegetation. Conv. Long-Range Transbound. Air Pollut. Available at : http://www.icpmappinmg.org/2010.

Uprety, D.C., Garg, S.C., Bisht, B.S., Maini, H.K., Dwivedi, N., Paswan, G., Raj, A., Saxena, D.C., 2006. Carbon dioxide enrichment technologies for crop response studies. J. Sci. Ind. Res. (India). 65, 859–866.

Vainonen, J.P., Kangasjärvi, J., 2015. Plant signalling in acute ozone exposure. Plant. Cell Environ. 38, 240–252.

Vanaja, M., Maheswari, M., Ratnakumar, P., Ramakrishna, Y.S., 2006. Monitoring and controlling of CO2 concentrations in open top chambers for better understanding of plants response to elevated CO2 levels. Indian J. Radio Sp. Phys. 35, 193–197.

Varela, S.A., Weigandt, M.N., Willems, P., Bianchi, E., Diez, J.P., Gyenge, J.E., 2016. Physiological status of conifer seedlings treated with radiation, drought and frost stress mitigation techniques: a laboratory assessment. New For. 47, 87–103. https://doi.org/10.1007/s11056-015-9485-5

Velikova, V., Tsonev, T., Pinelli, P., Alessio, G.A., Loreto, F., 2005. Localized ozone fumigation system for studying ozone effects on photosynthesis, respiration, electron transport rate and isoprene emission in field-grown Mediterranean oak species. Tree Physiol. 25, 1523–1532.

Vitale, M., Scimone, M., Feoli, E., Manes, F., 2003. Modelling leaf gas exchanges to predict functional trends in Mediterranean Quercus Ilex forest under climatic changes in temperature. Ecol. Modell. 166, 123–134. https://doi.org/10.1016/S0304-3800(03)00129-7

Vitale, M., Salvatori, E., Loreto, F., Fares, S., Manes, F., 2008. Physiological responses of Quercus ilex Leaves to Water Stress and Acute Ozone Exposure Under Controlled Conditions. Water. Air. Soil Pollut. 189, 113–125. https://doi.org/10.1007/s11270-007-9560-4

Webb, R.A., 1972. Use of the Boundary Line in the analysis of biological data. J. Hortic. Sci. 47, 309–319. https://doi.org/10.1080/00221589.1972.11514472

Wesely, M.L., 1989. Parameterization of surface resistances to gaseous dry deposition in regional-scale numerical models. Atmos. Environ. 23, 1293–1304. https://doi.org/10.1016/0004-6981(89)90153-4

Wieser, G., 1997. Ozone Impact on Photosynthetic Capacity of Mature and Young Norway Spruce (Picea abies (L.) Karst.): External Versus Internal Exposure. Phyt. - Ann. Rei Bot. 37, 297–302.

Wieser, G., Matyssek, R., 2007. Linking ozone uptake and defense towards a mechanistic risk assessment for forest trees: Letters. New Phytol. https://doi.org/10.1111/j.1469-8137.2007.01994.x

Wieser, G., Tausz, M., 2006. Critical levels for ozone: further applying and developing the flux-based concept. n A UNECE Work. Report. BFW-Wien.

Wieser, G., Tegischer, K., Tausz, M., Häberle, K.H., Grams, T.E.E., Matyssek, R., 2002. Age effects on Norway spruce (Picea abies) susceptibility to ozone uptake: A novel approach relating stress avoidance to defense. Tree Physiol. 22, 583–590. https://doi.org/10.1093/treephys/22.8.583

Wilkinson, S., Davies, W.J., 2010. Drought, ozone, ABA and ethylene: new insights from cell to

plant to community. Plant, Cell Environ. 33, 510–525. https://doi.org/10.1111/j.1365-3040.2009.02052.x

Wittig, V.E., Ainsworth, E.A., Long, S.P., 2007. To what extent do current and projected increases in surface ozone affect photosynthesis and stomatal conductance of trees? A meta-analytic review of the last 3 decades of experiments. Plant. Cell Environ. 30, 1150–62. https://doi.org/10.1111/j.1365-3040.2007.01717.x

Wittig, V.E., Ainsworth, E.A., Naidu, S.L., Karnosky, D.F., Long, S.P., 2009. Quantifying the impact of current and future tropospheric ozone on tree biomass, growth, physiology and biochemistry: A quantitative meta-analysis. Glob. Chang. Biol. 15, 396–424. https://doi.org/10.1111/j.1365-2486.2008.01774.x

Wong, S., Cowan, I., Farquhar, G.D., 1979. Stomatal conductance correlates with photosynthetic capacity. Nature. https://doi.org/10.1038/282424a0

Woodrow, I.E., 1994. Optimal acclimation of the C3 photosynthetic system under enhanced CO2. Photosynth. Res. 39, 401–412. https://doi.org/10.1007/BF00014594

Zhang, L., Brook, J.R., Vet, R., 2002. On ozone dry deposition—with emphasis on non-stomatal uptake and wet canopies. Atmos. Environ. 36, 4787–4799. https://doi.org/10.1016/S1352-2310(02)00567-8

Zhang, W., Feng, Z., Wang, X., Niu, J., 2012. Responses of native broadleaved woody species to elevated ozone in subtropical China. Environ. Pollut. 163, 149–157. https://doi.org/10.1016/j.envpol.2011.12.035

Zhang, Y.Q., Wu, Q.P., Zhang, J.M., Yang, X.H., 2011. Effects of ozone on membrane permeability and ultrastructure in Pseudomonas aeruginosa. J. Appl. Microbiol. 111, 1006–1015. https://doi.org/10.1111/j.1365-2672.2011.05113.x

Zong, R., Yang, X., Wen, L., Xu, C., Zhu, Y., Chen, T., Yao, L., Wang, L., Zhang, J., Yang, L., Wang, X., Shao, M., Zhu, T., Xue, L., Wang, W., 2018. Strong ozone production at a rural site in theNorth China Plain: Mixed effects of urban plumesand biogenic emissions. J. Environ. Sci. 71, 261–270. https://doi.org/10.1016/J.JES.2018.05.003

List of scientific publications produced during the PhD course

Published papers

Conte, A., Fares, S., Salvati, L., Savi, F., Matteucci, G., Mazzenga, F., ... & Cremonese, E. (2019). Ecophysiological responses to rainFall variability in grassland and forests along a latitudinal gradient in Italy. *Frontiers in Forests and Global Change*, *2*, 16.

Fares, S., Savi, F., Fusaro, L., Conte, A., Salvatori, E., Aromolo, R., & Manes, F. (2016). Particle deposition in a peri-urban Mediterranean forest. *Environmental pollution*, *218*, 1278-1286.

Fares, S., Conte, A., & Chabbi, A. (2018). Ozone flux in plant ecosystems: new opportunities for long-term monitoring networks to deliver ozone-risk assessments. *Environmental Science and Pollution Research*, *25*(9), 8240-8248.

Fares, S., Alivernini, A., Conte, A., & Maggi, F. (2019). Ozone and particle fluxes in a Mediterranean forest predicted by the AIRTREE model. *Science of The Total Environment*, *682*, 494-504.

Paoletti E., Alivernini A., Anav A., Badea O., Carrari E., Chivulescu S., Conte A., Ciriani M.L.; Dalstein–Richier L., De Marco A., Fares S., Fasano G., Giovannelli A., Lazzara M., Leca S., Materassi A., Moretti V., Pitar D., Popa I., Sabatini F., Salvati L., Sicard P., Sorgi T., Hoshika Y. (2019). Toward stomatal-flux based forest protection against ozone: the MOTTLES approach. *Science of The Total Environment*.

Submitted

Hoshika Y., Fares S., Pellegrini E., Conte A., Paoletti E., (2019). Water use strategy affects avoidance of ozone stress by stomatal closure in Mediterranean trees –A modelling analysis–. *Plant, Cell & Environment.*